Distributed Energy Storage Systems: Microgrid Application, Market-Based Optimal Operation and Harmonic Analysis

Reza Arghandeh Jouneghani

Dissertation submitted to the faculty of the Virginia Polytechnic Institute and State University in partial fulfillment of the requirements for the degree of

Doctor of Philosophy
in
Electrical Engineering

Robert P. Broadwater (Co-Chair)
Virgilio A. Centeno (Co-Chair)
Jaime De La Ree Lopez
Parviz Ghandforoush
Amos L. Abbott

March 27 2013
Blacksburg, VA

Keywords: Distribution Network, Optimization, Control, Microgrid, Energy Storage, Harmonics, Economical Operation

Copyright© 2013 Reza Arghandeh

Distributed Energy Storage Systems: Microgrid Application, Market-Based Optimal Operation and Harmonic Analysis

Reza Arghandeh Jouneghani

ABSTRACT

The need for modern electricity infrastructures and more capable grid components brings attention to distributed energy storage systems because of their bidirectional power flow capability. This dissertation focuses on three different aspects of distributed energy storage system applications in distribution networks. It starts with flywheel energy storage system modeling and analysis for application in microgrid facilities. Then, a market-based optimal controller is proposed to enhance the operational profit of distributed energy storage devices in distribution networks. Finally, impact of multiple distributed energy storage devices on harmonic propagation in distribution networks is investigated.

This dissertation provides a comparison between batteries and flywheels for the ride-through application in critical microgrid facilities like data centers. In comparison with batteries, the application of FES for power security is new. This limits the availability of experimental data. The software tool developed in this dissertation enables analysis of short-term, ride-through applications of FES during an islanded operation of a facility microgrid. As a result, it can provide a guideline for facility engineers in data centers or other types of facility microgrids to design backup power systems based on FES technology.

This dissertation also presents a real-time control scheme that maximizes the revenue attainable by distributed energy storage systems without sacrificing the benefits related to

improvements in reliability and reduction in peak feeder loading. This optimal control algorithm provides a means for realizing additional benefits by utilities by taking advantage of the fluctuating cost of energy in competitive energy markets. The key drivers of the economic optimization problem for distributed energy storage systems are discussed.

In this dissertation, the impact of distribution network topology on harmonic propagation due to the interaction of multiple harmonic sources is investigated. Understanding how multiple harmonic sources interact to increase or decrease the harmonic distortion is crucial in distribution networks with a large number of Distributed Energy Resources. A new index, Index of Phasor Harmonics (IPH), is proposed for harmonic quantization in multiple harmonic source cases. The proposed IPH index presents more information than commonly used indices. With the help of the detailed distribution network model, topological impacts of harmonic propagation are investigated. In particular, effects of mutual coupling, phase balance, three phase harmonic sources, and single phase harmonic sources are considered.

Acknowledgements

Above all, I am grateful to the almighty God, my Maker and Friend, for providing me with the physical, emotional, and spiritual support I needed to complete my PhD.

I would like to express my sincere gratitude to my advisor Dr. Robert Broadwater for his significant role in my life. He provided me with the guidance, assistance and support that I needed during my PhD study. He gave me encouragement and confidence to venture into research experience on my own and branch out into new research horizons. The engineering principles he taught me are not only accurate but also very practical to industry. I am also grateful for his friendship and patience during my PhD study. He is the best advisor I can imagine.

I am deeply grateful to my Co-Adviser Dr. Virgilio Centeno for his constant support and guidance from beginning of my PhD study. Our discussions opened my eyes to new ideas and approaches to my research. I appreciate his passion for helping me progress in my research. Thank you for your priceless time.

I would also like to thank Dr. Saifur Rahman for his great influence on the way I approach not only my research but also other challenges in life. We had many invaluable conversations on the first section of my dissertation in particular and on the Philosophy of Research in general. He is a great mentor for technology development. Moreover, Dr. Manisa Pipattanasomporn in Virginia Tech Advanced Research Institute (VT-ARI) provided me with a deep insight into taking a whole-system approach to my research work. She helped me a lot in my first steps at Virginia Tech.

I would like to thank Dr. Jaime De La Ree, Dr. Parviz Ghandforoush, and Dr. Amos Abbott for serving on my PhD advisory committee. Dr. De La Ree gave me many constructive comments during our group meetings in the power systems lab. Dr. Ghanforush from the college of Business supplied very interesting advice on my dissertation in term of economic optimization. He kindly gave me the time for

our constructive conversations on business side of engineering. I appreciate the attentiveness Dr. Abbot gave to my academic progress and the perspective he brought to my research as a professor from a different area within ECE.

I also have special thanks for Dr. Lamine Mili whose teaching style I found very engaging and helpful to the rest of my academic journey. I expect that the courses that I took under his instruction will prove fruitful throughout my career.

I would also like to thank Dr. Majid Amidpour, my advisor at Khajeh Nasir Toosi University of Technology, in Tehran, Iran, for laying a good foundation for my later research and encouraging me to go on for my PhD. I also would like to thank Dr. Mohammad Reza Jafari Nasr, Dr. Mohammad Hassan Panjeshahi and Dr. Ali Ghaffari for providing instructive advices from different perspectives to improve my research work.

I would like to thank Electrical Distribution Design (EDD) Inc. for providing me with the resources necessary for me to conduct my dissertation, in particular, the Distributed Engineering Workstation (DEW) software, which is a great and unique tool for smart grid design, planning and operation.

Because of the academic environment, I have crossed paths with many graduate students and professionals who have influenced and enhance my academic experience and my daily life! I like to thank my great friends in VT-ARI ,Younel Teklo, Sai Krovvidi, Shengnan Shao, Sixiang Yang and especially Mahmoud El Gammal who always supported and helped me 24-7! I would like to thank Marija Telbis-Forster as the graduate coordinator in VT-NVC for her countless helps and supports. I would like to thank my friends, classmates and labmates in EDD as I recall the good times we enjoyed together in the past two years. Murat Dilek and Kevin Russell supplied their expertise, Ahmet Onen supplied his good sense of humor, Jearmy Woyak supplied his delicious banana bread, Jaesung Jung supplied his financial advice, and Roddy DeHart his collections of sci-fi movies and toys. Besides all of the fun, I learned a lot from all of them.

As long as I am writing names, I cannot forget that of Saeed Keshani, my most constant friend since a long time ago. He provided me a lot of support and encouragement over the years like a brother. To make a long story short, he is my pillar of support. I don't want to miss any opportunity to thank him! I would also like to thank all my friends in Blacksburg, especially Hanif Livani. Well, I can only say that without him school life would have been so boring. His kindness, sense of humor, and his Ray-Ban glasses made him an outstanding friend. I am indebted to him for helping me get away from my studies so that I didn't become a reclusive nerd. I also would like to thank Reza Sarlak, a great friend who inspired me with his great talent in Tonbak (the goblet drum from Persia) and his sense of humor. Meeting him in Blacksburg was a great happening.

I would to thank my uncle, Abbas Arvaneh. He and his family, Mersedeh and Tia, are my only relatives in states. These years far from my parents and sisters would have been intolerable without my uncle's family care and kindness. I am so proud of them.

Finally, and most deeply, I would like to dedicate this work to my parents. They did provide me with more than just my genes, life and soul. My mother is a chemistry teacher. My interest in science and education started early in my life when she took me to her classes and provided me with books and movies about science and engineering. My father is an Oil and Gas industry expert. My interest in energy goes back to my childhood when he took me to refineries and oil production facilities. I am also thankful for my lovely sisters who are both engineers, Azar a computer engineer and Rahil an electrical engineer. I am so lucky to have these kind and selfless sisters. The love, education and support of my family are the base of my academic achievements, and they always have my back. This long journey would have been impossible without their support.

Thank you and God Bless all of you

To my Mother Soodabeh Arvaneh, my first teacher,

my Father Ali-Asghar Arghandeh, my lifetime inspiration

and my beloved Sisters, Azar and Rahil

Table of Contents

Figures Outline

Tables Outline

Chapter 1 : Introduction

1.1. Introduction

Environmental concerns, global warming and fossil fuel prices along with demand growth create a shift in the expectations of consumers and utilities to move toward renewable energy resources, electric vehicles, and higher qualitative electricity supplies. The advent of Smart Grid is an answer to the need for reform in power systems. The smart grid aims to create high penetration levels of renewable energy resources to create a more sustainable energy supply. It appreciates electric vehicle adoption and efficient components [1]. Generally speaking, smart grid seeks to make the grid reliable, secure and efficient [2]. However, there are number of challenges in addition to the offered opportunities with smart grid.

Renewable energy resources are intermittent and non-dispatchable. The inability to control output of renewable resources results in operational challenges in power systems. Moreover, the rising share of electric vehicles in the automotive market increases stress on distribution networks. Moreover, grid reliability requirements need investment and retrofitting of conventional power systems.

Recently, demand response programs came to help conventional grids transition to the smart grid. Demand response is load control approaches to decrease peak [3]. It is performed by customers and in some cases by utilities. Demand Response programs are highly dependent on customer demand behavior and their participation in such programs [4]. However, many customers are not willing to decrease their convenience or invest efforts in changing their behavior to alleviate utilities challenges. Demand Response alone will not allow penetrating high levels of intermittent renewable energy resources into the grid. Moreover, in terms of major problems in supply side or outages, demand response cannot help. Therefore, they are not an ultimate solution for reliable and secure operation of distribution networks.

These operational challenges can be addressed by energy storage systems. Energy storage systems can be used to control the effect of intermittent renewable energy resources. Furthermore, energy storage systems are applied for ancillary services, peak reduction, mitigating contingencies in distribution and transmission networks, and improve power systems reliability and flexibility. This dissertation is shaped around energy storage system applications in distribution networks. It includes modeling and simulation, optimal economic operation, and harmonic impacts of such systems on distribution networks. However, the algorithms and impact studies are expandable to other Distributed Energy Resources (DER) inside the distribution network.

1.2. Background Information

1.2.1. Energy Storage Systems for Distribution Networks, Cons and Pros

Distribution network enhancements via the smart grid concept in addition to advent of the Microgrids bring generation sources near customers. Distributed energy resources, more sensitive electronic loads, and large numbers of power electronic interfaces create more stress and limitations for distribution network planning and operation. Renewable energy resource integration, power quality, power flow re-distribution, network restoration, supply and demand control, and electricity market-based operation are areas that have recently gained attention of power system experts. It is worthwhile to mention that distributed energy resources, along with new technologies for supply and demand control in distribution networks, help in central station generation and transmission capacity utilizations and expansion plans. Energy storage systems are applicable in all areas. The challenges in the distribution network need specific types of analysis and technologies fitted for the distribution network with solutions that can extend up to customer houses. Distributed Energy Storage systems have come to realize the critical need for energy buffering and control at distribution levels. Energy storage units add more degrees of freedom to the power system with bi-directional power flow capabilities. Distributed energy storage systems represent a new class of power grid components and require new algorithms, standards, economics, planning and operation paradigms.

The bi-directional capability of energy storage systems means the power supply and demand can be detached as far as the energy storage capacity allows. The reserve capacity of energy storage units provides immediate energy for back-up power, ancillary services and quick response applications [5]. Energy storage systems offer economic advantages by regulating charging and discharging to capitalize on fluctuating electricity prices or regulating line loading and demand to optimize power system utilization. At the transmission level, energy storage improves the effective capacity of lines. At the distribution level, it improves power factor and efficiency. From the power system planning point of view, energy storage applications can mitigate the need for more transmission or generation capacities. Energy storage systems defer investments for distribution network expansion by reducing power system flows needed to supply peak loads.

Wind and solar energy resources usually have their own maximum at hours different from the peak load. Energy storage systems in addition to renewable firming, add dispatchability to such intermittent energy resources. The renewable resource dispatchability provides ancillary service benefits for distribution and transmission network stockholders. The similar economic incentives are provided by

energy storage owned by customers for small scale renewable resources integration and demand control purposes. Figure 1-1 illustrates energy storage benefits for utilities under two categories, service-based benefits and market-based benefits [6].

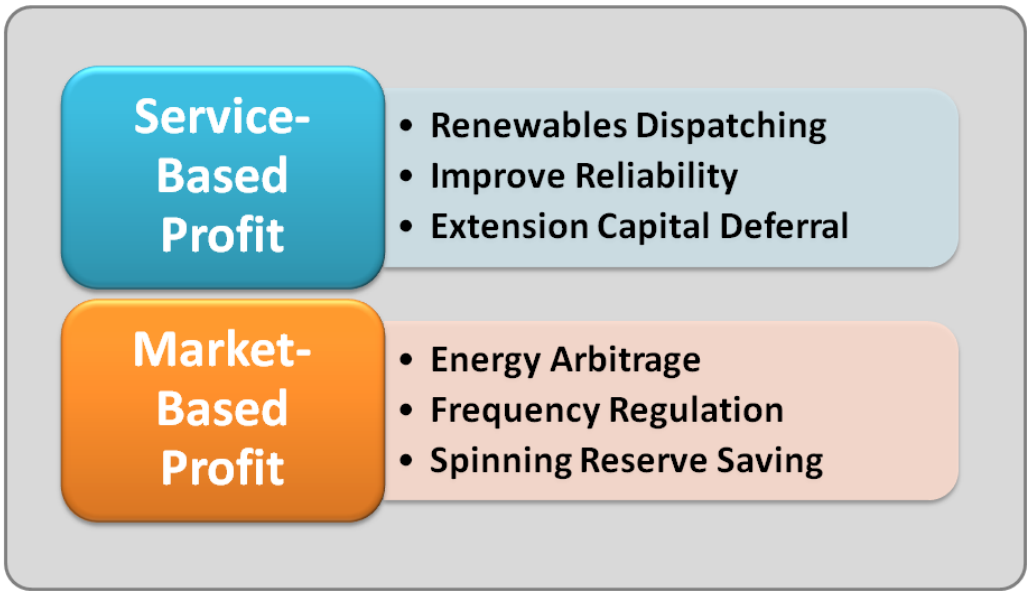

Figure 1-1 , Service based and market-based benefits of energy storage systems

The main challenge of energy storage systems is reducing overall cost of the batteries, especially for small scale applications. However, battery manufacturers are utilizing different materials and manufacturing techniques to cut down energy storage cost. Increased interest in intermittent renewable resources and dynamic prices of electricity provide more incentives for using batteries. Also, reusing electric vehicle (EV) batteries for grid support applications has potential for economic benefits. Allocating EV batteries for second-use applications leads to environmental benefits by delaying disposing and recycling of EV batteries [7]. The financial benefits of energy storage systems can be highlighted in Figure 1.2.

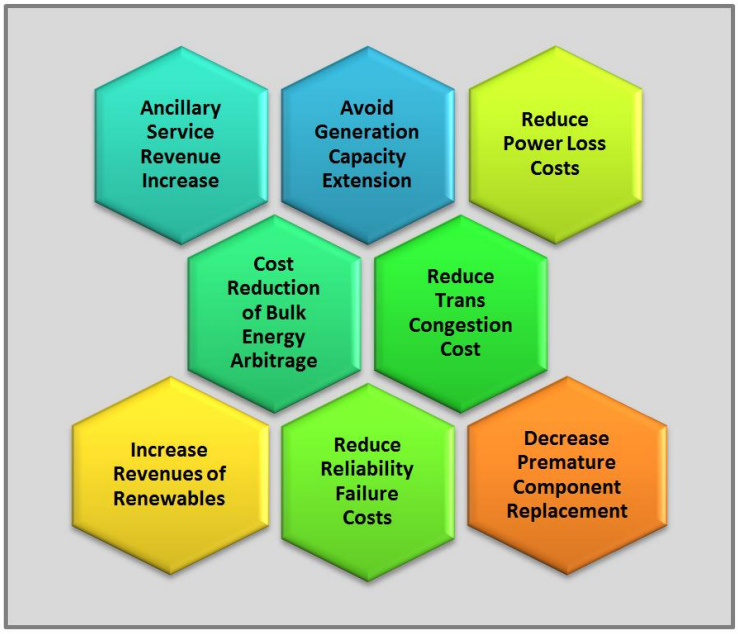

Figure 1-2. Economic Benefits of Energy Storage Systems

1.2.2. Energy Storage System Applications

Energy storage system (ESS) technologies are available in a wide selection of capacity and discharging times. Energy storage delivers many benefits to electric power systems at the generation, transmission, and distribution levels. At the generation and transmission levels, one of the potential benefits of storage systems is the ability to defer new generation capacity and transmission line upgrades. Storage can be installed at or near load centers often easier than generating units. It can also operate in conjunction with demand response programs.

At the distribution level, storage can be used in substations to enhance power factor and improve system reliability [5]. At the load level, it can be implemented to perform peak shaving and load balancing. It can store energy from distributed renewable energy resources until it is needed for off-grid or grid connected conditions. Figure 1-2 shows different applications of energy storage systems [6]. Each application needs specific battery capacity and ranges of discharge times.

1.2.3. Energy Storage Technologies

There are many energy storage technologies for power system applications. Different technologies have different characteristics, which result in different advantages and disadvantages. Pumped hydro facilities and lead acid batteries have been successful examples for many years. Other technologies

require advancements to become practical and economic for applications. The electricity storage systems can be divided into four main categories [8]:

- Mechanical energy storage systems (Flywheels, Compressed air, Hydroelectric)
- Electrical energy storage systems (Super Capacitors, Super conductors)
- Electrochemical energy storage systems (Batteries, Hydrogen)
- Thermal energy storage systems (Ice, Molten salt)

Figure 1-3 represents various storage technologies published by Electricity Storage Association (ESA) in terms of total power and energy capacity time [6].

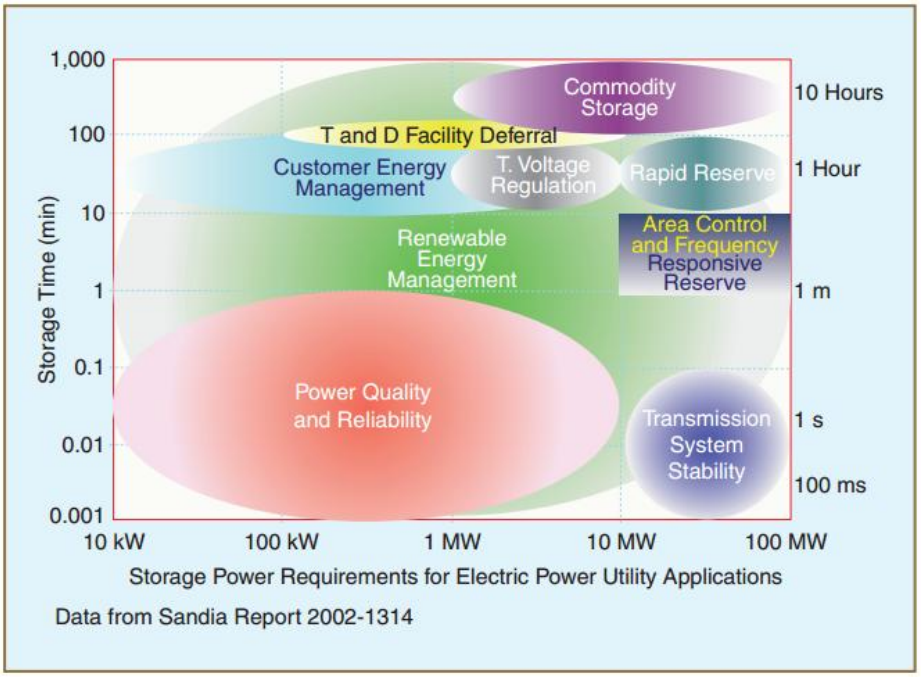

Figure 1-3, Different applications of energy storage systems with corresponded capacity and discharge time (Courtesy Electricity Storage Association) [6]

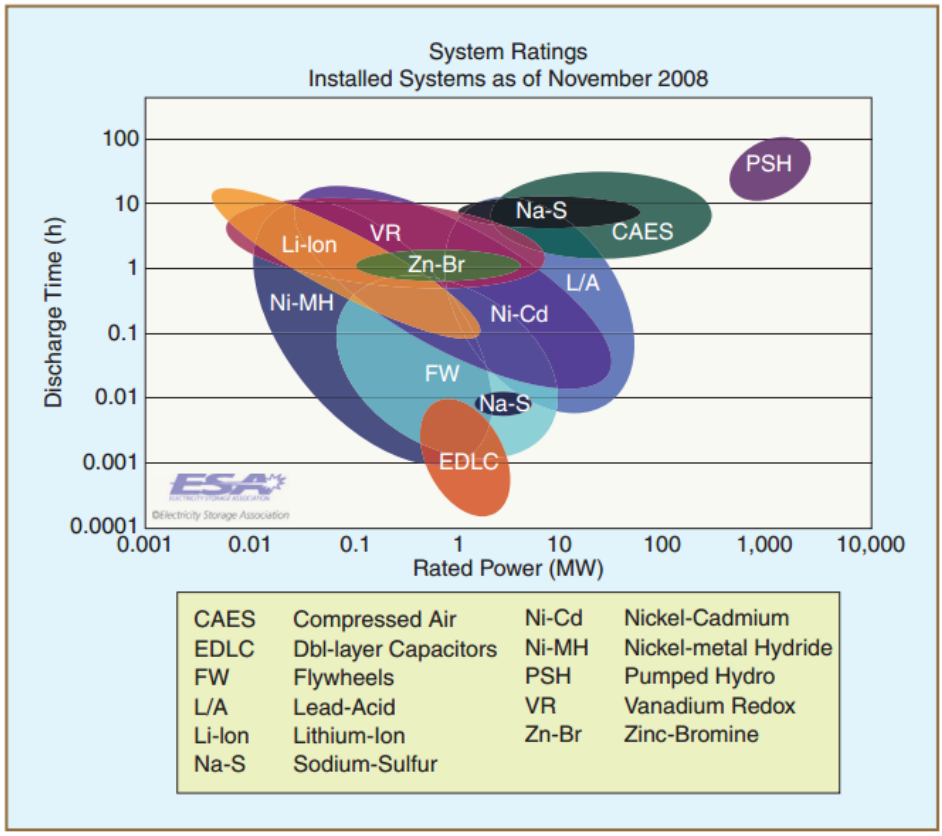

Figure 1-4, Different technologies of energy storage systems in term of rated power and discharge time (Courtesy Electricity Storage Association) [6]

A number of energy storage technologies that are more common for utility scale applications are presented as follows:

Sodium Sulfur Batteries:

Since 1984, Tokyo Electric Power Company (TEPCO) and NGK Insulators Ltd (NGK) began a joint program to develop the Sodium Sulfur (NaS) battery energy storage systems for load leveling and power grid stabilization. In a NaS battery cell, sodium is used as a negative electrode and sulfur is used as positive electrode. There is a metal container inside the beta alumina tube to prevent over current and internal temperature rise for safety purposes. The NaS battery operates between 300˚C and 360˚C with an equipped electrical heater to maintain the temperature [9]. The battery temperature increases during the discharging and standby status and decreases during charging. Cells inside the module are anchored in place by filling and solidifying them with sand, which is used to prevent fires and as a means of lateral

support [10]. The commercially available NaS batteries are designed to discharge as long as 7 hours. For quick discharge applications, they can provide power up to 5 times the rated power for some minutes.

Flow Batteries:

Flow batteries are emerging energy storage devices that can serve many purposes in energy delivery systems. They operate like conventional batteries, storing and releasing energy through a reversible electrochemical reaction with an almost limitless number of charging and discharging cycles. They differ from a conventional battery in two ways; 1) the reaction occurs between two electrolytes, rather than between an electrolyte and an electrode and 2) the two electrolytes are stored in external containers and the electrolytes are circulated through the cell stack as required. The flow battery is scalable to any power and energy. More cell stacks create a greater power rating and more electrolyte volume leads to higher energy capacity. They operate in ambient temperature [11]. One of the advantages of flow batteries is that their construction is based on plastic components in reactor stacks, piping, and tanks for holding the electrolytes. Therefore, the batteries are relatively light in weight and have a long life [12].

Lead Acid Batteries:

The lead acid batteries are the oldest battery technology. They have the lowest cost because of their technology maturity. The amount of energy (kWh) that a lead-acid battery can deliver is not fixed and depends on its rate of discharge. They are used in power plants for back-up power as a black start source. They are ideal for applications with low duty cycles. The research and efforts on advanced lead acid battery technologies target the life cycle expansion for these types of batteries [13].

Lithium-Ion Batteries:

The Lithium-Ion (Li-Ion) battery technology can be applied in different sizes and shapes to fit in available space [12]. They are lighter in terms of energy density. The Li-Ion battery development for PHEV applications result in lower prices and better performance. Li-Ion batteries will benefit from economy of scale over the next years because of variety of their applications [14].

Flywheels:

The flywheel is one of the oldest technologies in human hands. It is a rotating disk which can store kinetic energy. The stored energy can be used to produce electricity. Flywheels have a specific spinning time based on its natural momentum. Nowadays, many designs are available for flywheels and some of them are developed for use as Flywheel Electricity Storage Systems (FESS). Generally, flywheels can be

classified as either low speed or high speed. The speed of former is in thousands revolutions per minute (rpm), while that of the latter is at tens of thousands rpm [15].

Thermal Storage:

Thermal storage devices are usually designed to deploy in commercial or residential buildings. Ice storage devices can make ice during off-pick hours at nights and used for air cooling during the peak hours of the next day. In cold climates, ceramic heat sinks can capture thermal energy during off-peak hours and power the heating system during peak hours [3].

Other Storage Technologies:

Pump storage and compressed air storage technologies are considered large-scale storage systems. There are over 90 GW of pumped storage in operation worldwide, which is about 3 % of global generation capacity. Pumped storage plants are characterized by long construction times and high capital expenditure. Pumped storage is the most widespread energy storage system in use on power networks. Its main applications are for energy management, frequency control and energy reserves.

1.2.4. Distribution Network Simulation and Analysis Platform

The Distributed Engineering Workstation (DEW) software is used in this dissertation for power system analysis and system integration. It is the object oriented software based on the generic analysis approach. It is developed more than 20 years ago at Virginia Tech [16].

The Generic Analysis approach is a combination of physical network modeling and generic programming. The physical network modeling is developed for both steady-state and dynamic analysis of system models. Generic programming is one step beyond object oriented programming. It is based on the use of iterators that access and manipulated objects. In DEW, iterators are referred to as topology iterators, and are used to access and manipulate network objects in respect to physical connections. The topology iterator represents a graph-based approach that does not need to maintain or use matrices in analysis [17]. It eliminates very large system matrix updates following changes in system topology created by such things as sectionalizing device operations or equipment failures. With topology iterators, after any topological change model updates will operate only at the local component topology in constant time [17, 18]. The network solution approach used in DEW is also referred to as Graph Trace Analysis (GTA). Research on GTA has been conducted for many years at Virginia Tech [18, 19].

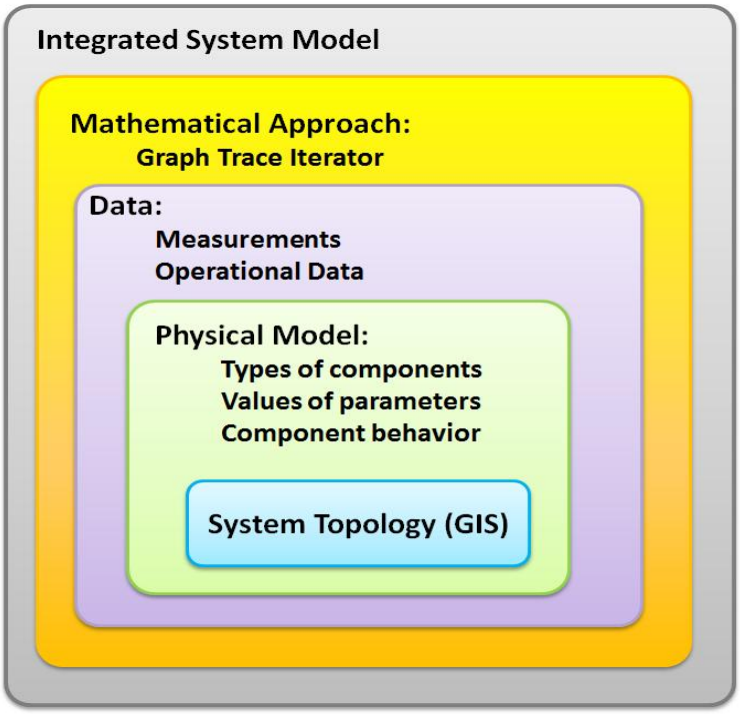

Figure 1-5, Major functional parts of DEW software

In DEW the analysis approach uses one model for all types of analysis. The technology is referred to as Integrated System Model (ISM). The scope of ISM includes transmission and distribution networks through customer loads. It easily displays and manipulates GIS system data [20]. Currently, commercialized power system software packages often use different models for different applications [21]. The ISM allows using a common model for different aspects of smart grid like planning, reliability, substation engineering, operation, and load forecasting. Figure 1-5 shows the major functional parts of the DEW software.

1.3. Dissertation Objectives and Research Questions

The advent of smart grid brings new trends to power systems, like distributed renewable energy resource integration, electric vehicles, decentralized management and control, and deregulation of electricity markets. The need for modern electricity infrastructures and more capable grid components brings attention to distributed energy storage systems because of their bidirectional power flow capability. The objective of this dissertation is to model, simulate and analyze energy storage systems in distribution networks with insights into the electricity market, economic benefits, reliability, efficiency and power quality. This dissertation is classified into three sections. It starts with distributed energy storage system modeling and application to microgrid facilities. Then, a market-based optimization algorithm is proposed

to enhance the operational value of energy storage devices in distribution networks. A Distributed Energy Resources (DER) harmonic impact study is also presented. This study considers the interactive impacts of multiple harmonic sources on each other, proposing new measurement indices and visualization approaches. The distribution network topology and phase balance impact on harmonic propagation are investigated.

This dissertation investigates a number of challenging questions related to smart grid energy storage. Major tasks performed along with the questions and subtasks associated with each task are now presented:

Task 1: Modeling and simulation of distributed energy systems for critical microgrid facilities

In this research, the selected technology for the critical microgrid application is the flywheel.

Q.1.1*. What type of energy storage technology is a better fit for critical microgrid applications, such as data centers? What are the challenges for conventional battery-based back-up power sources in data centers?*

Subtask 1.1. Compare flywheels and batteries for critical microgrid facilities applications

Q.1.2*. How can flywheel technology be used for ride-through applications in microgrids?*

Subtask 1.2. Develop flywheel energy storage detailed model and model evaluation

Subtask 1.3. Analyze flywheel energy storage system performance in critical microgrids

Task 2: Economic control and optimization of Community Energy Storage (CES) systems in competitive electricity markets

The research is part of the Department of Energy smart grid demonstration project to implement community energy storage systems for grid support. The research questions and their associated dissertation objectives are as follows:

Q.2.1*. What are the potential advantages of community energy storage systems in distribution networks?*

Subtask 2.1. Investigate potential benefits of Community Energy Storage for distribution networks operators

Q.2.2*. How can the community energy storage system operational profits be enhanced in distribution networks?*

Subtask 2.2. Design hierarchical real-time control and optimization architecture for CES units to increase their operational profits

Q.2.3*. What is the multi-objective optimal solution for using distributed energy storage systems simultaneously considering dynamic market price, reliability, and network efficiency?*

Subtask 2.3. Develop market-based economic optimization algorithm for CES application

Subtask 2.4. Analyze different trade-offs for CES economic operation

Q.2.4*. What economic benefits can be realized by using energy storage systems to take advantage of real-time and day ahead dynamic market prices?*

Subtask 2.5. Analyze impact of real-time and day ahead LMP price differences on operational profits

Q.2.5*. How can the detailed three-phase distribution network model in this dissertation improve the simulation and analysis results in comparison to previous studies?*

Subtask 2.6. Apply the detailed multiphase model for distribution network for more realistic investigation of CES adoption on distribution networks

Subtask 2.7. Calculate the aggregated impact of a fleet of CES units on the distribution network

Subtask 2.8. Analyze the impact of CES on renewable energy resources integration in distribution networks

Subtask 2.9. Alleviate electric vehicle adoption impact on distribution transformer overloading through the CES system operation

Task 3: Harmonics interaction from Multiple Distributed Energy Resources on Distribution Networks

The harmonic impact of different DER resources in distribution networks and the effect of such DER sources on each other from the harmonic perspective are analyzed in this task. The research questions and objectives associated with this task are as follows:

Q.3.1. *What are the impacts of multiple inverter-based distributed energy resources like PV and community energy storage systems on harmonic distortion in distribution networks?*

Subtask 3.1. Investigate harmonic impact from multiple sources on distribution networks

Q.3.2. *What are the challenges of common harmonic measurement indices?*

Subtask 3.2. Calculate the harmonic impact with commonly used indices and investigate how these indices predict distortion for distribution networks with multiple harmonic sources

Q.3.3. *Are new indices for harmonic distortion that involve interacting harmonic sources needed?*

Subtask 3.3. Investigate new harmonic measurement indices for interactive harmonic propagation assessment

Q.3.4. *How do harmonics generated from multiple harmonic sources interact?*

Subtask 3.4. Create the structure to simulate the interactive harmonic propagation in distribution networks

Subtask 3.5. Conduct sensitivity analysis to find the effect of each harmonic source's magnitude and phase angle on the total harmonic emission

Q.3.5. *How can phase balance affect the harmonic distortion in distribution networks?*

Subtask e 3.6. Perform simulation to show effect of phase balance on interactive harmonic propagation

Q.3.6. *How does distribution network topology impact the harmonic propagation?*

Subtask 3.7. Analyze impact of network topology on harmonic propagation through different case studies

Subtask 3.8. Study the impact of interactive harmonic sources on the customer side and at the substation

Subtask 3.9. Simulate single phase harmonic current propagation through other phases than the injection phase to quantize impact of mutual coupling on harmonic propagation

1.4. The Contents of Dissertation

The rest of this dissertation chapters are organized as follows. Chapter 2 covers literature review. Chapter 3 presents flywheel energy storage ride-through application for critical microgrids. A comparison between the new flywheel energy storage (FES) technology and the conventional battery energy storage technology for data centers is presented in this chapter. Then, the detail FES model is applied for case study analysis. In chapter 4, Community Energy Storage (CES) systems are introduced for distribution network support. This chapter provides a multi objective economic optimization algorithm to provide more profit for distribution network operators. Chapter 5 presents the interactive multiple harmonic analysis and impact study. It investigates the harmonic propagation through the novel and common harmonic assessment indices. In chapter 6, the impact of distribution network topology on harmonic propagation is investigated. The last chapter, chapter 7, is the conclusion of conducted researches in this dissertation.

1.5. Published Works Related to the Dissertation

1.5.1. Publications for Modeling and Simulation of Flywheel Energy Systems for Critical Microgrid Facilities

1. [*Journal*] R. Arghandeh, M. Pipattanasomporn, and S. Rahman, "**Flywheel Energy Storage Systems for Ride-through Applications in a Facility Microgrid**," Smart Grid, IEEE Transactions on, vol. 3, pp. 1955-1962, 2012.
2. [*Conference*] R. Arghandeh, M. Pipattanasomporn , S. Rahman, "**Modeling and Simulation of Flywheel as a Ride-through Device for Securing Critical Loads in a Data Center**", IEEE Power and Energy Society General Meeting, Detroit, MI, Jul 2011

1.5.2. Publications for Economic control and optimization of Community Energy Storage (CES) systems in competitive electricity markets

3. [*Journal*] R. Arghandeh, J. Woyak, R. Broadwater, "**Economic Control of Distributed Energy Storage Systems in Competitive Energy Markets**", IEEE Transaction on Smart Grid, (Submitted)
4. [*Conference*] M. Perov, R. Arghandeh, R. Broadwater, "**Concept and application of distributed compressed air energy storage systems integrated in utility networks**", ASME 2013 Power Conference, Boston, MA, Jul 2013
5. [*Conference*] R. Arghandeh, R. Broadwater, "**Control of Distributed Energy Storage System for Optimal Solar Energy Penetration**", ASME 2012 Power Conference, Anaheim, CA, Jul 2012
6. [*Conference*] R. Arghandeh, R. Broadwater, "**Distributed Energy Storage System Control for Optimal Adoption of Electric Vehicles**", IEEE Power and Energy Society General Meeting, San Diego, CA, Jul 2012

1.5.3. Publications for Interactive Harmonics from Distributed Energy Resources (DER) in Distribution Networks

7. [*Journal*] R. Arghandeh, A. Onen, J. Jung, R. Broadwater, "**Topological Impact Study of Interactive Harmonics from Distributed Energy Resources**," International Journal of Electrical Power & Energy Systems, Elsevier, (Submitted)
8. [*Journal*] R. Arghandeh, R. Broadwater, "**Interactive Assessment of Multi-Harmonic Sources in Distribution Networks"**, IEEE Transaction on Smart Grid, (Submitted)

9. [*Conference*] R. Arghandeh, R. Broadwater, "**Harmonic Impact Study For Distributed Energy Resources Integrated into Power Distribution Networks**", ASME 2013 Power Conference, Boston, MA, Jul 2011

Chapter 2 Literature Reviews

In this chapter, previous works related to the research questions presented in section 1.3 are presented. The knowledge gaps related to those questions and the dissertation novelty are presented. Literature reviews are classified under three main tasks as follows:

2.1.1. Modeling and simulation of distributed energy systems for critical microgrid facilities.

Q.1.1*. What type of energy storage technology is a better fit for critical microgrid applications, such as data centers? What are the challenges for conventional battery-based back-up power sources in data centers?*

The rapid increase in electricity demand in data centers has resulted in a number of research efforts. Many previous publications in this area focus on topics related to power management, which are approaches for determining demand reduction [22] or minimizing total electricity costs using selected optimization techniques and demand response [4, 23]. There are not many publications that address issues of back-up power and energy storage units in data centers. These systems are crucial for maintaining continuous operation of a data center microgrid and can provide ride-through capability for sensitive loads.

Traditionally, energy storage systems in data centers are battery-based [24]. Available literatures in this field are related to the energy storage modeling and analysis for stand-alone power systems or uninterruptable power sources. Authors in [25, 26] discuss different control approaches for battery-based back-up power systems.

There are a considerable number of studies on different energy storage technologies. [27] presents life cycle cost analysis for batteries. In [28], life cycle cost information are presented for a large scale flywheel. [29] shows flywheels have higher energy efficiency than batteries without the need for air conditioning system. From environmental point of view, creation, maintenance and disposing of batteries have dramatic effects on natural environment [27] . However, there is not any literature that specifically compares flywheel and battery energy storage technologies for ride-through applications in data centers. This dissertation compares batteries and flywheels for back-up power system application in data centers and similar facility microgrids.

While most of data center energy storage technologies are based on batteries, flywheels have gained more attention in recent years as they can provide ride-through capability for critical loads in a data center. Batteries are mature technologies, but flywheels have better characteristics in terms of higher efficiency, compactness, footprint, and operation temperature for data center applications. Batteries are less efficient than flywheels. They have less energy density, so they require a larger footprint than flywheels. To economically compare batteries and flywheels, life cycle cost analysis, including both capital and maintenance costs, should be used. This is to account for the fact that the life of flywheels is estimated at 20 years, whereas that of batteries is estimated at three to five years.

The conducted analysis in this dissertation shows flywheel advantages in comparison to batteries for data center applications from different aspects which are not addressed in previous literatures.

***Q.1.2**. How can flywheel technology be used for ride-through applications in microgrids?*

Previous works on modeling and analysis of flywheel applications are available in the literature [30]. Some have applied flywheels to prevent voltage sag and improve power quality [31]. Authors in [32] propose a rotary uninterruptable power supply (UPS) system based on the flywheel energy storage (FES) unit. Authors in [33] introduce appropriate electric machines to drive flywheels. Authors in [34] present new designs for the power electronics interface of FES. There are also papers focusing on the mechanical aspects of FES [28, 29]. Existing literatures on flywheels do not provide an insight into how FES can be used to provide ride through applications in critical microgrids.

This dissertation proposes a detailed model for Flywheel Energy Storage (FES) as a capable distributed energy storage technology for critical microgrid facilities like data centers. Moreover, a software tool based on MATLAB/SIMULINK® is presented to simulate and analyze the flywheel application for data center back-up power systems.

2.1.2. Economic control and optimization of Community Energy Storage (CES) systems in competitive electricity markets

Distributed energy storage devices may improve reliability by providing standby power when equipment outages would otherwise force customer interruptions. Distributed Energy Storage systems are the second aspect covered in the dissertation.

***Q.2.1**. What are the potential advantages of community energy storage systems in distribution networks?*

The authors in [35] present a comprehensive review of battery technologies and their impact on power systems. [36] discusses different energy storage applications in the smart grid. [37] discusses success stories of commercialized energy storage projects. The authors in [38, 39] analyze energy storage systems (EES) for utility scale applications. In [6] authors review different applications of energy storage in distribution networks. They proposed energy storage devices can reduce equipment loading during peak hours, thereby allowing the utility to delay equipment upgrades and to decrease pre-mature aging in network components. Authors in [40] use energy storage for power quality enhancement. Frequency regulation and spinning reserve control are addressed in [41]. Authors in [42, 43] review ESS applications in automotive industries.

In [44-46], authors show EES can also help with renewable energy resource integration into distribution networks. Based on their findings, volt-var control, frequency regulation, and demand response program support are among other benefits of distributed energy systems for utilities. Authors in [47] investigate islanding issues for distributed energy storage systems.

Distributed, controllable energy storage devices offer several significant benefits to electric power system operations. Reliability improvement, power quality enhancement, ancillary services, demand response program support, and renewable energy resource firming are among them.

The Community Energy Storage (CES) is a new architecture of distributed energy storage systems that is considered in this dissertation. The CES units are located at the secondary of distribution transformers. CES provides the most reliable service to customers, since the primary system may be compromised, even to the point of distribution transformer failure, and the energy storage system may still serve the customer.

This dissertation presents a means of realizing additional benefits for utilities by taking advantage of the fluctuating costs of energy in competitive energy markets which is not addressed in previous literatures. These benefits are so great that they sometimes outweigh the high cost of installing the energy storage devices and the communication infrastructure to support them. By combining electricity market information with real-time control of energy storage devices, utilities may enjoy year-round economic benefits from the storage devices in addition to the benefits mentioned above.

Q.2.2*. How can the community energy storage system operational profits be enhanced in distribution networks?*

Many researchers have focused on large scale energy storage applications [48], but fewer have attempted to realize year-round benefits from distributed energy storage systems. The authors of [49-51] looked at the problem from the perspective of controlling customer-owned storage devices that integrate other generation sources. Authors in [52] focused on the voltage fluctuation issue due to high penetration of photovoltaic panels in commercial buildings. The customer owned ESS provides voltage regulation in exchange for subsidies from utilities to cover battery costs. The authors in [53] proposed a stochastic optimal load management for a residential customer with DER and ESS. However, the proposed approach minimized the electricity cost in a real-time manner without considering the system's day ahead behavior.

The presented optimization algorithm in this dissertation is the multi-objective economic solution for community energy storage systems operation. It brings more profit for distribution network operators considering electricity market prices in addition to reliability and stand-by energy capacity. The multi-objective problem solving algorithm, the market-based optimization approach, and the energy storage system hierarchical architecture which are presented in this dissertation are not addressed in previous studies.

***Q.2.3**. What is the multi-objective optimal solution for using distributed energy storage systems simultaneously considering dynamic market price, reliability, and network efficiency?*

Studies that are more relevant to this dissertation are [54, 55]. [54] presented a load management approach for a large load aggregator to determine the electricity price for participation in the day ahead market. A lumped load was considered with grid scale energy storage, and distribution level system topology was not considered. In [55] a distributed energy storage system is applied to minimize the forecasting error of DER generation and to decrease the uncertainty in electricity markets without considering cost benefits and efficiency issues.

The sizing and placement optimization problem for systems with DER and energy storage systems have been well-researched [56, 57]. However, operations of energy storage systems in the competitive energy markets in conjunction with customer service reliability and network efficiency have not been addressed in available literatures. This dissertation presents a real-time control and optimization scheme that maximizes the revenue attainable by energy storage systems without sacrificing the occasional benefits related to improvements in reliability and reduction in peak feeder loading.

This dissertation introduces the multi-objective mathematical approach and its associated constraints (at CES battery level and at feeder level) to achieve the maximum economic profit. The day-ahead load forecasting and day-ahead market prices are considered in the optimization algorithm presented here.

This dissertation applies the optimization solver developed in DEW environment by EDD Inc. that has short computational time even for a large distribution network.

In this dissertation, a novel combination of trade-offs related to transformer loading, feeder loss, and LMP price prediction is considered that are not addressed in previous literatures. The correlation of real-time and day-ahead LMP price has a direct impact on the cost savings potential. This observation and its ramifications are not addressed in previous studies.

***Q.2.4**. What economic benefits can be realized by using energy storage systems to take advantage of real-time and day ahead dynamic market prices?*

The increasing adoption of intermittent renewable energy resources (DER) and the technologic merit for batteries in recent years bring more attention to energy storage systems (ESS) as viable solutions [45, 58, 59]. In [58] authors use a fuzzy clustering optimization approach while considering system security constraints to maximize the renewable energy utilization integrated with a pumped storage unit. Authors in [59] explored sodium–sulfur battery application for ancillary services in electricity markets. Reference [45] provides a general overview to load leveling with solar power generation and storage under a Time of Use (TOU) price scheme. However, the electricity market and the effect of time varying loads were not considered in that reference.

In this dissertation, the price of energy at future hours is needed to determine the optimal charging and discharging schedule for the CES units. The presented dissertation applies a unique combination of day ahead Local Marginal Prices (LMP) and real-time LMP in addition to the distribution network load forecast. The proposed CES scheduling algorithm determines optimal hours for charging and discharging based on the day ahead LMP and modifies the schedule with real-time LMP continually.

Since the real-time Local marginal Price (LMP) is not known in advance, the utility may use the day-ahead LMP. It may use its own LMP forecast too. The other novelty of this dissertation is analyzing the impact of day ahead LMP and real-time LMP differences on attainable profit from the CES operation.

The distribution network load forecast is the other primary driver of the economic optimization. Load forecasting estimates the load profile for each distribution transformer for the next 24 hours. The distribution transformer loading is necessary for each battery's day ahead schedule.

***Q.2.5**. How can the detailed three-phase distribution network model in this dissertation improve the simulation and analysis results in comparison to previous studies?*

Most papers related to distribution use single line model for distribution networks [60]. However, they ignore three phase phenomena like loading and balancing. A large group of previous studies use lumped load models for simplification purposes or they apply Norton equivalent model for the distribution network [61, 62].

This dissertation applies a detailed, multi-phase model of the distribution network that considers all circuit components, including distribution transformers and secondary distribution. The detailed network model is needed to schedule community energy storage (CES) units based on the customer loads and the distribution transformers connected to each CES unit. This detailed model provides more realistic analysis results than previous studies.

2.1.3. Impact of Interactive Harmonics from Multiple Distributed Energy Resources on Distribution Networks

Q.3.1. *What are the impacts of multiple inverter-based distributed energy resources like PV and community energy storage systems on harmonic distortion in distribution networks?*

The harmonics related to DER and CES inverters raise concerns for power system engineers and operators. The harmonics generated by inverter interfaced devices and Plug-in Electric Vehicles (PEV) can cause distortion in power system voltages and currents. In addition to the power quality issues, harmonics can have economic impacts on distribution networks. Harmonics can decrease efficiency, create thermal losses and may overload network components. These effects cause premature aging and failure in power system devices. The harmonic impact study for a single harmonic source is a well-researched topic. Harmonic measurement and filtering are discussed in plenty of literatures. However, conventional researches mostly consider harmonics as a local phenomenon with local effects [63, 64].

This dissertation investigates harmonic propagation and interactions of multiple harmonic sources in the distribution network as compared with many literatures that investigate harmonics locally and at the device-level.

Q.3.2. *What are the challenges of common harmonic measurement indices?*

In terms of harmonic distortion quantization, the Total Harmonic Distortion (THD) is the most common index in standards and literature [65, 66], but THD is based only on the magnitude of the distorted waveforms.

In this dissertation a new index is proposed that considers phase angles and in some instances to be discussed provides more insight into harmonics.

Q.3.3. *Are new indices for harmonic distortion that involve interacting harmonic sources needed?*

In this dissertation a new index is introduced that is called the Index of Phasor Harmonics (IPH). IPH incorporates both magnitude and phase angle information in evaluating distorted waveforms resulting from the interaction of multiple harmonic sources. The advantages of IPH as compared to common harmonic indices (THDV and THDI) are illustrated.

Q.3.4. *How do harmonics generated from multiple harmonic sources interact?*

There are few papers that demonstrate harmonics produced by DER sources like PV and energy storage devices [67-69]. Even fewer papers study harmonic effects on large scale distribution networks [60, 62, 70]. However, the interactive effect of harmonics produced by multiple DER sources on each other and their aggregated effect on the distribution system are not addressed in previous literatures.

In this dissertation, the aim is simulating and analyzing multiple harmonic source interactions. As harmonics from different harmonic sources propagate and interact, the interactions can result in harmonics being reduced or increased. This dissertation seeks to provide further insight into such interactions which are not addressed in previous literature.

Q.3.5. *How can phase balance affect the harmonic distortion in distribution networks?*

Published studies on phase balance and harmonics have focused on particular devices, such as transformers, or inverters [71, 72]. The other novelty of this dissertation is due to the consideration of the impact of phase balance on harmonic propagation thoughout the distribution network itself.

Q.3.6. *How does distribution network topology impact the harmonic propagation?*

Even less literature demonstrate the impact of harmonic propagation in distribution networks. Authors in [61] proposed a method to find harmonic source locations in distribution networks. However, the authors use the Norton equivalent model for the distribution network. [73] analyzes harmonic distortion in different distribution transformer types. [74] conducts the sensitivity analysis to find vulnerable buses in distribution networks for placing harmonic filters, but the authors use the Thevenin equivalent model at each bus instead of the topological model of the circuit. [60, 62] show the impact of aggregated

harmonics from Distributed Generation units in distribution networks; however, they use single-phase equivalent line models and do not consider three phase line models.

The proposed approach in this dissertation benefits from the detailed distribution network model. This detail of distribution system modeling is not addressed in previous harmonic analysis literature. This dissertation seeks to more precisely investigate the impact of distribution network topology and conductor phase couplings on harmonic propagation.

This detailed circuit model used in the work here provides for more realistic harmonic propagation simulations. Multiphase and unbalanced load models help to demonstrate realistic harmonic propagation in distribution networks.

Chapter 3 : Modeling and Simulation of Flywheel Energy Systems for Critical Microgrid Facilities

3.1. Introduction

Flywheel energy storage (FES) devices are appearing as viable alternatives to other types of battery storage technologies for securing critical loads during momentary power interruptions. Flywheel refers to a rotating mass that stores energy in the form of kinetic energy. It can serve as a short-term backup power source when the main energy source fails. The FES has been deployed in many applications, which include – but are not limited to – space systems, telecommunications, and data centers.

This chapter discusses specifically the application of FES in a data center microgrid. Due to the proliferation of the Internet and web-based activities together with cloud computing, data centers have become a significant and growing power consumer. Data centers cannot tolerate even a momentary interruption. Therefore, backup power is a vital part of such microgrids.

Conventionally, backup power units consist of batteries and diesel generators. Batteries handle critical loads before diesel generators startup. Batteries are mature technologies, but flywheels have better characteristics in terms of higher efficiency, compactness, footprint, and operation temperature for data center applications [75].

This chapter focuses on developing a software tool to model, analyze and simulate the use of FES units in a facility microgrid. The proposed tool includes a library of selected commercial FES systems. A user can also create any customer-defined flywheels by entering certain parameters. The tool is developed in the MATLAB/SIMULINK® environment with a user friendly Graphical User Interface (GUI). MATLAB/SIMULINK® is a powerful simulation environment that has the ability to model and simulate different power systems. Therefore, the developed FES model can be integrated into different microgrid architectures. It is expected that the proposed software tool can compensate for the lack of real data of FES through modeling and simulation.

Section 3.2 discusses review of previous work. Section 3.3 describes the competitiveness of FES as compared to traditional battery energy storage in a facility microgrid. Section 3.4 discusses mathematical formulation of FES in MATLAB/SIMULINK®. The FES simulation model is discussed in section 3.5, together with the model validation. The case study of a facility microgrid, based on a data center, is

presented in section 3.6 to demonstrate how a FES can help improve the load serving capability during an islanded operation of a microgrid.

3.2. Overview of Previous Works

Along with the rapid increase in electricity demand in data centers, many previous publications focus on topics related to their power management, which are, for example, approaches for determining demand reduction [22] or minimizing total electricity costs using selected optimization techniques and demand response [4, 23]. There are not many publications that address issues of back-up power and energy storage units in data centers. These systems are crucial for maintaining continuous operation of a data center microgrid and can provide ride-through capability for sensitive loads.

Traditionally, energy storage systems in data centers are battery-based [24]. Available literatures in this field are related to energy storage modeling and analysis for stand-alone power systems or uninterruptable power sources. Authors in [25, 26] discuss different control approaches for battery-based back-up power systems. While most of data center energy storage technologies are based on batteries, flywheels have gained more attention in recent years as they can provide ride-through capability for critical loads in a data center.

Previous works on modeling and analysis of flywheel applications is available in the literature. Some have applied flywheels to prevent voltage sag and improve power quality [31]. Authors in [32] propose a rotary uninterruptable power supply (UPS) system based on the flywheel storage unit. Authors in [33] introduce appropriate electric machines to drive flywheels. Authors in [34] present new designs for the power electronics interface of FES. There are also papers focusing on the mechanical aspects of FES [28, 29]. Existing literatures on flywheels do not provide an insight into how FES can be used to provide ride through applications in data centers.

3.3. Comparison of Flywheels and Batteries

Flywheels are emerging technology with specific characteristics that make them viable energy storage system in comparison to batteries. This section investigates the competitiveness of flywheels against batteries. Flywheels have higher efficiency. They can cause overall energy cost reduction in data centers [75]. Flywheels have higher life cycle with little decrease in efficiency [76]. Flywheel has fewer footprints and generates less heat than batteries. Also, flywheels operate in ambient temperature. These factors can result in the tremendous less cooling system requirements. Furthermore, battery rooms need separate ventilation system for toxic gases evacuation [77].

Above all, batteries are susceptible to undetectable internal failures, even with regular maintenance [77]. Such these unnoticeable failures are the reason for 20% of battery based energy storage failures in data centers. The research on flywheel and battery systems' operation indicates that the failure possibility of lead-acid battery is seven times more than that of the flywheel [78]. From environmental point of view, creation, maintenance and disposing of batteries have dramatic effects on natural environment. Flywheel is a large step toward green data centers [27].

Although flywheels have many advantages over traditional battery systems, there are some challenges for deployment of flywheels in facility microgrids. Firstly, flywheels can only serve loads for a short period of time, i.e. in tens of seconds. They should therefore be used in conjunction with other types of power generation to serve the loads for longer period of time. Secondly, flywheels involve a more complex installation because they are new on the technology horizon. Furthermore, there are no established standards for operation, safety regulations for flywheels. The lack of historical operational data is also another challenge for flywheel performance analysis.

To economically compare batteries and flywheels, life cycle cost analysis, including both capital and maintenance costs, should be used. This is to account for the fact that the life of flywheels is estimated at 20 years [79], whereas that of batteries is estimated at three to five years. Therefore, batteries will need to be replaced every three to five years. The internal stand-by power consumption is 0.01 % of capacity for battery and it is 1% of capacity for flywheel [80]. Based on the operational cost analysis by California Energy Commission presented in [81] -- for a lead acid battery and a flywheel that have the same capacity of 250 kW (note that the battery system has 15-minutes backup time, while the flywheel can serve loads for 20 seconds at its rated capacity) -- although the initial capital cost of the flywheel is more that of the battery of equivalent size, the 20-year life cycle cost calculation shows that flywheels have less cumulative ownership cost than batteries after three to four years.

3.4. Short-Term vs. Long-Term Energy Storage Systems for a Data Center Microgrid

To provide power for continuous operation during a utility outage, data centers typically deploy diesel generators coupled with a battery UPS system. Critical loads (IT and some lighting loads) are connected to the battery UPS, and backed up with diesel generators. At the moment of outage, UPS will handle the transient and momentary interruption until the diesel generator output achieves proper voltage and frequency. The recommended ride-through time for a battery UPS system is 15 minutes. Alternatively, a backup power system can be designed with less ride-through time using a more reliable storage

technology, like flywheels, in combination with back-up generators [82]. A flywheel unit can typically serve connected loads at its rating for 10-20 seconds depending on its specifications. This is enough time for a diesel generator to startup.

This section focuses on the idea that 15 seconds energy storage is enough for data center applications. In fact, the 15-minute ride-through time of batteries is superfluous for the following reasons: Firstly, 1 minute was assumed for a "soft shutdown" of protected computer loads. However, for a data center a "soft shutdown" is intolerable [78]. Secondly, it is not logical to perform a "second crank" on a standby diesel generator after waiting 15 minutes. In the rare case that the engine does not start during the first 5-6 seconds, it is unlikely it will start in the next 15 minutes [82]. Finally, the 15-minute ride-through time has a destructive impact on the thermal runaway in the servers. After outage, IT loads have the highest priority to serve with batteries. Therefore, cooling system shutdowns and it cause dramatically temperature increase in servers. The research on data centers [78] shows that in a reliable designed backup power system, diesel generators should start within 5-6 seconds after outage to avoid thermal runaway in servers. Therefore, backup generators starts in case of any failure and emergency without considering the type of energy storage system. The 15-second flywheel operation time should provide sufficient starting up time for diesel generators.

3.5. Mathematical Formulation of Flywheel Energy Storage (FES)

The FES consists of a flywheel and a machine that acts both as a motor and a generator. During normal operation, the flywheel system converts electrical energy from the grid to kinetic energy using the motor. The kinetic energy is stored in the spinning flywheel. During outages or emergencies, the stored kinetic energy is converted back into the electrical energy by the generator. This energy is then transferred to the connected electrical loads. Table 3.1 shows the nomenclature for the presented formulations.

Table 3-1 Flywheel formulation nomenclature

E	: Energy of flywheel (kW-sec)
E_{stored}	: Stored energy in flywheel (kW-sec)
P	: Power of flywheel (kW)
m	: Rotating mass (kg)
v	: Linear speed (m/sec)
ω	: Angular speed (rad/sec)
ω_{max}	: Maximum angular speed (rad/sec)
r	: Radius of flywheel(m)
J	: Polar moment of inertia (kg.m^2)
ρ	: Density of rotating mass (kg/ m^2)

l	: Length of flywheel (m)
K_0	: Torque conversion factor
η_{fw}	: Efficiency of flywheel

In this chapter, the flywheel model is developed based on the mathematical equations for kinetic energy in a rotating mass. Two components affect the flywheel performance: the polar moment of inertia and the rotational speed [83, 84]. (3-1) represents the kinetic energy formula. This is the equation to calculate the stored energy in a body of mass m moving in a straight line with the velocity v [83]:

$$E = \frac{1}{2} m \cdot v^2 \tag{3-1}$$

The above formula implies that a body of mass m can store more energy within a higher velocity. A flywheel is a rotating mass; therefore, (1) can be rewritten based on the angular speed ω, as shown in (3-2). The flywheel radius is r:

$$E = \frac{1}{2} m \cdot (r \cdot \omega)^2 \tag{3-2}$$

The other important factor used to model the flywheel energy storage is the polar moment of inertia *J*. It has the unit of mass multiplied by the radius squared. For the straight solid cylinder with radius *r*, the polar moment of inertia is [84]:

$$J = \int r^2 \cdot dm = m \cdot r^2 \tag{3-3}$$

Flywheel mass *m* with density ρ and length *l* can be represented as:

$$m = \pi \cdot \rho \cdot l \cdot r^2 \tag{3-4}$$

Substituting (3-4) into (3-3), polar moment of inertia can be represented as (3-5).

$$J = \pi \cdot \rho \cdot l \cdot r^4 \tag{3-5}$$

Considering (3-2), (3-4), and (3-5) the stored kinetic energy in a flywheel can be achieved from (3-6), where *J* is the polar moment of inertia and ω_{max} is the maximum angular speed of flywheel.

$$E_{stored} = \frac{1}{2} \cdot J \cdot \omega_{max}^2 \tag{3-6}$$

ω_{max} depends on the material characteristics of the flywheel and is available from flywheels datasheets. For design purposes, ω_{max} can be calculated from (3-7). In (3-7), σ is tensile strength; ρ is the density of flywheel rotor material; s is safety margin for flywheel healthy operation which is also available from manufacturers' datasheets [85].

$$\omega_{max} = s \cdot \frac{1}{r} \cdot \sqrt{\frac{\sigma}{\rho}} \tag{3-7}$$

Equation (3-8) shows that the angular speed during a discharge period yields to a piecewise-defined function[34]. Flywheel discharging has two regions: the constant speed and exponential reduction speed.

$$\omega(t) = \begin{cases} \omega_{max} & t \le T \\ \omega_{max} \cdot e^{-\frac{K_0}{J} \cdot t} & t \ge T \end{cases} \tag{3-8}$$

K_0 is the torque conversion factor from mechanical to electrical energy. T is the time duration of flywheel rotation in the ω_{max} speed. For commercial flywheels, T is available in datasheets. To find T in design cases, the engineering rule of thumb is applied in (3-9) [86]. The P_{max} is the maximum nominal power of the flywheel.

$$T = \frac{J \cdot \omega_{max}^{\ 2}}{2 \cdot P_{max}} \cdot \tag{3-9}$$

The flywheel discharging characteristic is explained with the (3-10) and (3-11) [34]. Replacing ω in (3-6) with $\omega(t)$ from (3-8) leads to (3-10):

$$E = \frac{1}{2} \cdot J \cdot \omega(t)^2 \tag{3-10}$$

The power of flywheel at exponential region is the derivative of energy in (3-9) with respect to the time:

$$P = \begin{cases} P_{max} & t \le T \\ \eta_{fw} \cdot \omega_{max}^2 \cdot e^{-\frac{2K_0}{J} \cdot t} & t \ge T \end{cases} \tag{3-11}$$

The η_{fw} is efficiency of flywheel. This factor takes into account the required energy in order to keep the flywheel spinning, or the flywheel standby loss. The full load standby loss of a flywheel is from 0.2% to 2% of the total capacity depending on manufacturers [87]. Flywheel UPS consists of the flywheel and the power electronics components. According to the literature and the manufacturers' data sheets, flywheel UPS efficiency is in the range of 95% to 98% [88].

3.6. FES Modeling and Simulation Tool

3.6.1. Overview of the FES Simulation Tool

The (3-10) and (3-`11) are the basis for the proposed flywheel modeling and simulation tool. The tool is developed in the MATLAB/SIMULINK® environment with a user friendly GUI. Several commercially available flywheels have been modeled as a part of the proposed FES simulation tool. Users have two choices for FES simulation, either to use commercial FES models in the developed flywheel library or to customize their own FES.

Figure 3-1 illustrates the generic block diagram of the FES model developed in MATLAB/SIMULINK®. As shown, the FES model is composed of two subsystems, namely the flywheel subsystem and the generator/motor subsystem. Inputs to the FES simulation tool are: voltage and current measurements at the load bus which are the signal to control flywheel power output. For a customized flywheel model, additional flywheel characteristics are required as user-defined inputs, including flywheel maximum and minimum rotating speeds (rad/sec), power capacity (kW), energy capacity (kW*sec), efficiency, charging duration, discharge duration at maximum power (sec), and discharge duration at half of maximum power (sec). Outputs of this model are the flywheel power output (kW), energy output (kW-sec) and rotating speed (rad/sec).

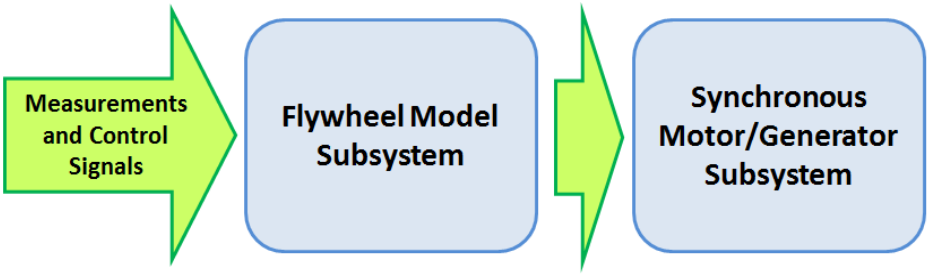

Figure 3-1 Generic block diagram of the proposed FES model in MATLAB/SIMULINK® .

3.6.2. The Flywheel Subsystem

The typical discharge time of a flywheel ranges from 10 to 30 seconds [88-90]. Flywheel charging from the totally discharged point to the totally charged point needs 1 to 10 minutes, depending on FES technologies and manufacturer designs [90, 91].

The control of FES is based on the balance of power supply and demand. If the available power is more than the load, flywheel starts charging to absorb the excess power. During a utility disturbance or lack of power, the flywheel is discharged to handle critical loads. Then, after diesel generators start and the system voltage and frequency are stabilized (ramp-in time), flywheels are recharged from the diesel generators. Figure 3-2 depicts flywheel charging and discharging cycles.

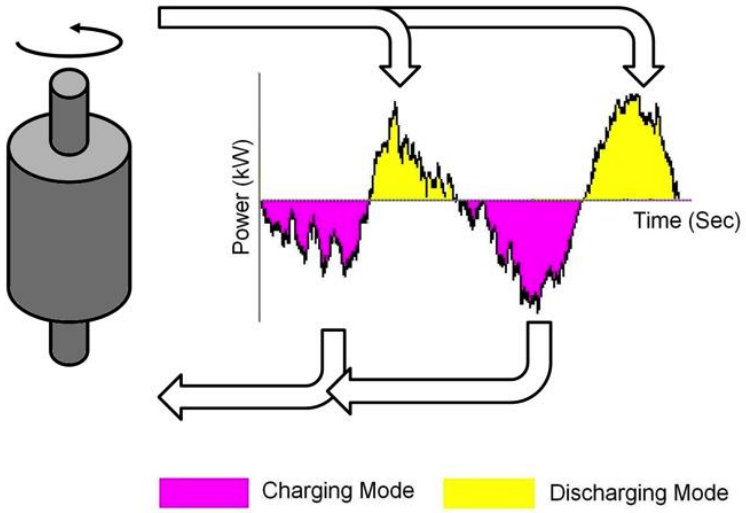

Figure 3-2 Flywheel control signal for charging and discharging modes.

The flywheel subsystem consists of the discharge and charge sections. The exponential function shown in (3-11) is the basis for the calculating the charging and discharging power. Figure 3-3 and Figure 3-4 represent the implementation of power discharging and charging functions, respectively, in the MATLAB/SIMULINK® environment.

The discharging section consists of the mathematical function in (3-11) and a switch that is controlled by the external signal from the load bus. The discharging of FES is activated when the voltage and current measurements on the load bus indicate shortage of power.

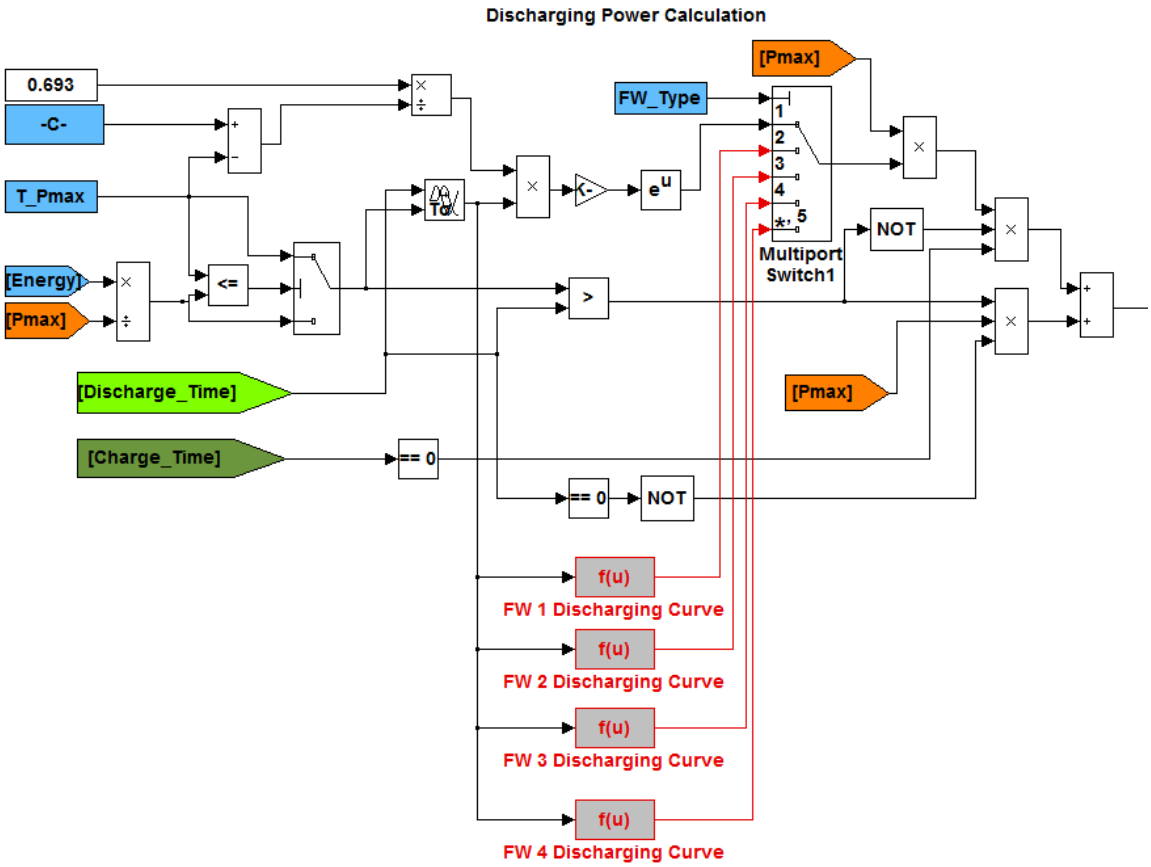

Figure 3-3 Discharging section of the flywheel model.

The charging power calculation is presented in Figure 3-4. This part of the model consists of the mathematical function (3-11) and a switch that is controlled by the signal from the load bus. The charging of FES is activated when the voltage and current measurements on the load bus indicate excess power.

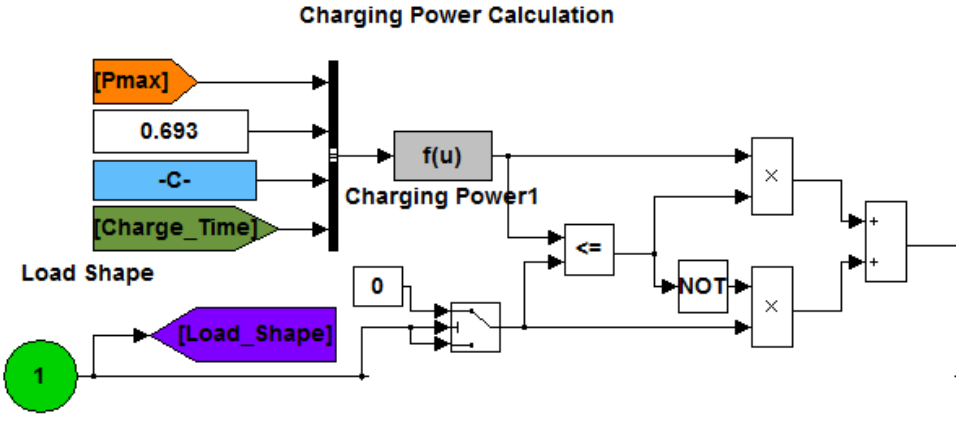

Figure 3-4 Charging section of the flywheel model.

The flywheel rotational speed can be calculated based on (3-6), which is shown in (3-12).

$$\omega = \sqrt{\frac{2E}{J}} \qquad (3-12)$$

On the right hand side of (3-12), the flywheel energy E can be determined from the output of the developed FES model. The polar moment of inertia J can be calculated using (3-5) based on the manufacturer supplied information.

3.6.3. Motor Generator Subsystem

Different types of electric machines can be used in an FES. The most common types are induction machines, and permanent magnet synchronous machines (PMSM) [92]. They have higher torque to current ratio and higher power density than other machines [93]. In this chapter PMSM is used for the FES model. The standard PMSM model provided in the MATLAB/SIMULINK® library is used with some modifications. The model of diesel engine is presented in Figure 3-5.

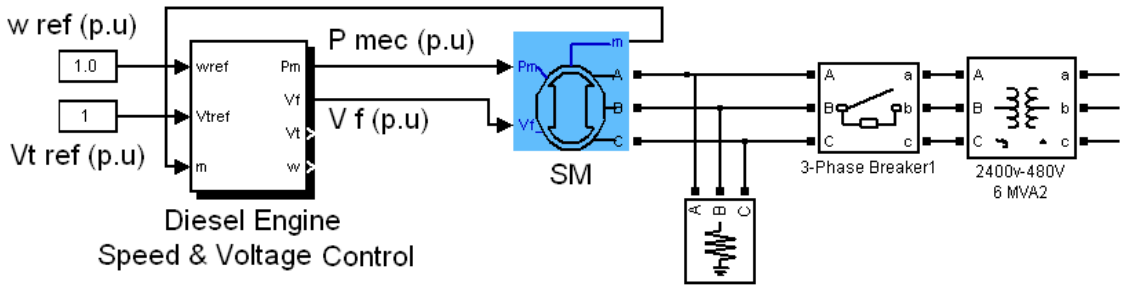

Figure 3-5 MATLAB/SIMULINK® model of a synchronous motor/generator unit.

3.6.4. FES Simulation Results and Model Validation

To validate the proposed FES model, authors have developed four flywheel models of different sizes, following the specifications of four commercial flywheels available from different manufacturers: (i) a 120kW flywheel unit, (ii) a 150kW flywheel unit, (iii) a 160kW flywheel unit, and (vi) a 250kW flywheel unit.

The model outputs are compared with the manufacturers' data as presented in Figure 3-6. The dashed lines are the manufacturers' data, while the solid lines are the simulation results. Figure 3-6 indicates that simulation results are consistent with the flywheel's experimental data from the manufacturers. These four flywheel units are built-in into the flywheel library as mentioned earlier. Based on (3-11), flywheel

discharging has two operation regions. In the first region, output power is constant. In the second region, output power has exponential decreasing trend.

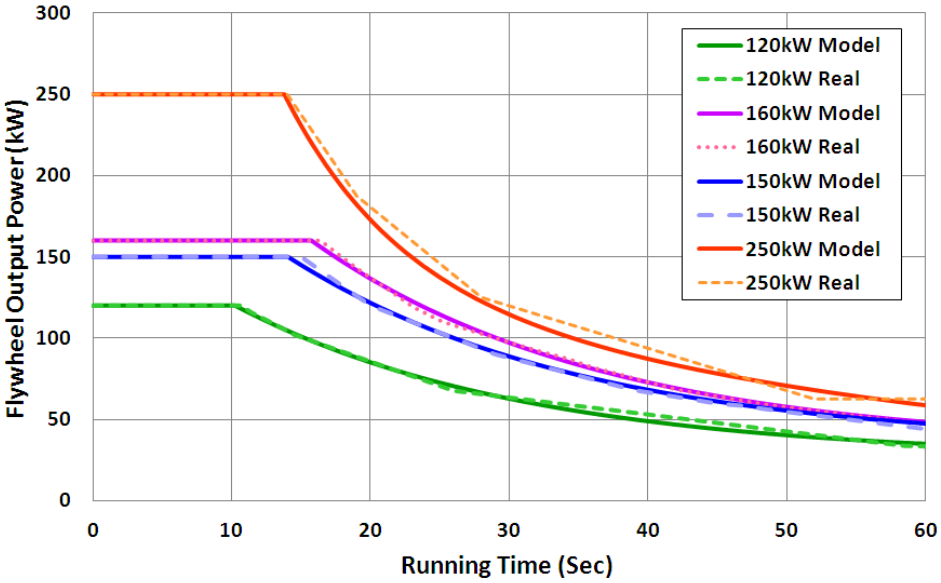

Figure 3-6 Flywheel discharging characteristics for four different flywheel units.

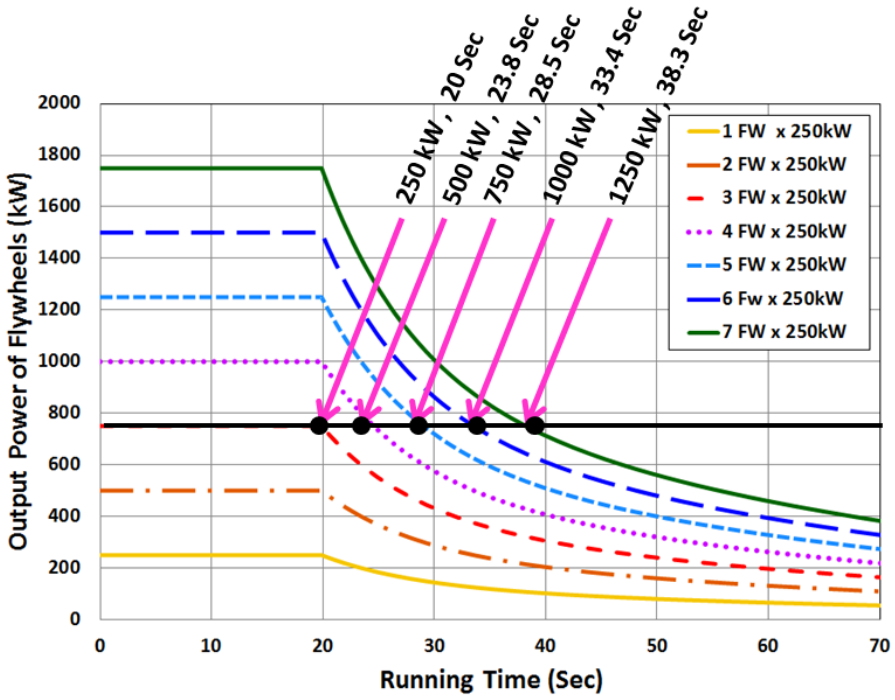

Figure 3-7 Different running times for different numbers of 250 kW flywheel units connected in parallel.

Each flywheel unit has a specific running time. If there is a need for a longer running time, more flywheel units can be paralleled. The design tool developed and presented in this chapter also helps the user to find a sufficient number of flywheels for a specific running time. The tool can demonstrate the output of multiple flywheel units connected in parallel. It calculates the running time for each case. Figure 3-7 illustrates how additional flywheels in parallel can meet the load for a longer time. In this case, to achieve 750 kW power for 20 seconds, at least three 250 kW flywheels should be paralleled. Four 250 kW flywheels can serve the 750 kW load for 33.4 seconds.

3.7. The Case Study

The developed FES model is coupled with a diesel generator in the case study of a data center, as described below. This case study aims at demonstrating the impact of flywheel on the load serving capability and frequency of a data center power system during a utility disturbance.

3.7.1. The System Specification

To analyze the impact of a flywheel operated in parallel with a diesel generator to provide backup power for data center loads, a realistic set of specifications from a data center in Virginia is taken into account. Table 3-2 presents electrical specifications of the case study [94].

Since the power system configuration of any data center is confidential, the N+1 power system architecture, available in the IEEE 493-2007 standard [95], is used to allow modeling and simulation of the FES in a data center presented in this study. See Figure 3-8. In this system, the primary system voltage is 34.5 kV, and the secondary voltage is 480 Volts.

Table 3-2 Specifications of A Data Center

PEAK LOAD	1.55 MW
BACKUP SYSTEM	• Flywheel UPS
COOLING SYSTEM	• Evaporative chilled water system
POWER	• Secured from two substations • Northern Virginia Electric Cooperative (NOVEC) supplies power
ELECTRICAL INFRASTRUCTURE	• N+1 system • 2x2.1 MW diesel generators • Primary voltage: 34.5 kV • Secondary voltage: 480 V • Multiple power and cooling paths • 120 hours diesel fuel storage at full load

As shown in Figure 3-8, there are two parallel diesel generators that connect to the generator switchboard to provide backup power for a data center. One of the two generators operates in emergency conditions (N_{gen}+1, N_{gen}=1). The other generator serves as a backup. There are four parallel flywheel systems and at any given time. Three of them are connected to sensitive loads (N_{FW}+1, N_{FW}=3) and one is an extra unit; therefore it has the N+1 architecture. "G" represents diesel generator, "ATS" represents automatic transfer switch and "PDU" is power distribution unit.

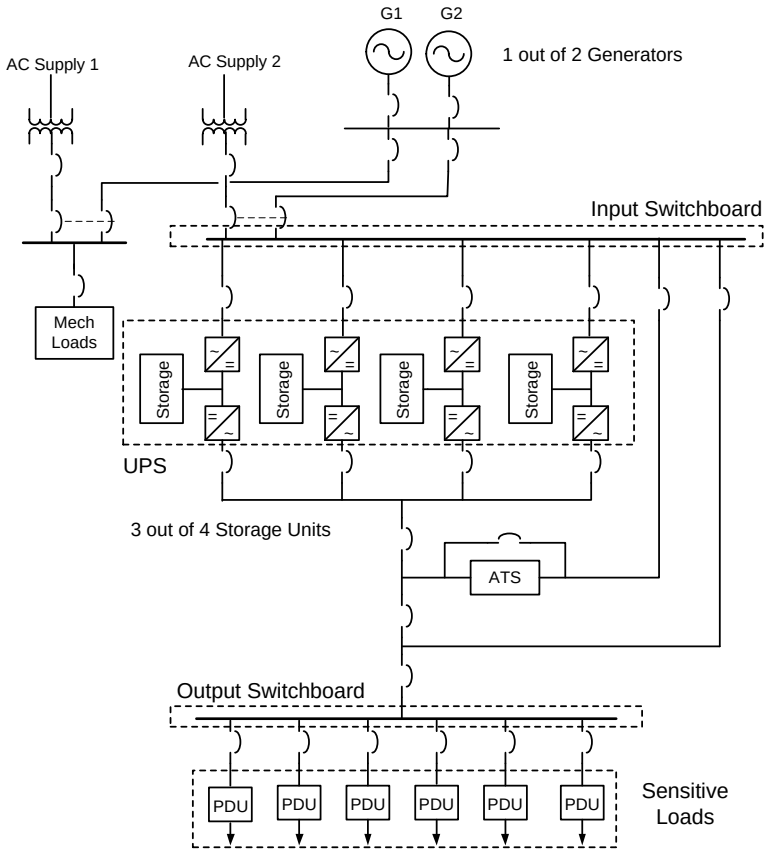

Figure 3-8 (N+1) backup power architecture for a data center in accordance to the IEEE 493-2007 [95].

3.7.2. Scenario Description

Of all data center loads, the HVAC loads - which constitute about 50% of the total load - can be interrupted momentarily. On the other hand, all IT and computing hardware, such as computers, servers, routers, storage devices, telecom devices and some lighting loads, need uninterruptible power supply. These critical loads constitute approximately the other 50% of the total data center loads. Therefore, the size of flywheels should be designed accordingly to cover all critical loads in the data center, which is 750kW (three out of four 250 kW units operating at the same time) during back-up generator startup in the test case being studied.

During a disturbance, the FES systems operate to support critical loads. If the outage lasts for more than five seconds, the diesel generator will start and take over all data center loads. This time is typically 10 seconds [96] [97]. After the electricity is restored, the diesel generator should be operated for extra 5 to 15 minutes. This extra operation time helps the generator to have the "cool-down period" before shutting down [96]. The cool-down period is vital for the diesel generator life cycle. Additionally, the flywheel will be charged by the generator during this time, if needed.

3.8. Simulation Results

Figure 3-9 illustrates the simulation results, showing the operation of the flywheels and the diesel generator when a utility outage occurs at t=0 sec. The solid line is the total load of the system (kW) and the dashed line is the diesel generator power output (kW). At the time of the power outage (t=0), flywheels operate to provide ride-through capability for the critical loads (750kW). Since the outage is longer than 5 seconds, the diesel generator starts (t=5 sec). After the diesel generator has synchronized with the system (t=17 sec), the rest of the data center loads are served, and the flywheel changes from its discharging mode to its charging mode.

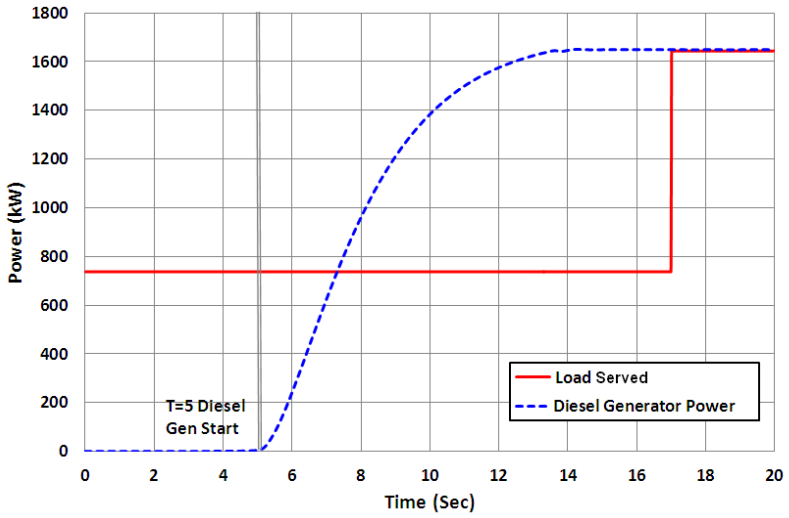

Figure 3-9 Snapshot of electrical power (kW) at the load bus after the outage.

At this time, the load served (the solid line) is the total data center load plus the flywheel charging. The generator output (dashed line) matches both the data center load and the flywheel charging load. Once the flywheel is fully charged (t > 190 sec – not shown), the diesel generator output will decrease to the total data center load level.

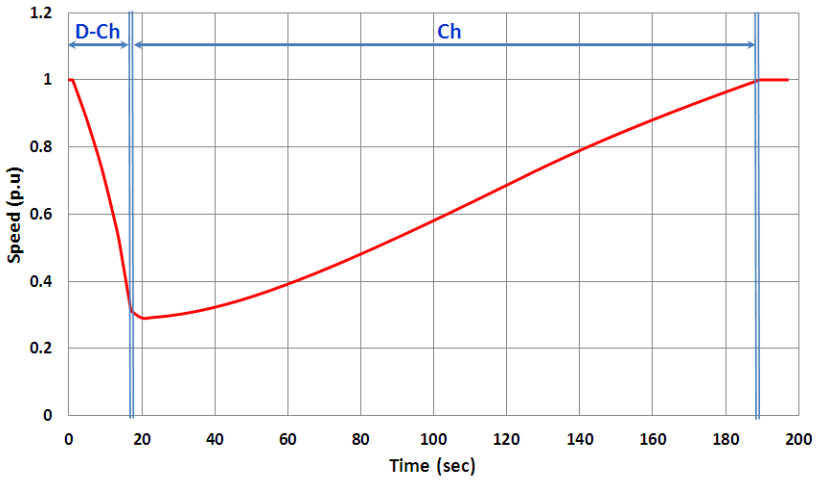

Figure 3-10 Flywheel speed during charging and discharging periods: D-Ch and Ch indicate flywheel discharging and charging periods, respectively.

Figure 3-10 shows the flywheel speed during its operation. During the first 5 seconds, the flywheels discharge to serve the critical loads and the flywheels' speed decreases. The system waits for 5 seconds to confirm that it is the real power outage before starting the diesel generator. Once the generator starts at t=5 sec, it takes some time – as shown in the simulation results – before it can fully synchronize with the system and serve the loads at t=17 sec. After picking up the loads, the generator charges the flywheels until t=190 sec. The flywheels charging time is in accordance with the charging range, 2-3 minutes, indicated by the flywheel manufacturer [36]. During the charge period, the flywheels speed increases, as indicated in Figure 3-10.

In addition to providing continuous power supply, flywheels also stabilize the frequency at the load bus. Figure 3-11 presents frequency deviation at the load bus during the simulation. The solid line represents frequency response of the system with flywheels. The dashed line shows frequency response of the diesel generator after it starts at t=5 sec. Note that the frequency is stabilized at around t=16 sec before the diesel generator synchronizes with the system at t=17 sec.

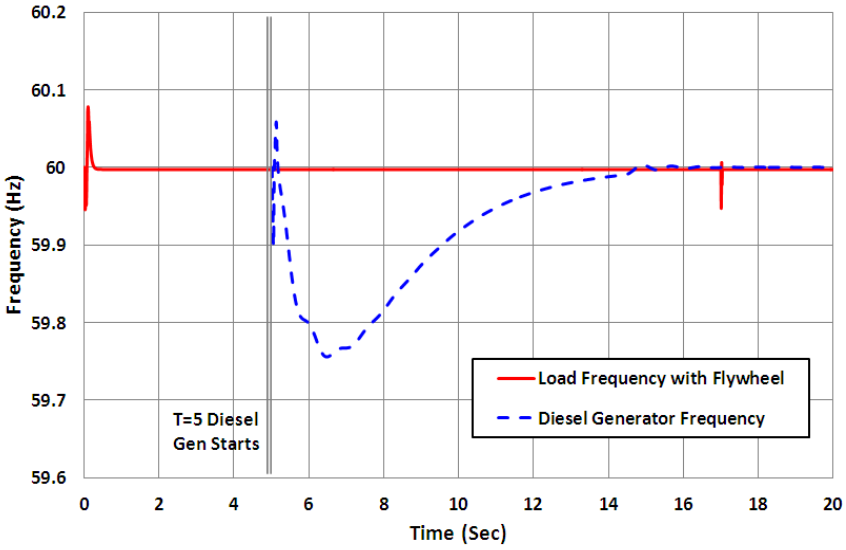

Figure 3-11 The frequency deviations after the power outage with flywheels (solid) and without flywheels (dashed).

Figure 3-11 indicates that flywheels can significantly decrease the system frequency deviation. During its startup (t=5-17 sec), the generator frequency goes down as low as 59.75 Hz. This results in the system frequency deviation of 0.25 Hz from the nominal frequency of 60Hz. With the flywheels, the maximum frequency deviation decreases to 0.06 Hz. This deviation meets the maximum allowable frequency deviation for sensitive loads of 0.12 Hz or 0.2% of the normal frequency [95].

3.9. Chapter Conclusions

This chapter presented a tool for modeling and simulation of a flywheel energy storage (FES) system in a microgrid environment. The FES model was validated by comparing simulation results with manufacturer supplied data. To demonstrate the use of the developed FES model, a case study of a facility microgrid based on a data center application was presented. This study showed the operation of the FES coupled with a diesel generator to serve the data center's critical loads during a utility outage. Results indicated that the FES, coupled with the generator, can deliver secure and resilient power to support critical loads during a utility outage. Since FES applications to provide power security and resiliency for a mission-critical facility are new on the horizon, there is a lack of experimental data for use in microgrid studies. The proposed software tool bridges this gap by enabling facility engineers and system designers to run several what-if analysis scenarios -- that is, to analyze the operation of a facility microgrid with the incorporation of a FES system coupled with traditional fuel-based generators as a backup power source.

Chapter 4 Economic control and optimization of Community Energy Storage (CES) systems in competitive electricity markets

4.1. Introduction

Distributed energy storage devices may improve reliability by providing standby power when equipment outages would otherwise force customer interruptions. Additionally, energy storage devices can reduce equipment loading during peak hours, thereby allowing the utility to delay equipment upgrades and to decrease pre-mature aging in network components [39]. They can also help with renewable energy resource integration into distribution networks. Volt-Var control, frequency regulation, and demand response program support are among other benefits of distributed energy systems for utilities [44-46]. These benefits are so great that they sometimes outweigh the high cost of installing the energy storage devices and the communication infrastructure to support them [44].

This chapter presents a means of realizing additional benefits for utilities by taking advantage of the fluctuating costs of energy in competitive energy markets. By combining electricity market information with real-time control of energy storage devices, utilities may enjoy year-round economic benefits from the storage devices in addition to the occasional benefits mentioned above.

The increasing adoption of intermittent renewable energy resources (DER) into the power grid and technologic merit for batteries in recent years brings more attention to energy storage systems (ESS) as viable solutions [45, 58, 59]. In [58] authors used a fuzzy clustering optimization approach while considering system security constraints to maximize the renewable energy utilization integrated with a pumped storage unit. Authors in [59] explored sodium–sulfur battery application ancillary services in an electricity market. Reference [45] provides a general overview to load leveling with solar power generation and storage under a Time of Use (TOU) price scheme. However, the electricity market and the effect of time varying loads were not considered.

Many researchers have focused on large scale energy storage applications [48], but fewer have attempted to realize year-round benefits from distributed energy storage systems. The authors of [49-51] looked at the problem from the perspective of controlling customer-owned storage devices that integrate other generation sources. Authors in [52] focused on the voltage fluctuation issue due to high penetration

of photovoltaic panels in commercial buildings. The customer side ESS provided voltage regulation in exchange for subsides from utilities to cover battery costs. The authors in [53] proposed a stochastic optimal load management for a residential customer with DER and ESS. However, the proposed approach minimized the electricity cost in a real-time manner without considering the system's day ahead behavior.

Studies that are more relevant to this chapter are [54, 55]. [54] presented a load management approach for a large load aggregator to determine the electricity price for participation in the day ahead market. A lumped load was considered with grid scale energy storage, and distribution level system topology was not considered. In [55] a distributed storage system is applied to minimize the forecasting error of DER generation and to decrease the uncertainty in electricity markets. CES is addressed in the Department of Energy Smart Grid recovery act of 2009 [98].

The sizing and placement optimization problems for systems with DER and ESS have been well-researched. However, the operations of ESS in the competitive energy markets in conjunction with customer service reliability and distribution network efficiency have not been addressed. Moreover, energy storage systems placed on the secondary of distribution transformers have not been investigated thoroughly. This chapter presents a real-time control scheme that maximizes the revenue attainable by energy storage systems without sacrificing the occasional benefits related to improvements in reliability and reduction in peak feeder loading. The day ahead load forecasting and day ahead market prices are considered in the optimization algorithm presented here. In this chapter, a novel combination of trade-offs related to transformer loading, feeder loss, and LMP price prediction is considered that is not addressed in other literatures.

The chapter is organized as follows: section 4.2 is a discussion concerning CES infrastructure. Section 4.3 describes the CES service requirements. Section 4.4 presents the control and optimization algorithm. In sections 4.5 and 4.6 case studies and simulation results are discussed.

4.2. Community Energy Storage (CES) Infrastructure

CES units may be more flexible than large substation batteries [99]. While the smaller size appropriate for secondary-level power does not take advantage of economies of scale, researchers have proposed means of reducing production costs [36, 100, 101]. Perhaps more important than cost, such placement provides the most reliable service to customers, since the primary system may be compromised, even to the point of distribution transformer failure, and the energy storage system may still serve the customer. This chapter supposes that the CES units are owned and operated by an electric

utility and thus may be aggregated for optimal operation. CES can increase capacity, efficiency and reliability of distribution circuits due to the functions illustrated in Figure 4-1.

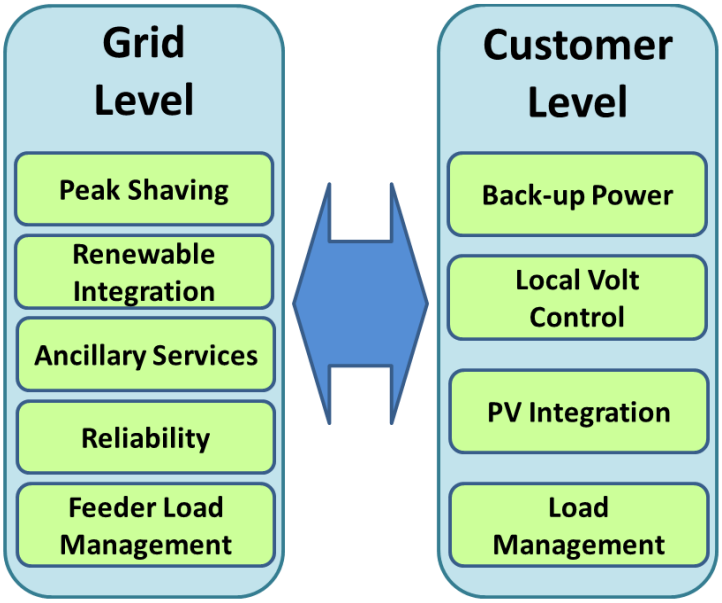

Figure 4-1 DES advantages at grid and customer levels.

There are several key factors that affect the successful deployment of CES systems. The high cost of batteries, lack of standards, and infrastructure needed for controlling DER units seem to be barriers. Some strategies can help to provide a sustainable growth for DER adoption and CES deployment. Reusing Plug-in Electric Vehicle (PEV) batteries for stationery energy storage purposes enables battery manufacturers to increase the production and decrease the price of batteries with the expanding market [101]. Other business models involving third-party ownership such as "battery leasing" and "battery as a service" may result in reduced DES prices. Moreover, standardizing the CES units can effectively keep manufacturing costs down [36].

The CES units operate under a hierarchical control system, as illustrated in Figure 4-2. Each individual unit is controlled by a local controller, called the CES Control Unit (CCU), which manages secondary voltage and serves the load when islanded. When not islanded, the CCU controls the CES to charge or discharge based on commands sent from a Group CES Control Unit (GCU) whose set point is given by a centralized Distribution Control Center (DCC) [102] or directly controlled by the DCC as part of the utility DMS.

The algorithm presented here runs in the DCC, where the LMP data, forecasted load, and operational alerts, such as storm predictions, are available. Each CCU sends local information, such as the stored

energy and transformer loading, back to the DCC by means of the GCU, so that the data may be used by the control algorithm. Due to the required infrastructure for the smart grid demonstration, it is assumed that the distribution network has appropriate communication facilities for such data harvesting and transmission.

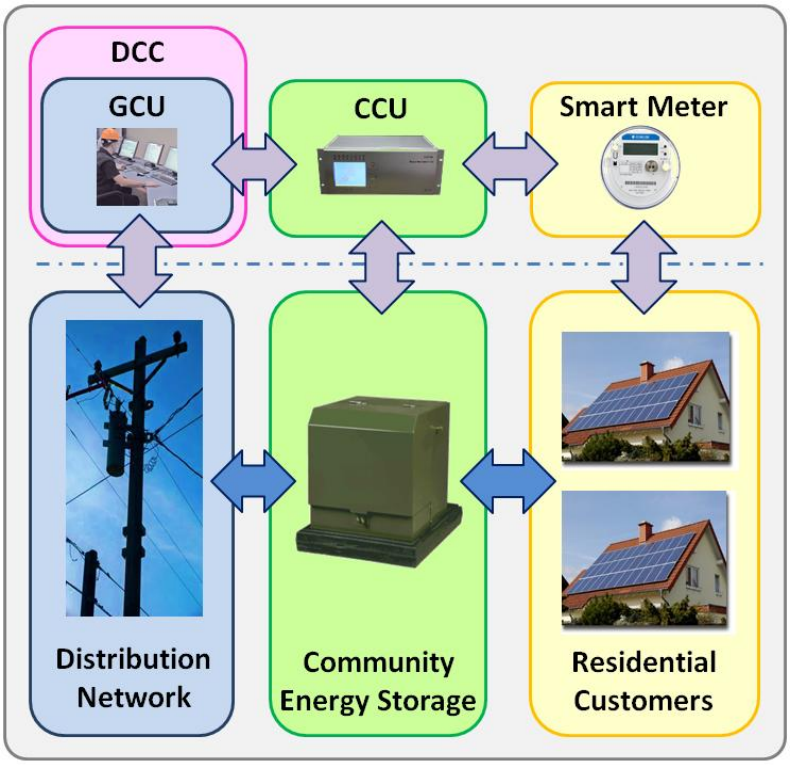

Figure 4-2 CES system control layout

4.3. CES Service Requirements

Since the CES units are located on the secondary sides of transformers, load management involves, at the secondary level, preventing transformer overloads and low voltages, and, at the feeder level, preventing primary overloads and low voltages. The secondary level constraints (particularly transformer loading) are integrated into the economic scheduling for each CES unit, while the primary level constraints are handled at the feeder level, which involves operating many CES units in a coordinated or aggregated manner. Such constraints are described in more detail in section 4.5.

The reliability benefits also take precedence over the energy cost savings. While the utility could decide to keep the CES units at maximum storage or above some fixed storage level (static reserve capacity) so as to be able to sustain the maximum possible outage durations, such lengthy outages may be extremely uncommon, thus resulting in under-utilization of the CES units. Rather than using a static

reserve capacity, the CES units can be managed with a dynamic reserve capacity, meaning that the stored energy is kept at a sufficient level to serve an outage for a given duration (HR). For example, suppose that customers on a given feeder may be restored through manual switching efforts which require two hours (HR = 2) to complete. In this case the CES unit only needs to keep enough energy to serve an outage at that transformer for two hours. During peak load conditions the full capacity of the battery may be needed to provide energy for two hours, but during light load conditions the battery may need only a small percentage of its maximum capacity. If storm information is available to the DCC, the reserve capacity may be modified in anticipation of longer restoration times. The modeling of the dynamic reserve capacity will be discussed in detail in the next section.

The load management constraints and the reserve capacity constraints may be in conflict. Preventing an overload may require violating the dynamic reserve requirement. Here it is assumed better to prevent outages at the present time than to prepare for potential future outages.

4.4. Control and optimization Algorithm

4.4.1. Energy Cost Savings

The objective of the control algorithm is to optimize energy cost savings over time. However, the reliability requirements and components capacity are forced as constraints in this optimization problem. When a CES unit charges, the utility incurs the cost of the energy entering into the unit ($R_{tCh} < \$0$), and when the CES unit discharges, the utility saves the cost of the energy supplied by the unit ($R_{tDch} > \$0$). The utility is thus accounting for the difference in energy costs in its own balance sheet as a cost savings.

In addition to the energy going into or out of the CES units, the utility may also count the change in feeder losses in its cost savings calculation. That is, when the CES unit is charging, the load has increased, and there will be greater losses in the feeder and substation due to the increased current. Similarly, when the CES unit discharges, the losses on the feeder decrease and the CES control may take "credit" for such cost savings. Combined with the cost savings due directly to the CES output energy, this net cost savings will be termed "revenue" when taken separately (R_{tCh}, R_{tDch}), and "operating profit" or "profit" when combined ($Ch/Dch\ Pair_{profit}$, Sch_{profit}).

4.4.2. Principle Drivers of CES Optimization

Since the goal is to maximize profit by taking advantage of CES stored energy in excess of the reserve energy, the two primary drivers of the optimization algorithm are the LMP prediction (cost of energy) and the load forecast (availability of energy).

In regulated electric energy markets the Locational Marginal Price (LMP) is computed in real-time based on bids from energy producers, losses and line congestion. These prices are called the real-time LMPs and represent the incremental cost to supply load to a given region at a given time [103]. In addition to the real-time LMP market, there is a day-ahead LMP market, wherein energy producers bid their expected costs one day ahead [104].

In order to determine the optimal charging and discharging schedule for the CES units, the price of energy at future hours is needed. Since the real-time LMP price is not known in advance, the utility may use either the day-ahead LMP, or, if it has a better prediction of its own costs based on generators that it operates, it may use its own LMP forecast. The simulation reported here uses the day-ahead LMP price and compares the profit with that attainable from an ideal prediction (ie, a prediction that exactly matches the LMP prices that occur over the next 24 hours).

The distribution network load forecast is the other primary driver of the economic optimization. Load forecasting helps to find how much load will be on each distribution transformer for the next 24 hours. The distribution transformer loading is necessary for each battery's day ahead schedule. The 24-hour load forecast for each transformer is based on the "load research statistics" load estimation method that is developed in [105, 106]. The real-time demand at each distribution transformer with a CES unit is metered locally and provided to the DCC for use in the optimization algorithm to refine the load forecast. Weather data may also be used to refine the load forecast [107].

4.4.3. CES Optimization Formulation

In real-time control the optimization algorithm first calculates the optimal charge/discharge schedule for each CES unit for the next 24 hours, and then issues the commands through the DCC for the first hour's optimum operation. Each CES unit is scheduled independently using the same formulation, but the constraints will be set up differently as the corresponding measurements differ. Table 4-1 shows the nomenclature for CES formulation.

Table 4-1 CES Formulation nomenclature

Sch_{profit}	: CES Scheduling profit ($)
P_t^{CESout}	: Output power of the CES in hour *t* (kW)
$P_t^{FeedLossRed}$	: Reduction in feeder losses in hour *t* (kW)
$P_t^{CESLoss}$	: CES loss function (kW)
P_{max}^{Ch}	: Maximum charge rate (kW)
P_{max}^{DCh}	: Maximum discharge rate (kW)
P_{MinPri}	: Minimum CES power for primary issues (kW)
P_{MaxPri}	: Maximum CES power for primary issues (kW)

P_{max}^{Trans}	: kVA rating of the transformer
P_{max}^{Trans}	: Load in hour *t* (kW)
ΔC_t	: Change in stored energy in hour *t* (kWh)
$\Delta C_t^{(i)}$	: Change in ΔC_t decided upon in iteration *i*
C_{max}	: Maximum CES capacity (kWh)
C_{min}	: Minimum CES capacity (kWh)
$C_{Rsv\ t}$	: CES reserve capacity at hour *t* (kWh)
SS_{Max}	: Maximum iteration step size (kW)
NT	: Number of time points
$Ch/DchPair_{profit}$	:CES Charging and Discharging pairs
a_t, b_t, c_t	: Interpolation coefficients
K_{config}	: Battery cell configuration coefficient
R_{cell}	: Battery cell internal resistance
L	: Transformer loading
R_{tCh}	: Charging Revenue (Cost) in hour *t*
R_{tDch}	: Discharging Revenue (Cost) in hour *t*
H_R	: Outage duration (Hours)

Mathematically, the objective function then has 24 independent variables—the kW outputs at each hour—and one dependent variable (the total profit). Thus, the objective function to be optimized is given in (4-1) per the definitions provided in the Nomenclature section.

$$Sch_{profit} = max \sum_{t=0}^{23} LMP_t * (P_t^{CESout} + P_t^{FeedLossRed}) \tag{4-1}$$

P_t^{CESout} stands for CES power output between the t^{th} and $^{tth-1}$ hours. The sign convention used here associates a positive P_t^{CESout} with discharging and a negative P_t^{CESout} with charging. Similarly, $P_t^{FeedLossRed}$ is negative when the losses increase.

As noted, the total feeder losses do not need to be calculated for each output; rather, only the change in feeder losses needs to be calculated accurately. Since feeder losses are quadratic for radial distribution systems, the change in losses due to any given CES unit's output are computed by interpolating a quadratic polynomial defined by three points relating CES output to feeder losses.

$$P_t^{FeedLossRed} = a_t \times (P_t^{CESout})^2 + b_t \times P_t^{CESout} + c_t \tag{4-2}$$

The coefficients a_t, b_t, and c_t are calculated in advance using power flow calculations on the feeder for three different output levels for each battery. Thus, rather than running a power flow computation on the entire feeder at every iteration in the scheduling algorithm, only three power flow runs per battery are required.

Since the CES outputs are assumed to be constant for the entire hour, the conversion of output power (kW) to stored energy (kWh) involves only the identity function. However, the CES units do not operate at perfect efficiency and the losses incurred during both charging and discharging must be considered. Equation (4-3) relates the actual CES output power to the change in stored energy ΔC_t, where the internal losses $P_t^{CESLoss}$ are a function of the CES internal resistance which is provided by battery manufacturer.

$$\left|\Delta C_t\right| = \left|P_t^{CESout} + P_t^{CESLoss}(P_t^{CESout})\right| \tag{4-3}$$

Any model may be used to compute the CES internal losses, but the algorithm may not converge to the correct solution if the loss function $P_t^{CESLoss}$ (P_t^{CESout}) is non-convex. For a simple model consisting of a constant voltage source in series with a resistor, the CES loss function becomes that in (4-4).

$$P_t^{CESLoss} = \frac{K_{config} * R_{cell}(temp)}{(V_{cell})^2} * (P_t^{CESout})^2 \tag{4-4}$$

The K_{config} is the configuration coefficient. It depends on the number of series and parallel battery cells in the CES module. V_{cell} is the battery cell output voltage. R_{cell}(temp) is the internal resistance of a single cell, and is a function of the cell temperature.

As mentioned in the CES Service Requirements, section III, the operation of the CES units includes both secondary (local) and primary (fleet) constraints. Each CES unit has responsibility first to meet the local constraints, such as preventing a distribution transformer overload, and then to serve with other CES units in a fleet to meet primary constraints, such as preventing an overload at the substation exit cable.

Even before the secondary power system constraints are imposed upon the schedule, the physical constraints of the CES units must be met, per the manufacturer's specifications. These constraints include power output (kW) constraints and stored energy (kWh) constraints.

The output power constraint in each hour is given in (4-5). The negative sign in front of P_{max}^{Ch} reflects the sign convention used here, where charging is "negative output."

$$-P_{max}^{Ch} \le P_t^{CESout} \le P_{max}^{DCh} \qquad \forall 0 \le t \le 23 \tag{4-5}$$

The CES stored energy constraints are modeled in (4-6). C_{min} and C_{max} are the minimum and maximum levels of energy that can be stored in the CES unit, per the manufacturer's operating recommendations. It prevents the battery from full drainage.

$$C_{min} \le \left|C_t\right| \le C_{max} \qquad \forall 0 \le t \le 23 \tag{4-6}$$

Once the physical CES constraints have been computed, the power system primary and secondary constraints must be computed. The local loading measurements and load forecast are first used to set bounds on the CES unit outputs so as to prevent transformer overloads. These constraints take the form shown in (4-7).

$$\left|P_t^{Load} - P_t^{CESout}\right| \le P_{max}^{Trans} \tag{4-7}$$

P_{max}^{Trans} may be set equal to the kVA rating of the transformer. Although the reactive component of the load will add to the total kVA loading on the transformer, the CES unit may supply power to the system through an inverter, and that inverter may supply VARs up to a certain limit. Since transformer ratings are not firm ratings (a transformer may be slightly overloaded with minimal impact on reliability and transformer life), this approximation was deemed appropriate.

Together with the availability of stored energy in the CES unit, the transformer loading constraint is used to calculate the CES availability for primary-level control. Power flow analysis is then used to check for primary-level overloads and low voltages. If such primary-level problems exist, the CES fleet will be used to attempt to alleviate those problems. These changes create additional constraints, as described in (4-8), to be placed upon the economic optimization.

$$P_{MinPri} \le P_t^{CESout} \le P_{MaxPri} \; \forall 0 \le t \le 23 \tag{4-8}$$

While the formulation of this algorithm focuses on individual CES units independent of other CES units, additional CES units may greatly affect the participation each unit plays in resolving primary-level constraints. Each CES schedule is different because each transformer has a different loading pattern.

Figure 4-3 depicts how these constraints are implemented. While the formulation of this algorithm focuses on individual CES units independent of other CES units, additional CES units may greatly affect the participation each unit plays in resolving primary-level constraints. Each CES schedule is different because each transformer has a different loading pattern as before.

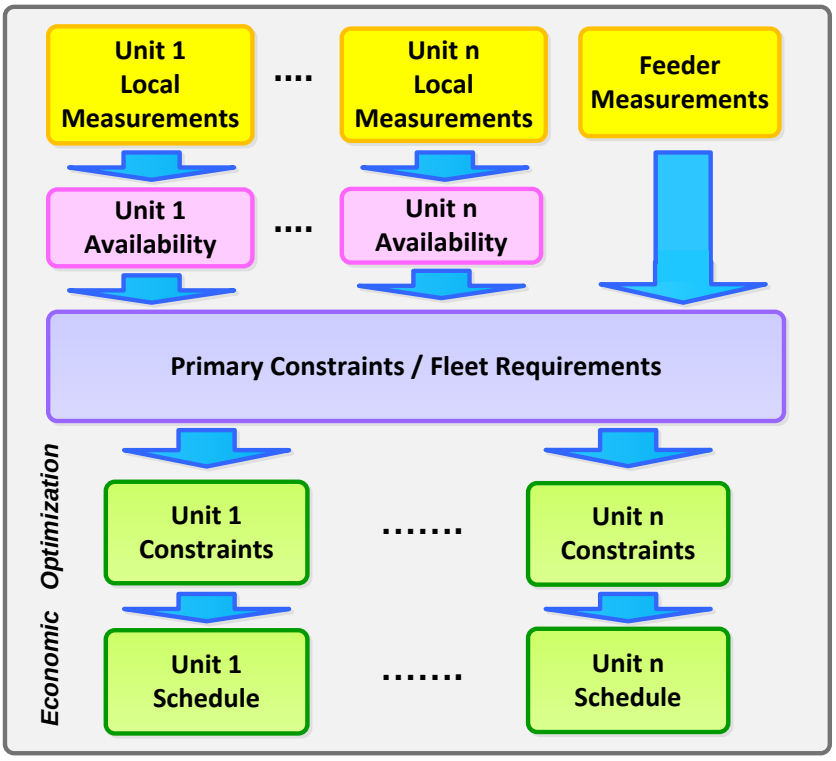

Figure 4-3 Primary and secondary constraint handling.

As mentioned in section III, the reserve capacity may be either static or dynamic. If static, the user specifies $C_{Rsv\,t0}$ directly. If dynamic, then the reserve capacity may be calculated by

$$C_{Rsv\,t_0} = \int_{t_0}^{t_0+H_R} Ld(t)dt \tag{4-9}$$

where the loading on the transformer Ld(t) is based on typical customer load curves [16-17] modified based on recent measurements and available load forecast information at that location.

Recall that each CES unit is placed at a different transformer; placing multiple CES units at the same transformer would require scheduling the two units together as a single optimization problem. The reserve energy is therefore constrained by (4-10) below.

$$-C_{Rsvt} \le \Delta C_t \le C_{max} \qquad \forall 0 \le t \le 23 \tag{4-10}$$

4.4.4. CES Optimal Control Algorithm

Once the constraints and the interpolation points for the feeder loss functions have been computed, the CES units may be scheduled for optimal profit. The algorithm, depicted in Figure 4-4, first identifies

the schedule with minimum charging and discharging that satisfies the various constraints at each hour. If there are any infeasible constraints, the reserve capacity constraints will be violated before the transformer loading constraint is violated. Then, starting from the initial schedule, the algorithm proceeds to add equal amounts (kWh) of charging and discharging at each iteration, moving toward an optimal schedule.

Mathematically this algorithm may be viewed as a modified version of the gradient method for solving optimization problems. The "gradient" is the marginal cost of increasing a unit of energy stored or released during a given hour. This unit of energy $\Delta C_t^{(i)}$ is called the step size. The maximum step size SSMax is chosen by the user based on the level of accuracy required and the amount of execution time available.

$$\Delta C_t^{(i)} < SS_{Max} \qquad \forall\ 0 < t < 23 \tag{4-11}$$

The revenue R_t corresponding to a given unit of energy is expressed in (4-12). Note that R_t will be negative when charging and positive when discharging.

$$R_t = LMP_t \times (P_t^{CESout} + P_t^{FeedLossRed}) \tag{4-12}$$

At each iteration, charging is added to only one hour and discharging is added to another hour, based on the charge/discharge pair with the maximum profit as given by

$$\begin{aligned} Ch/Dch\,Pair_{profit} = max(R_{t_{Ch}} + R_{t_{Dch}}) \\ \forall\, 0 \le t_{Ch} \le 23, \\ 0 \le t_{Dch} \le 23, \\ t_{Ch} \ne t_{Dch} \end{aligned} \tag{4-13}$$

The charging and discharging added at each iteration maintain a consistent time-integrated amount of energy stored inside the CES unit, which means that, due to internal losses in the batteries and inverter, the actual output and input seen external to the CES unit will be slightly different.

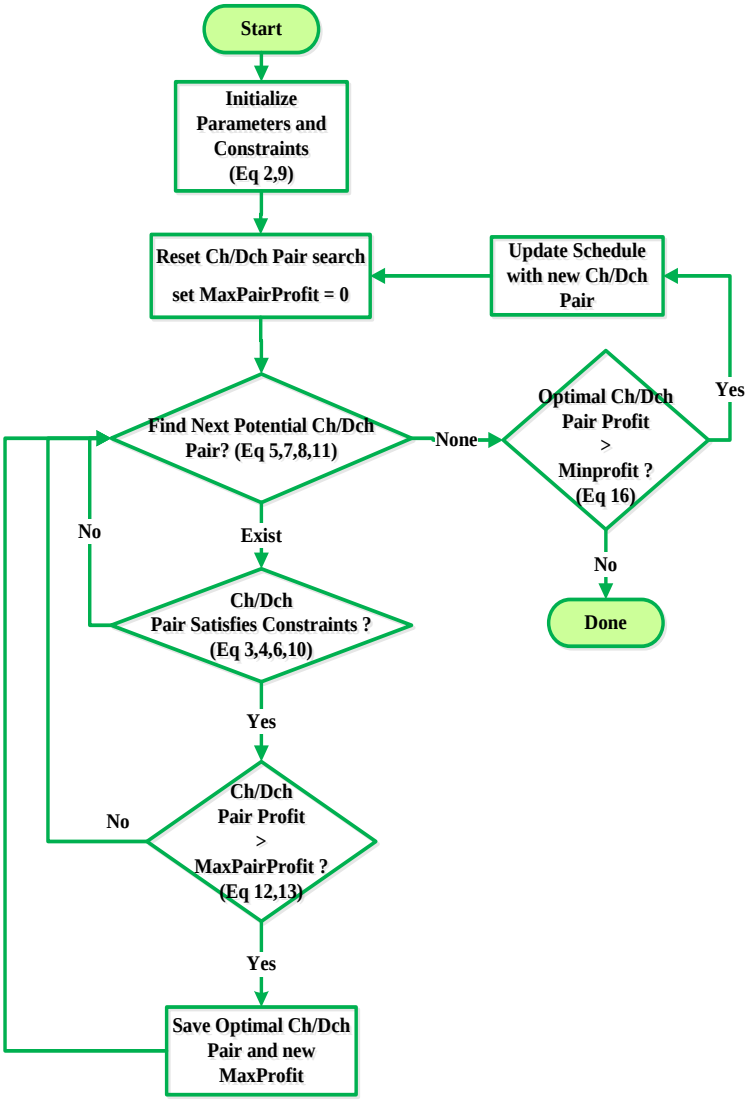

Figure 4-4 Economic optimization flowchart for each CES unit.

The algorithm developed here is more "greedy" than a normal gradient method. Once a certain charging or discharging amount has been scheduled for an hour, it does not scale back charging or discharging amounts in any hour during any iteration. When a constraint is reached in (4-10), the actual step size at that time slot ΔC_t may be smaller than SS_{Max}, but that time slot is then no longer considered in future iterations. Because of this "greedy" characteristic, the maximum number of steps required to find the optimal schedule for each CES unit can be calculated by

$$MaxSteps = \frac{max(P_{max}^{Ch}, P_{max}^{DCh})}{(SS_{Max})*(NT)} \tag{4-14}$$

,where NT is the number of time points. As long as both the function for the losses internal to the CES unit and the function for feeder losses are convex in all dimensions (as, for example, when the CES losses are modeled by a quadratic function dependent on a modeled internal resistance), the objective function as a whole is convex, so the algorithm converges to the optimal solution as the step size is reduced, where reasoning similar to the proof in [108] may be used.

$$\lim_{SS_{max} \to 0} (Sch_{profit_{opt}} - Sch_{profit}) = 0 \tag{4-15}$$

Finally, as a practical matter, the algorithm will only schedule charging and discharging when it can make greater than a certain minimum profit per kWh on the charge/discharge cycle. Since charging and discharging activity reduces the battery's life, the utility will set the minimum profit margin based on the CES unit's cost and life cycle information from the battery manufacturer.

$$\frac{Ch / Dch\,Pair_{profit_t}}{2 * \Delta C_t} > Minprofit \qquad \forall\ 0 < t < 23 \tag{4-16}$$

Thus, the algorithm will either stop when all time slots have been scheduled to a constraint or when the maximum charge/discharge pair profit is less than or equal to the minimum profit.

Finally, the algorithm should be run as frequently as the LMP prices or demand measurements change. Essentially, then, the 24-hour schedule is only used to decide what to do at the present time. The algorithm may be run again in another five or ten minutes to revise the current operation as the loading and energy costs have changed. Because of how quickly load and LMP prices change, it would be foolish to operate the CES units based on information that is almost 24 hours old—and often, it is foolish to operate based on information that is only 15 minutes old, as the LMP price is subject to occasional spikes. It is continuous process, when the time the "end of the day" arrives, the algorithm is already looking ahead to the end of the next day and adjusting the schedule accordingly.

Not only does the LMP price change rapidly but also the load forecasting may be very inaccurate 24-hours in advance. Again, by re-running the CES control algorithm every five or ten minutes with an updated load forecast, the CES units will be able to respond more quickly to changes in load.

4.5. Simulation Parameters

While the algorithm described above may be used with many varieties of storage technologies differing in rated output, storage capacity, and losses, the simulation presented here considers CES units

with Lithium-Ion cells as recommended in [46] with the following capabilities: 50kWh energy storage, maximum discharge rate of 25kW, and $R_{cell} = 0.003\Omega$ with 167 cells in parallel. Lithium-Ion battery self-discharge is neglected in this chapter. Table 4-2 shows the specifications of the DES units considered here. The DES unit has to provide the rated power and energy level after 1000 cycles in 25 ˚C ambient temperature.

During islanding, the DES has the capability to discharge up to 2.5 times the rated capacity for 3 seconds to serve motor inrush current. The minimum isolating contactor current rating of DES should be 400 Amps. The fault tolerance of DES unit restricts operation to transformer sizes less than or equal to 100KVA [20].

Table 4-2 CES Specification

Item	Unit	Default
Battery Type	-	Li-Ion
Power	kW	25
Capacity	kWh	50
Min AC Voltage	V	115
Max AC Voltage	V	125
Normal AC Voltage	V	117
Charging Rate	kW	25
Discharging Rate	kW	12.5

The load research data, customer billing information, and measurements from the primary sides of the distribution transformers are applied to model time varying loads in the Distributed Engineering Workstation (DEW) software [109]. The “profit” term in the following sections refers to the CES unit’s operational cost saving.

4.6. Simulation and Trade-Off Analysis

4.6.1. LMP Prediction Accuracy

Not surprisingly, the accuracy of the price forecast has a significant impact on the cost savings potential. The real-time price will often deviate from the day-ahead bids. In such cases, if the CES unit is charged when the price dips or discharged when the price rises, it is unable to take advantage of these fluctuations in price. The mature electricity markets normally have less LMP volatility in comparison to young electricity markets [110]. Figure 4-5 shows the difference between real time and day ahead LMP for the peak day of July 2009.

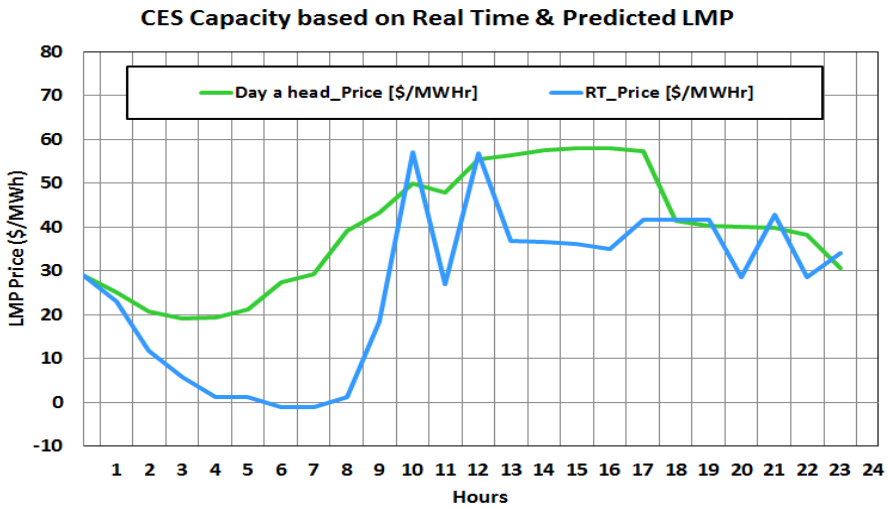

Figure 4-5 Real-Time and Day ahead LMP price for peak day in July 2009 with battery capacity for each price.

Smaller differences between real time and day ahead LMP market prices creates more benefits from DES economic scheduling because the charging and discharging of batteries are based on the electricity price prediction for the next 24 hours.

Table 4-3 shows the total profit for one month's operation calculated using the day-ahead prices as well as the total profit that could have been achieved if the real-time prices were known 24-hours in advance (an "ideal prediction"). Thus, there is a great incentive for utilities to revise the LMP forecast [111] when possible as equipment and loading data are updated. It is worth mentioning that the day ahead and the real time LMP prices are dictated by Independent System Operators (ISO) to utilities. Utilities do not determine the LMP prices. The difference of day ahead and real time LMP is because of unforeseen changes in generation capacity, transmission constraints or total demands in the ISO pricing software systems.

Table 4-3 LMP Accuracy Analysis

	PROFIT
Day-Ahead LMP	$101
Ideal Prediction	$185

4.7. Transformer Loading and Reserve Capacity

When the load is higher, more energy must be saved in case of an outage, so there is lower availability for participation in the energy market, resulting in smaller profits. On the other hand, when the system load is higher, the energy prices tend to be higher, resulting in higher profits. The simulation presented here uses the month of July, when both the load and the prices tend to be highest.

Since a higher load means less energy is available for market participation, a greater profit can be realized by placing the CES units on more lightly loaded transformers. Figure 4-6 illustrates this tradeoff, plotting the profit (cost savings) against the transformer loading. However, the CES placement does not only depend on the transformer loading. Sometimes utilities place CES in areas with more outages. Thus, with a heavily loaded transformer the utility is trading off operating profit for improved reliability.

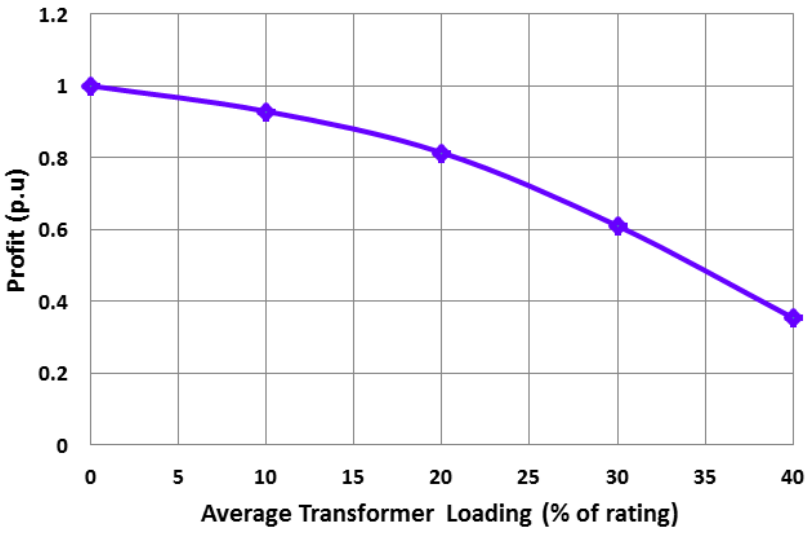

Figure 4-6 CES Operation profit vs. distribution transformer loading.

The dynamic reserve capacity is dependent not only on the load, but also on the number of hours' worth of load that the CES unit is expected to be able to serve in case of an outage. Figure 4-7 illustrates the tradeoff between the profit potential of the CES unit and the number of hours of reserve capacity. Utilities must decide how much reliability they are willing to risk to realize increased savings. Utilities with performance based rates (PBR) could use a plot like the one in Figure 4-7 to identify where the tradeoff between profit and reliability matches their PBR [112].

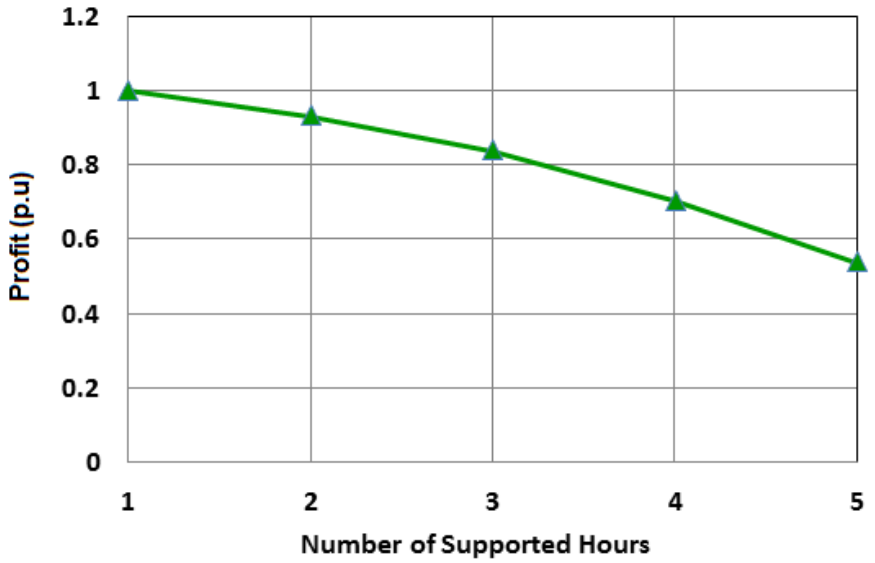

Figure 4-7 CES operational profit vs. number of hours for supporting loads following an outage.

For comparison, a static reserve margin is also assessed. Figure 4-8 compares the use of a static reserve capacity with a dynamic reserve capacity, where the static reserve capacity is fixed at the maximum capacity used by the dynamic reserve capacity. The static reserve capacity benefit is 39% less than the dynamic reserve capacity method at 80% transformer loading. In this curve a residential load is used; customers with different load shapes would see different variations between dynamic and static reserve capacity.

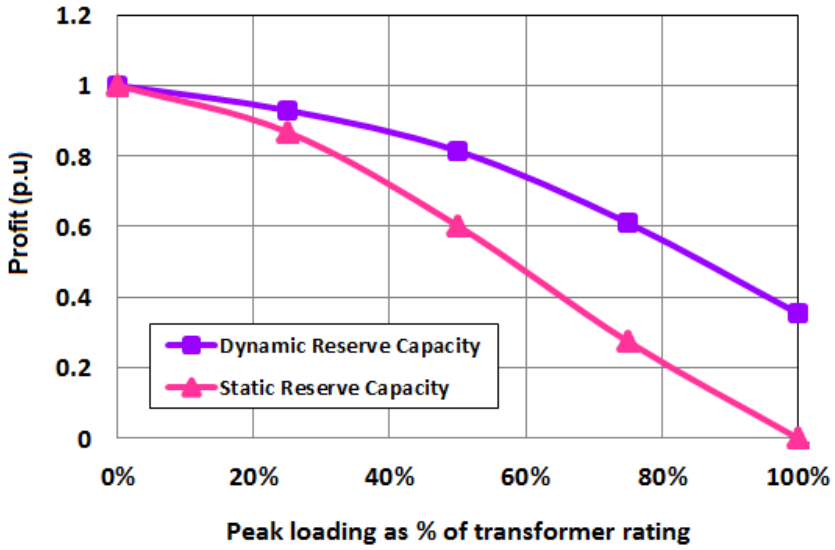

Figure 4-8 CES dynamic and static reserve operational benefits

Figure 4-9 shows the tradeoff between profit and fixed (static) reserve capacity. While a dynamic reserve margin offers a greater potential cost savings, computing the dynamic reserve margin depends heavily on accurate load forecasting. A utility with a poor load forecasting capability may be limited to using a static reserve capacity. Similarly, a customer with a constant load profile has a static reserve capacity.

Alternatively, Figure 4-9 can be understood as depicting the tradeoff between energy storage size and cost savings, as opposed to reliability and cost savings.

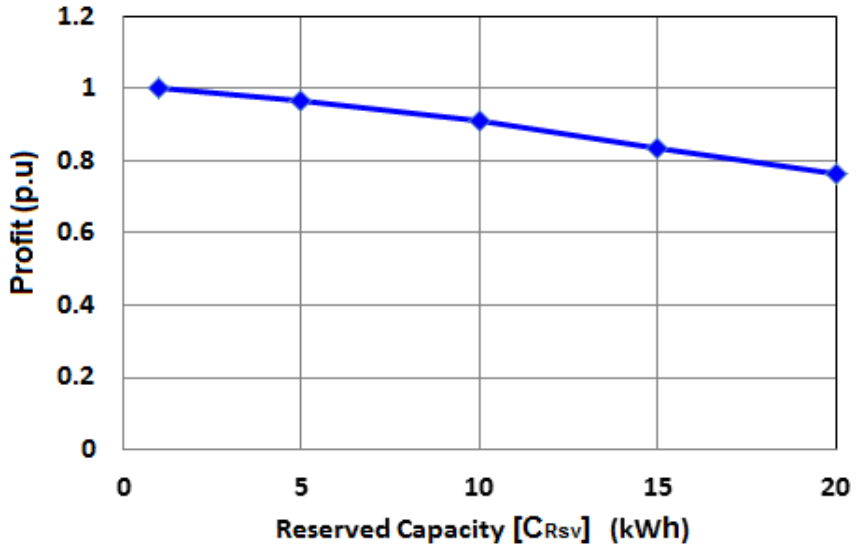

Figure 4-9 CES Operational profit vs. different fixed reserved capacity of a CES.

The cost savings potential is not only limited by the reserve capacity (stored energy) but also by the output power required to prevent overloads on a transformer.

4.7.1. Feeder Losses

The significance of feeder losses is presented in Table 4-4. The profit is calculated for a single month for a single CES unit far from the substation on a moderately loaded feeder. Two approaches are used to schedule the CES charging/discharging. The first approach includes feeder loss reduction as a part of the objective function, see (1), as well as the internal battery losses. The second approach ignores the feeder losses in optimization, but still incorporates internal battery losses. Note that an ideal LMP "prediction" is used to isolate the effects of the increased accuracy in the objective function from the effects of inaccuracy in the LMP prediction.

Table 4-4 Profits For a CES Unit in One Month

Objective Function	Profit ($)	Computational Time (Sec)
LMP Price + Loss Function	185	337
LMP Price	182	90

Table 4-4 shows that the feeder losses have a very small impact on the total cost savings attainable by optimization, but the computational time to calculate feeder losses is almost three times the total computational time for maximizing the objective function. The quality of the price forecast and the internal battery losses both outweigh the feeder losses in determining the optimal schedule.

4.7.2. Optimization Step Size

Table 4-5 shows the effects of changing the optimization step size on the profit achieved by the algorithm, where the optimization is performed for an entire month for the LMP price case (second case in Table 4-4). Since most of the cost savings comes from hours with unusually high or unusually low LMP prices, changing the step size has relatively little impact on the cost savings realized by the algorithm, but it has a significant impact on the computational time. Note that the actual step size used in each iteration depends also on the constraints – even if the step size is 5 kWh, if the battery only has 2 kWh remaining stored energy in a given hour, the step size effectively becomes 2 kWh for that iteration.

Table 4-5 CES Optimization Step Size

Step Size (% of Max Battery Capacity)	Computational Time for One Month (sec)	Profit for One Month ($)
2	90	101
5	65	101
10	57	101
20	55	100

4.7.3. CES Units Aggregated Response

The circuit used for case study is in a residential area with a 1769 kVA annual peak load on 13.2 kV distribution lines. 20 CES units are located on the circuit with total capacity of 1MWh. CES places are shown in Figure 4-10. The CES units are located beside the lightest loaded transformers to have more potential profit.

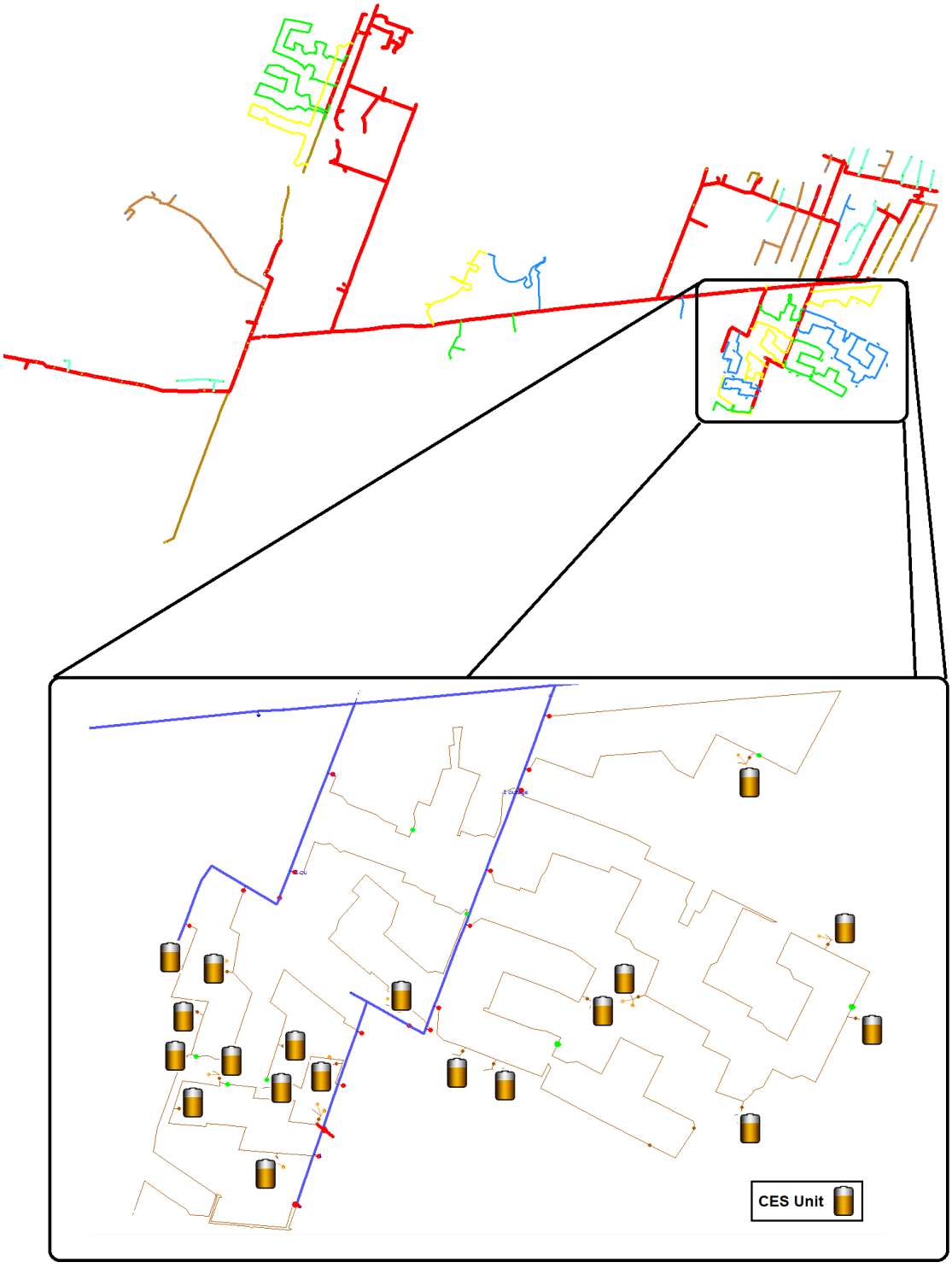

Figure 4-10 Case study circuit schematic

Figure 4-11 depicts the aggregated 20 CES units scheduling effect on the feeder loading for a day in July. It shows the consistency of CES scheduling with the real time LMP price. During LMP low price

hours (6AM - 9 AM), CES units charge to store energy. At the peak hour and more expensive LPM prices, CES units discharge to make a profit and decrease peak load.

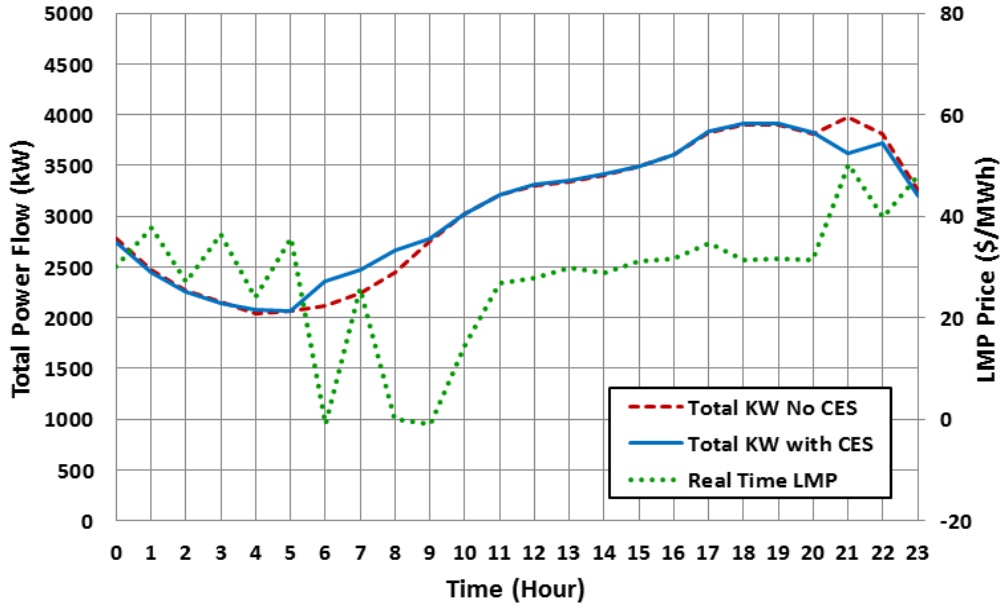

Figure 4-11 Feeder load profile for aggregated 20 CES units.

4.8. CES Application Analysis

4.8.1. CES and Electric Vehicle Adoption

Plug-in electric vehicles (PEV) refer to a class of vehicles that can use both fuel and electricity, independently or dependently. PEV can be considered as a Battery Electric Vehicle supplied with an internal combustion engine to increase the vehicle driving range. Moreover, PEV is like a conventional Hybrid Electric Vehicle with an extended electric driving range and battery charging capability [113]. PEV are classified based on the all-electric range (AER) that they can be driven only on battery. PEV-X is a representation for X miles AER [114]. The PEV-20, which is used in case study, refers to a PEV with 20 miles driving range on battery. To evaluate the impact of PEV on distribution circuits, the availability of grid connected electrical vehicles to the grid must be taken into account. The duration of PEV availability can be determined based on the National Household Travel Survey (NHTS) database. With time information about the departure and arrival times of vehicles, it is possible to estimate where, when, and how long PEV are connected to the grid. One of the factors extracted from the NHTS survey is the daily miles driven by each vehicle. The most common daily travel in the US is in the range of 25-30 miles. Figure 4-12 shows the percentage of vehicles vs. daily travel distance in US [114].

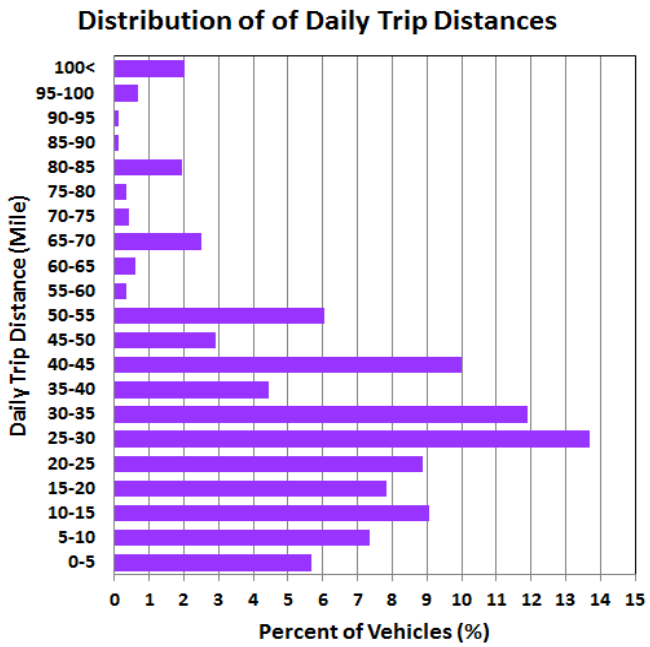

Figure 4-12 Distribution of daily trip distance in US based on NHTS survey[113].

The other important factor in the PEV load profile is the charging start time. Some literature assumes that owners will start to charge PEV once they arrive home [115, 116]. An average vehicles home arrival time can be extracted from the NHTS survey. With the help of Monte Carlo simulations on the census data and the average of arrival time to home, a probability distribution of the PEV charging start time is achieved (see Figure 4-13) [117].

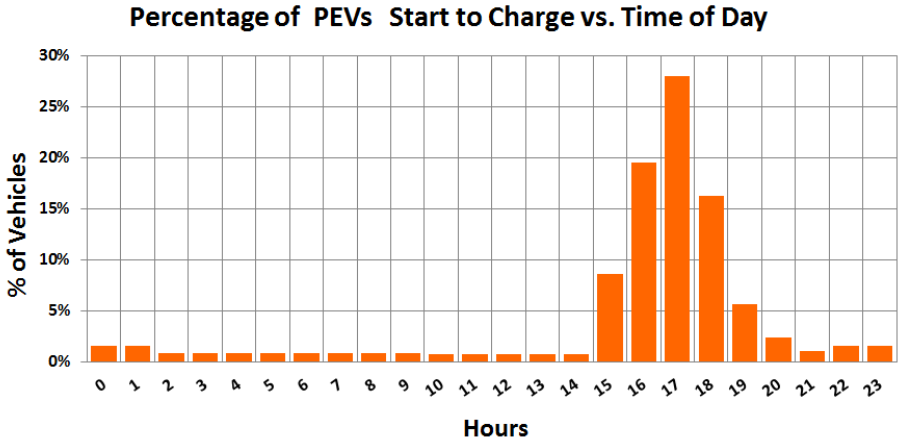

Figure 4-13 Probability distribution of start time for PEV charging[116].

The type of PEV has a major effect on the load profile. The 2001 NHTS user guide classified vehicles to seven vehicle type groups [118]. Most cars in residential areas are among types 1 to 4. Same

classification is used for PEVs (see Table 4-6). To clarify required energy for each type of PEV, the total battery capacity for different types of PEV-20 are presented in Table 4-6 [119].

Table 4-6 PEV Types and Capacity[118]

Vehicle Type	Description	Capacity (kWh)
1	Car	6.5
2	Van	7.5
3	SUV	8.7
4	Truck	10.1

There are a number of charging levels in previous research [120]. This research uses the level 1 charging with 110V/15A /1.44 kW in accordance to the National Electric Code (NEC) standard [121], because the 110V/15A outlets are available in all houses. Based on the level one charging and PEV capacity (Table 4-6), typical charging scenarios for all PEV types are illustrated in Figure 4-14. It is assumed that the battery is fully discharged at the start of charging time.

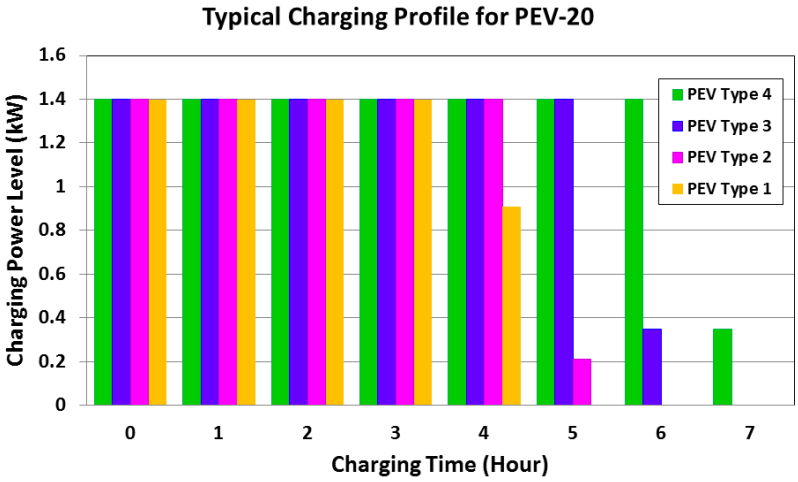

Figure 4-14 Typical charging profile for different types of electric vehicles[120].

The PEV type 3 is considered for simulation (blue column) in this chapter, because this type (SUV) is more popular than the PEV type 4 (Truck) in most residential areas and type3 cars have larger capacity than type 1 and type 2 [114].

Figure 4-15 depicts the effects of the transformer loading constraint on the DES charging/discharging schedule. In Figure 4-15, a high PEV adoption level creates a very large load between 5 and 9 P.M on an otherwise lightly loaded transformer. The CES constraints ensure that the battery retains sufficient charge

before and during this time frame to be able to prevent a transformer overload during the entire four-hour period in which the PEVs are being charged.

The PEV loads therefore affect the charge/discharge schedule in two ways. First, the overload caused by the PEVs causes the reserve capacity constraints to be overridden (the CES unit discharges, even though discharging will reduce the amount of time that the CES unit could supply the load if there were an outage). Additionally, the requirement to discharge during these hours limits the profit that could otherwise be gained by discharging the battery during more profitable hours.

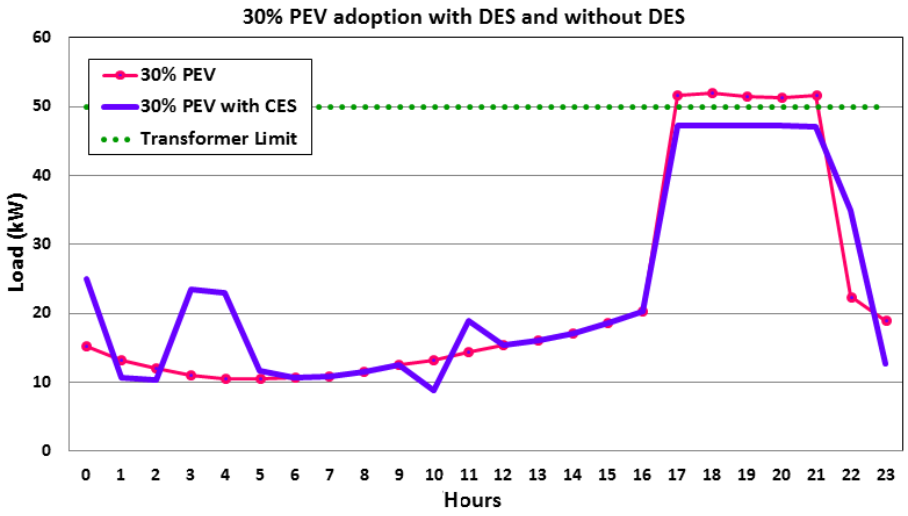

Figure 4-15 Load profile for different PEV adoption levels. Black line is the load profile with CES.

In Figure 4-16 the real-time prices are plotted together with the CES output and the internal capacity. Although the CES might have sold the energy between 2 and 4 P.M. to make a higher profit, it was forbidden from discharging so that enough capacity could be maintained to prevent the overload between 5 and 9 P.M. Of course, the LMP values are still higher between 5 and 9 P.M. than earlier in the day when the CES unit was charged, so the system is still achieving an operating profit while preventing the overload.

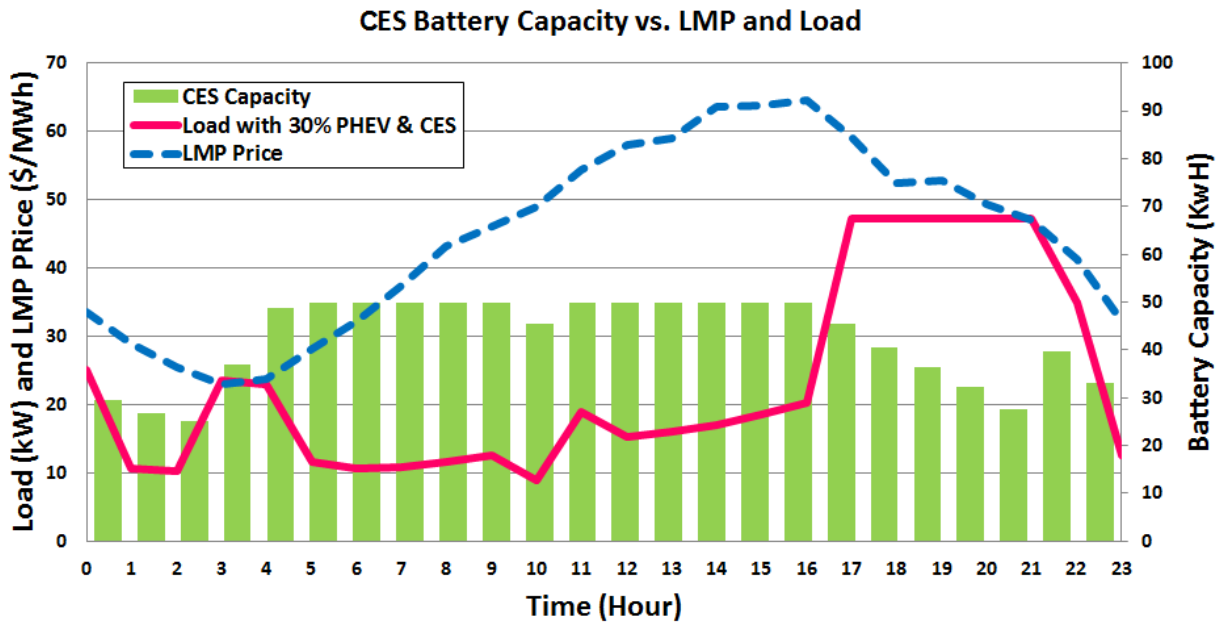

Figure 4-16 CES capacity with LMP price and load profile.

Since transformer overloading will impact CES profit potential, it is worth evaluating what levels of PEV adoption will cause such overloads. Table 4-7 shows the PEV adoption effects on overloading of distribution transformers spread throughout the circuit.

Table 4-7 PEV Adoption Effect on Distribution Transformers

Adoption %	0	10	20	30	40	50
Number of Overloaded Transformers	0	3	10	14	18	22

4.8.2. CES and Distributed Photovoltaic Sources Adoption

In this research three levels of Distributed Photovoltaic (DPV) sources adoption are considered in three scenarios. The aggregated PV capacities on the secondary of distribution transformer are Case 1- 0 kW, Case 2- 5 kW, Case 3- 10 kW and Case 4- 15 kW. Figure 4-17 shows the PV panel aggregated output at the peak day (July 5 2011).

The solar power generation data is based on the National Renewable Energy Laboratory (NREL) data from “In My Backyard” (IMBY) [122] and the “PVWatts” online tools [123]. These online PV power calculation tools use solar irradiation, metrological data and PV performance parameters to produce

hourly PV power data for any location in the United States. For this case study, the 1 kW PV panel outputs for the peak load day (July 5) is considered.

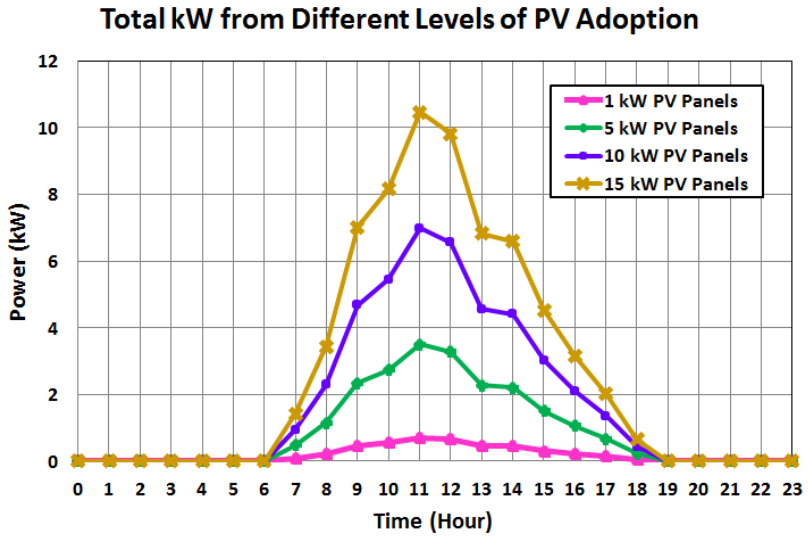

Figure 4-17 Different levels of aggregated PV panel output.

Figure 4-18 shows the results of DPV integration with aggregated residential loads, five houses, for the peak day. The yellow line represents the aggregated load of the five houses without DPV.

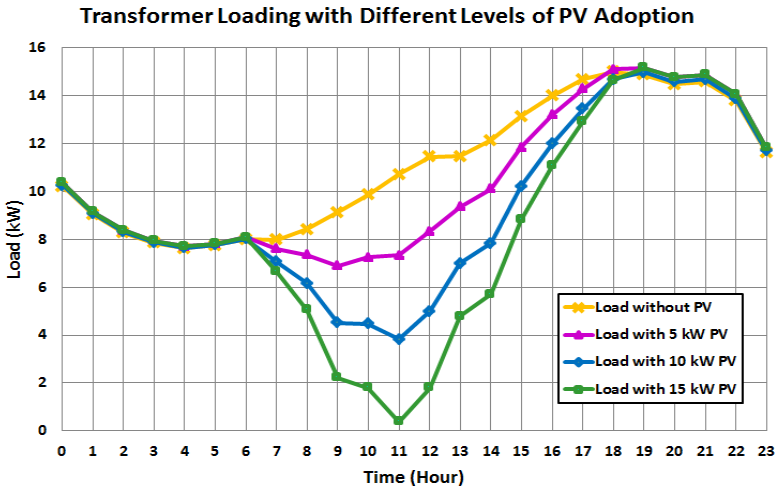

Figure 4-18 Aggregated load with different levels of DPV adoption (Case1 to 4).

The CES optimal control outputs for different DPV adoption levels are presented in Figure 4-19. From 5 AM to 9 AM the LMP price is low and demand is not high, therefore the battery charges to its maximum capacity during this period. From 9 AM to 6 PM, the battery keeps its capacity for peak hours, 6 PM to 9 PM. During the peak hours the battery starts to discharge to serve loads and decrease the peak

to avoid buying expensive electricity. At 9 PM the LMP has reached the highest price. Thus, the CES sells power to the grid at 9PM. The negative sign of load at 9 PM shows the reverse power flow from the CES to the grid.

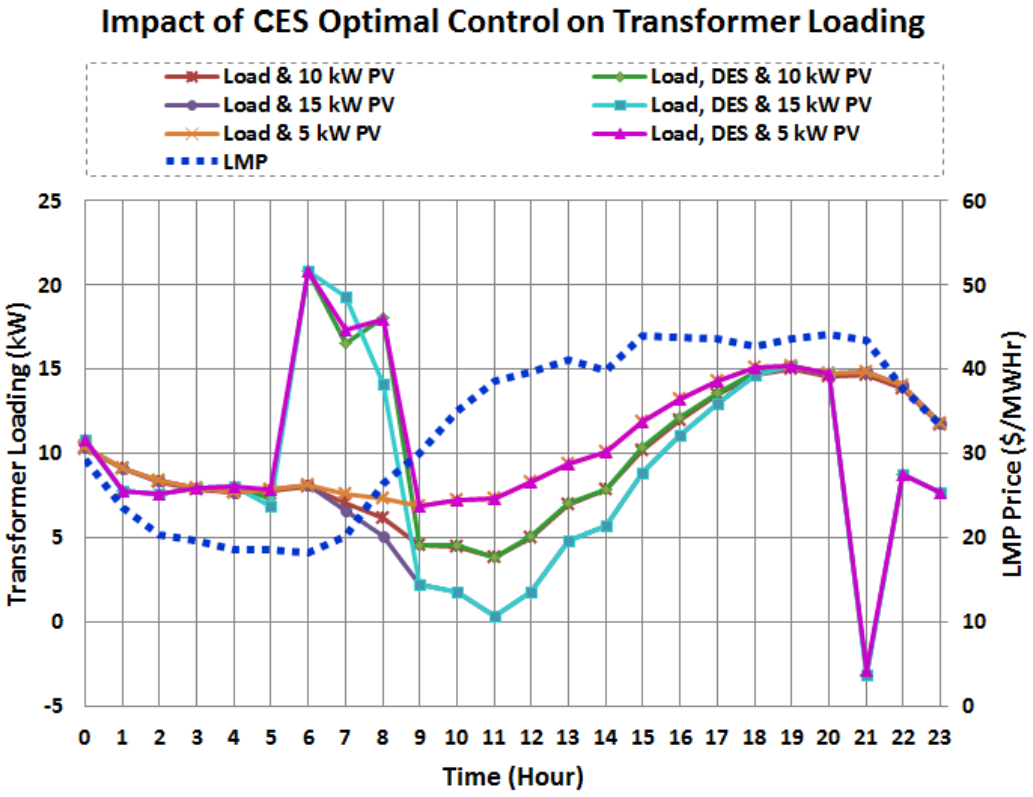

Figure 4-19 CES Optimal Control system output for different levels of DPV adoption. The dashed line represents the LMP price.

In Figure 4-20, the LMP price is plotted with the battery capacity and load profile for the 15 kW PV case. From 12 AM to 2 AM and from 10 PM to 12 AM the battery waits for the cheaper LMP prices. Therefore, it does not charge up to its maximum capacity. As mentioned in the previous figure, the battery keeps its maximum capacity for discharging during peak hours.

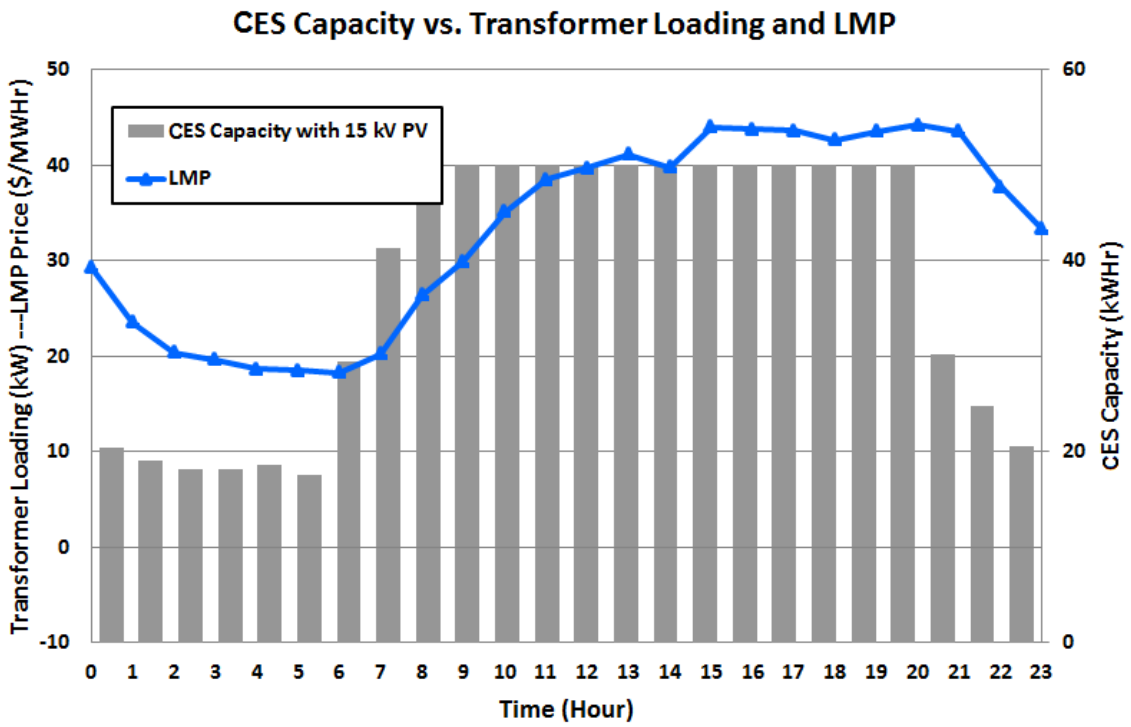

Figure 4-20 Battery capacity vs. real-time LMP price (Case 4).

In this chapter the CES units are owned by the utility company. Therefore, the CES operation benefits belong to the utility company. To calculate the DPV adoption effect on the CES operation benefits, four cases are considered. Case 1 is CES without DPV on the circuit. Cases 2, 3, and 4 have 5 kW, 10 kW, and 15 kW DPV capacity, respectively. Figure 4-21 presents the optimization results for these cases. As the DPV capacity increases at distribution transformers downstream, higher benefits are achieved by the CES operation. In case four, each CES unit makes $ 82.5 benefit over month of July 2011.

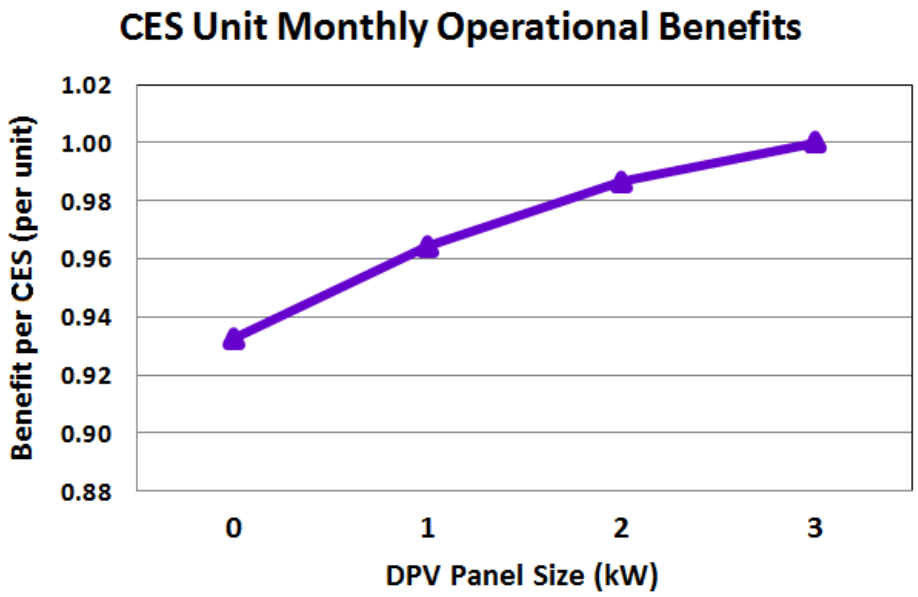

Figure 4-21 CES optimal control economic benefits (Case 1 to 4).

This chapter assumes DPV units are owned by customers. From the customer point of view, DPV installation allows serving part of their loads avoiding buying power from the utility company. Moreover, they can increase DPV revenue by selling PV active power to the grid. To calculate the customer benefit for all cases, the average electricity price in the New York state is considered to be 0.175 $/kWhr [124]. Figure 4-22 illustrates the electricity price for the aggregated load under the case study's transformer.

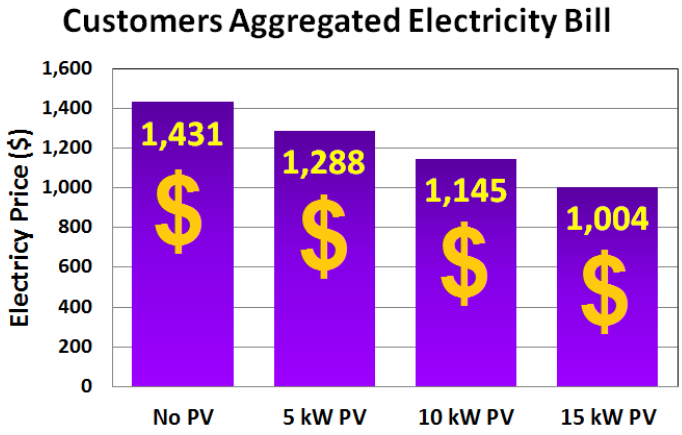

Figure 4-22 Electricity price for the aggregated load during different DPV adoption levels (Case 1 to 4) .

Figure 4-22 shows the trend of benefit growth based on the DPV size increase. Table 4-8 represents the average monthly benefit for each house based on three different distributed PV panel sizes for July 2011.

Table 4-8 Average benefit of DPV for each household for July 2011

Case #	Panel Size (kW)	Average Benefit ($/kW)
Case2	1	28.7
Case3	2	57.1
Case4	3	85.4

This chapter focuses on the operational cost of CES and DPV system in distribution networks. Based on the information in sections 3-A and 3-B, the CES and the DPV capital costs are still high. Therefore, business models involving third-party ownership such as "battery leasing" and "battery as a service" in conjunction with the tax reduction and governmental incentives may result in reduced CES and DPV installation costs. Designing such a business model is part of the future works. Furthermore, technologic advancements, market developments and enthusiasm of customers for green energy make the steady decline in PV and storage prices in near future [101].

4.9. Chapter Conclusions

This chapter presents utilities with a means of gaining year-round benefits from the control of community energy storage (CES) units. This dissertation presents a means of realizing additional benefits for utilities by taking advantage of the fluctuating costs of energy in competitive energy markets. By combining electricity market information with real-time control of energy storage devices, utilities may enjoy year-round economic benefits from the storage devices in addition to the occasional benefits mentioned above.

A mathematical formulation is presented for calculating the optimal charge/discharge schedule subject to a number of constraints. Analysis of some of the parameters and tradeoffs involved in operating distributed energy storage devices is presented, which provides insight into such considerations as inaccuracies in LMP price forecasts, transformer loading, reserve capacity, and feeder losses. The analysis shows the benefit is highly dependent on the accuracy of the LMP prediction and load forecasting. In the trade-off between accuracy and computational time, incorporating the feeder losses in the objective function has a rather small impact on the total profit, but a rather large impact on the computational time. While CES installations help meet power system reliability and capacity requirements, proposed optimal operating strategy further increases the value of the CES.

To demonstrate advantages of proposed optimal control algorithm for CES units, a number of case studies are considered in simulations. In case of high levels of Plugged-in Electric Vehicles (PHV)

adoption, CES supports the distribution transformers from overloading. CES brings more flexibility to the distribution networks. Moreover, Distributed Photovoltaic (DPV) sources penetration are addressed in case studies. The proposed optimal control system can improve the distribution network flexibility and reliability with combination of DPV and CES. The proposed algorithm for CES makes more benefits for utilities who operate CES with higher DPV installation and at the same time CES units decrease the stress on distribution transformers due to high level of solar power adoption.

Chapter 5 : Harmonic Impact Study for Multiple Harmonic Sources in Distribution Networks

5.1. Introduction

Smart Grid realization involves a steady increase in inverter-based components like Distributed Energy Resources (DER), energy storage systems, and plug-in electric vehicles. The harmonics related to DER inverters and the spread of power electronic devices raises concerns for power system engineers and operators. The harmonics generated by DER devices and Plug-in Electric Vehicles (PEV) can cause distortion in power system voltages and currents. In addition to the power quality issues, harmonics can have economic impacts on distribution networks. Harmonics can decrease efficiency, create thermal losses and may overload network components. These effects cause premature aging and failure in power system devices.

The harmonic impact study for a single harmonic source is a well-researched topic. Harmonic measurement and filtering are discussed in plenty of literatures. However, conventional researches mostly consider harmonic as a local phenomenon with local effect [63, 64]. There are few papers that demonstrate harmonics produced by DER sources like PV and energy storage [67-69]. Even fewer papers study harmonic effects on large scale distribution networks [60, 62, 70]. However, the interactive effect of harmonics produced by multi DER sources on each other and their aggregated effect on the distribution system are not addressed in previous literatures. The other uniqueness of this dissertation is application of the detailed multi-phase model of the distribution network that considers all circuit components, including distribution transformers and secondary distribution. Here harmonics are calculated for each phase throughout the multi-phase system, taking into account the mutual impedances among the phases. This detailed model provides for a more realistic analysis.

Published studies on phase balance and harmonics have focused on particular devices, such as transformers, or on three-phase unbalanced loads [71, 72]. In this dissertation, the effect of three phase balance on harmonic distortion at the distribution network level is addressed.

This dissertation discusses harmonics produced from multiple DER sources such as solar, wind and energy storage systems. The aim is simulating and analyzing multi-source produced harmonic interactions that could lead to concern in distribution networks from the view point of voltage and current harmonic

content and total harmonic distortion (THD). Traditionally, THD is the most used index for harmonics evaluation in standards and literatures [65, 66], but THD is only based on the harmonic magnitude. In this chapter a new index is proposed to consider the impact of interactive multisource phase angle on the harmonic distortion. The proposed index is called Index of Phasor harmonics (IPH). The sensitivity analysis is conducted to show the impact of each harmonic source magnitude and angle on overall distortion in the distribution network.

The chapter is organized as follows: section II is discusses harmonics phenomena in distribution networks. Section III describes the principle factors for harmonic analysis in distribution networks. Section IV presents simulations and results.

5.2. Harmonics Characteristics in Distribution Networks

5.2.1. Harmonics and Distribution Network Malfunctions

High level adoptions of distributed generation technologies like solar, wind, fuel cells and microturbines in addition to energy storage, PEVs, and power electronics based components, all within close proximity of one another, create concerns of how harmonics generated by one set of devices may interact with harmonics generated by other devices.

Harmonics can result in various malfunctions and failures in distribution networks. Transformer and conductor overheating and pre-mature aging, neutral conductor overloading, capacitor bank overstressing, abnormalities in protection system operation, thermal effects in electric machines, and control system errors are among the challenges for distribution network operation under harmonics emission [66, 125].

From an economic perspective, the harmonics resultant loss will increase the network operational cost. The pre-mature aging of network components caused by harmonics results in higher maintenance costs [126]. Moreover, harmonic distortion can affect energy metering equipment and decrease metering accuracy that can change electricity market transactions [127, 128].

5.2.2. Harmonic Measurements and Assessments

The AC electricity supply should ideally be a perfect sinusoidal voltage and current signal to every customer. The deviation from the perfect sinusoidal waveform is expressed in distortion terms. Harmonics in voltage and current waveforms can be represented as sinusoidal components with higher integer multiples of the fundamental frequency. A distorted voltage and current waveform are expressed by Fourier series as given by

$$I_{Total} = \sum_{h=1}^{\infty} \sqrt{2}\, I_h \cos(h\,\omega_0 t + \theta_h) \qquad (5-1)$$

$$V_{Total} = \sum_{h=1}^{\infty} \sqrt{2}\, V_h \cos(h\,\omega_0 t + \phi_h) \qquad (5-2)$$

where ITotal and VTotal are the nonsinusoidal current and voltage at the measurement point. Ih and Vh are current and voltage r.m.s values for the hth harmonic order. θh and φh are harmonic current and voltage phase angles. ω0 is the fundamental angular frequency and h is the harmonics order.

Total harmonic Distortion (THD) is an index that is widely used for power quality assessment in distribution and transmission networks. THD is defined for current and voltage respectively as [129]:

$$THDI = \frac{1}{I_1}\sqrt{\sum_{h=2}^{\infty} {I_h}^2} \qquad (5-3)$$

$$THDV = \frac{1}{V_1}\sqrt{\sum_{h=2}^{\infty} {V_h}^2} \qquad (5-4)$$

where THDI and THDV are THD values for current and voltage, respectively. I1 and V1 are the current and voltage r.m.s values for the fundamental frequency.

The Individual Harmonic Distortion (IHD) index presents the percentage ratio of current or voltage in the hth harmonic order with respect to the fundamental value. IHDI and IHDV are the IHD for current and voltage respectively as given by

$$IHDI = \frac{I_h}{I_1} \times 100 \qquad (5-5)$$

$$IHDV = \frac{V_h}{V_1} \times 100 \qquad (5-6)$$

Harmonics is a challenging and serious problem in distribution networks. However, interactive harmonic effects of DERS can intensify the problem. The Total Harmonic Distortion (THD) index is only based on signal magnitude. To help quantify the distortion caused by multiple harmonic source interactions, there is a need to consider phase angles of current and voltage waveforms.

In this dissertation, the Index of Phasor Harmonics (IPH) is proposed. The IPH is obtained by dividing the real part sums of the phasor harmonic waveforms by the algebraic sum of harmonic waveform magnitudes. Let us define

$$I_h^{Ph} = I_h \angle \theta_h \qquad (5-7)$$

$$V_h^{Ph} = V_h \angle \phi_h \qquad (5-8)$$

where I_h^{Ph} and V_h^{Ph} are phasor representation of current and voltage. The IPH equations are:

$$IPHI = \frac{\sum_{h=1}^{\infty} |I_h \cos(\theta_h)|}{\sum_{h=1}^{\infty} |I_h|} \qquad (5-9)$$

$$IPHV = \frac{\sum_{h=1}^{\infty} |V_h \cos(\phi_h)|}{\sum_{h=1}^{\infty} |V_h|} \qquad (5-10)$$

where IPHI and IPHV are Index of Phasor Harmonics for current and voltage waveforms.

When considering harmonic distortion, the conventional definition of power factor is modified to account for the contribution of higher frequencies on the power factor [66]. The modified power factor is called Total Power factor (TPF). Equation (11) shows the relationship between TPF and THD [126, 130]:

$$TPF = \frac{\cos(\delta_1)}{\sqrt{1 + THDI^2}} \qquad (11)$$

where δ1 is the angle between voltage and current at the fundamental frequency. The $\cos(\delta_1)$ called displacement power factor and the factor $1/\sqrt{1+THDI^2}$ is called distortion power factor.

5.2.3. Harmonics and Standards Perspective

Harmonic emissions are addressed in a number of standards and recommendations. The most widespread harmonic standards in the United States and the European Union are issued by IEEE and IEC. The harmonics standards can be classified into three categories: 1) standards related to power quality in distribution networks, 2) standards related to devices and harmonic sources, and 3) standards related to distribution network equipment installation and operation [126].

The IEEE-519, IEC-61000-6 and EN-50160 belong to the first group of standards. The IEEE-519 presents a joint approach for customers and utilities to limit nonlinear load harmonics [65]. The EN-

50160 focuses on voltage characteristics of public electricity distribution networks [131]. The IEC-61000-6 is mostly focused on harmonic limits for power quality at the planning level [132].

The IEC-61000-3-2 and IEC-61000-3-12 are subsets of the second group. They advocate harmonic limitations for low-voltage equipment [133].

The IEEE-1547-4.3 and IEC-61000-2 are classified under the third group of standards. The IEEE-1547 defines the requirements for distributed resource (DR) interconnections including harmonic distortions in DR applications [134]. The IEC-61000-2 defines harmonic limits for equipment immunity in LV and MV installations [135]. Figure 5-1 shows the voltage distortion limits from two different IEEE standards. The IEEE-1547 has more restricted limits in comparison to the older standards (IEEE-519).

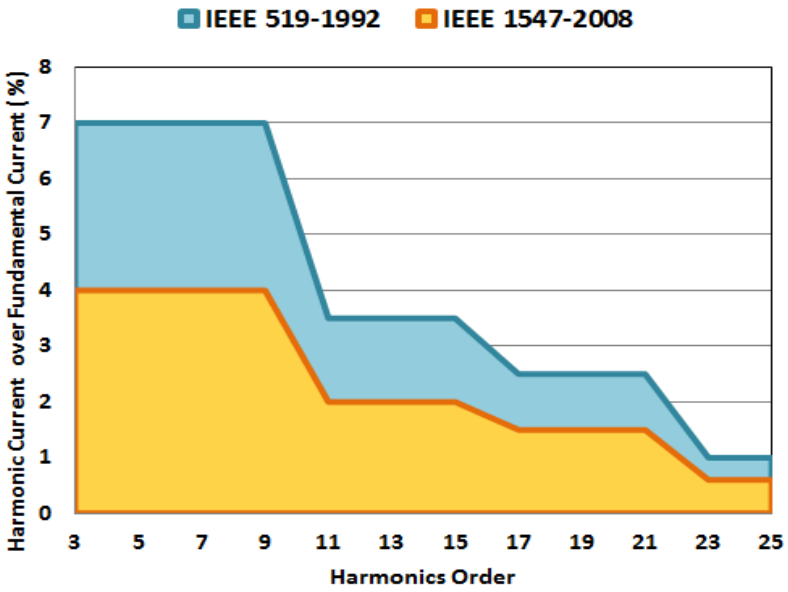

Figure 5-1 Harmonic current limits in accordance to IEEE519 and IEEE1547

5.3. Principle Factors for Harmonics Analysis in Distribution Networks

5.3.1. Architecture of Harmonic Analysis

In order to conduct harmonic analysis in power systems, the harmonic current propagation in circuits needs to be calculated. The fundamental frequency power flow analysis is the base for harmonic calculations. The power flow study provides steady-state circuit performance under the normal operating condition.

In addition to the power flow, the harmonic power flow is conducted to determine harmonic current and voltage emissions in the circuit for higher frequencies than the fundamental frequency. The harmonic power flow calculation helps in designing harmonic filters to avoid resonance conditions in distribution network.

To represent harmonic currents in equation (1), harmonic current sources, including magnitude and phase angle, are applied. These current sources inject harmonic currents at the location of the harmonic source. They are superimposing harmonic currents on top of the fundamental current waveform. The degree of voltage distortion depends on the harmonic current source characteristics and current propagation inside the distribution network. Harmonic current flow is affected by inductive and capacitive impedances, transformers and conductor configurations.

The major steps of harmonic analysis power flow algorithm used here are as follows:

Step 1: Initialize the distribution circuit parameters

Step 2: Run power flow for the fundamental frequency

Step 3: Modify the circuit for next higher harmonic calculation (change impedances)

Step 4: Run power flow for higher harmonic order (harmonic power flow)

Step 5: Store all power flow results for current harmonic order

Step 6: Check if the specified maximum harmonic order has been reached. If not, go Step 3. If yes, quit.

Step 7: Calculate harmonic indices

For the power flow calculation, the Distributed Engineering Workstation software package is used. Figure 5-2 depicts the algorithm for the harmonic analysis.

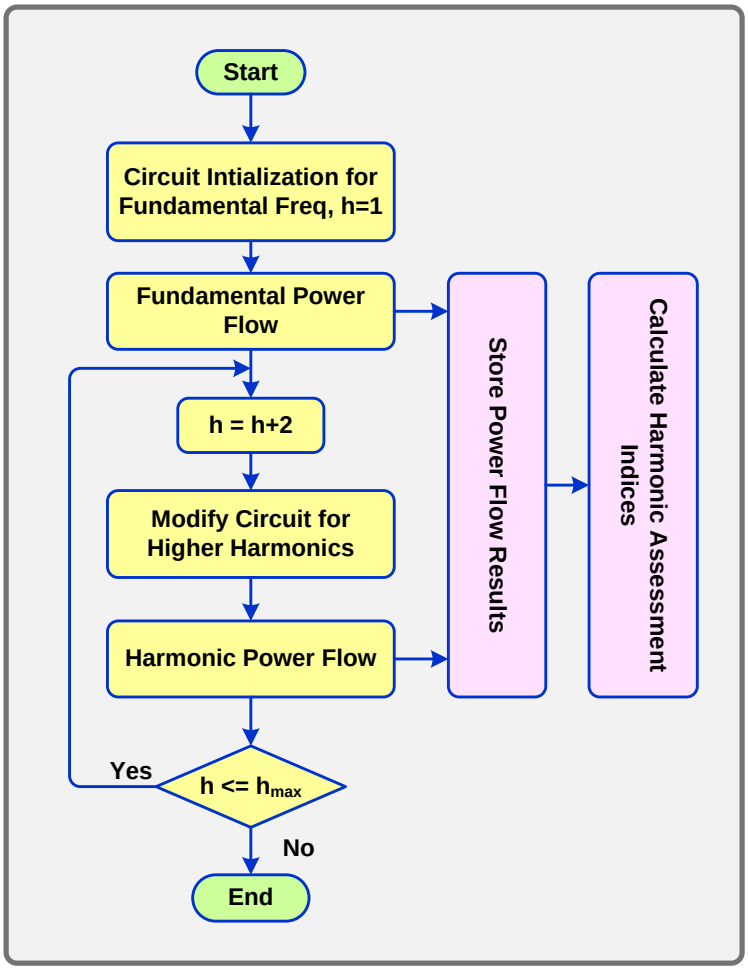

Figure 5-2 Harmonic Analysis Algorithm

5.3.2. Physical Network Model and Circuit Topology

One of the important factors in harmonic propagation is circuit topology. The harmonic simulation results are highly dependent on the circuit model. In this study, the circuit is 13.2 kV, Y-connected with 329 residential and commercial customers. The peak load is 9.5 MVA. The circuit model includes unbalanced, multiphase and single phase loads. The circuit contains two sets of three phase harmonic sources. Fig. 2 presents the circuit model.

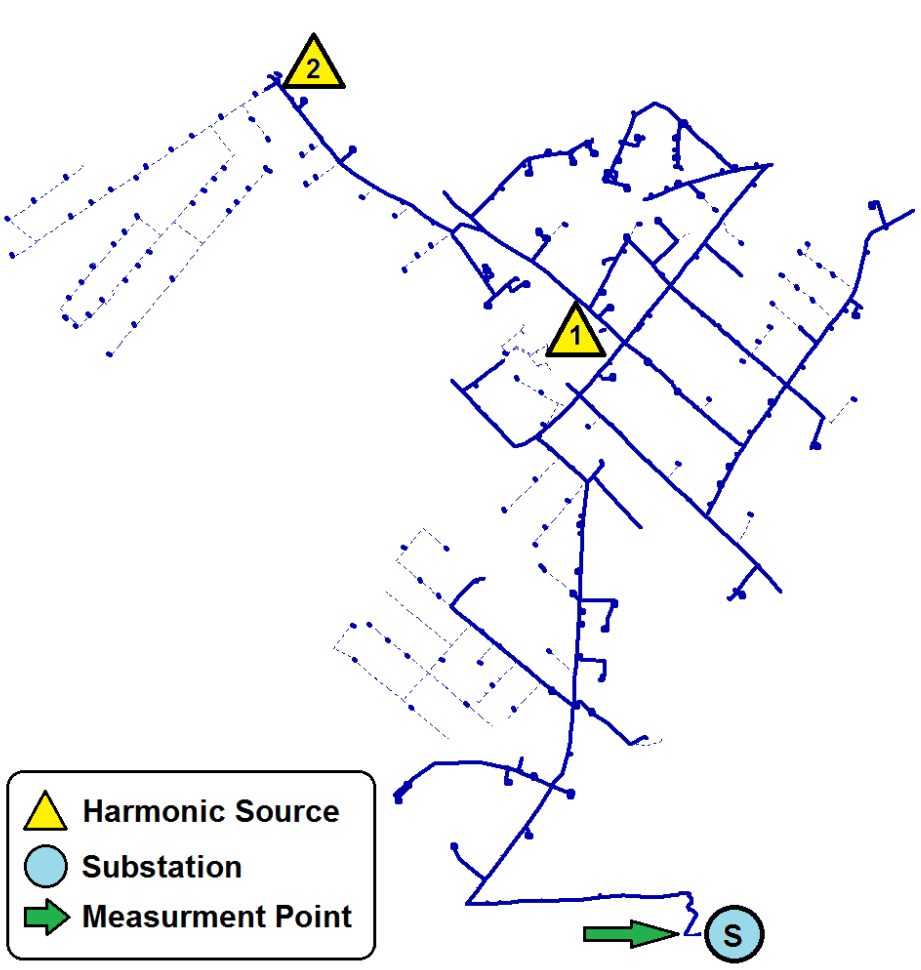

Figure 5-3 Schematic of distribution network model

5.4. Simulations, Results, and Discussions

Harmonic current emission through the distribution network is influenced by a number of factors related to the harmonic source and circuit characteristics. In this section, multiple harmonic source interactions based on different values of harmonic source magnitudes and angles are analyzed. To investigate three phase circuit loading effects on harmonic distortion, two case studies for unbalanced and balanced circuit are presented.

5.4.1. Simulation Assumptions

There are two 3-phase harmonic sources in the circuit which represent inverters connected to DER sources. It assumed that all three phase have the same current magnitudes. The configuration of three phase angle sequences used in the analysis is presented in Table 5-1 [129].

The inverter technology and DER type are not considered in this research. The research aim is the harmonic impact study apart from the harmonic source technology.

The dominant current and voltage harmonic observed through the simulation are of the 3ed, 5th, 7th, 9th and 11th orders. Harmonics of higher orders are neglected via their small values.

Table 5-1 Three Phase harmonic Angle Sequence

Order	Frequency	Sequence
0	60	+
3	180	0
5	300	-
7	420	+
9	540	0
11	660	-

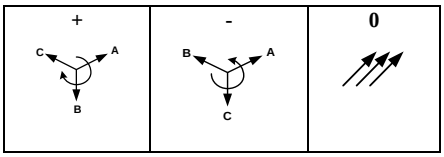

5.4.2. Impact of Multiple Harmonic Source Magnitudes

To show the effects of harmonic current source magnitude on the THD at the substation level, the simulation is conducted for different current magnitudes in the range from zero to ten (0, 2, 4, 6, 8, 10) amperes for both harmonic sources. The angles follow the sequences in Table 5-1.

Figure 5-4 and Figure 5-5 show respectively the variation of phase B THDI and THDV at the substation as a function of variation of the harmonic current source magnitudes. The HS in plots means harmonic source.

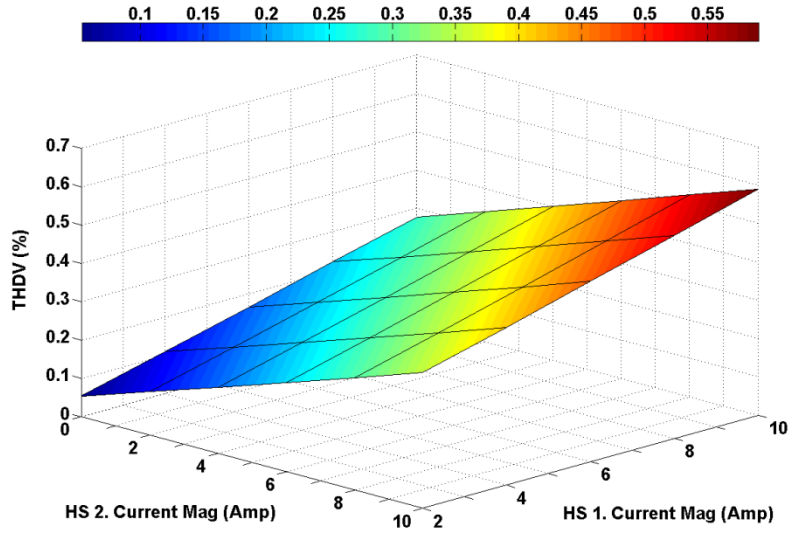

Figure 5-4 Multiple harmonic source THDV for different current magnitudes

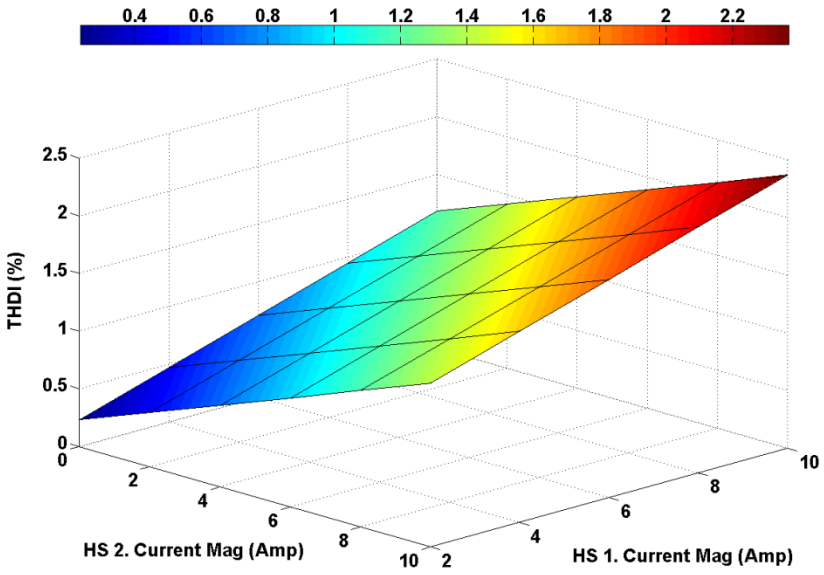

Figure 5-5 Multiple harmonic source THDI for different current magnitudes

Figure 5-4 and Figure 5-5 illustrate that the THD increases with increasing harmonic source magnitudes, and that the two sources act together to increase the THD. In Figure 5-4 and Figure 5-5, the surface cuts along the X (HS1) and Y (HS2) axes showing the rate of THDI and THDV increase versus magnitude of each harmonic source. The HS1 and HS2 slopes for THDI are 2.46 and 2.38 respectively. This means HS1 has more impact on total THDI at substation. The HS1 and HS2 slopes for THDV are

0.06 and 0.055 respectively. It is similar to the slopes observed with THDI. The IPHV for phase B is illustrated in Figure 5-6.

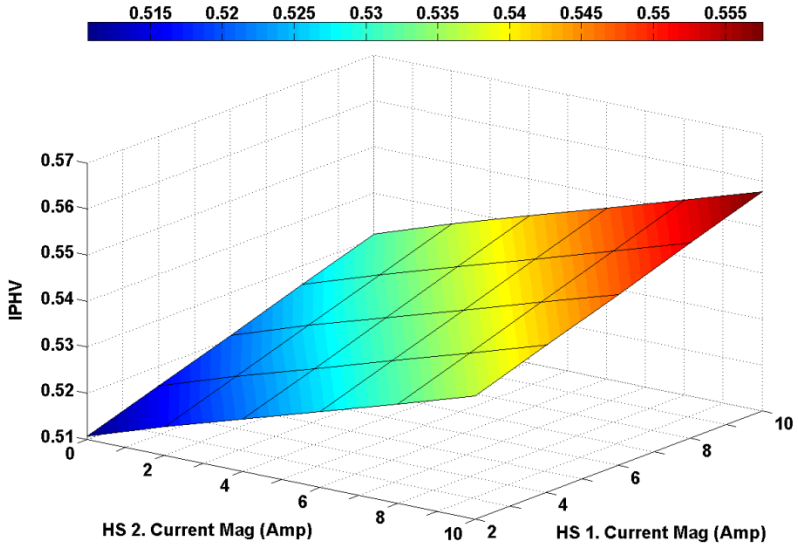

Figure 5-6 Multiple harmonic source IPHV for different current magnitudes

Figure 5-7 depicts the total power factor calculated values from equation (5-11). The surface in Figure 5-7 is descending gradually to lower power factor values as harmonic source magnitudes increase. Higher total power factor values mean less loss in the distribution network.

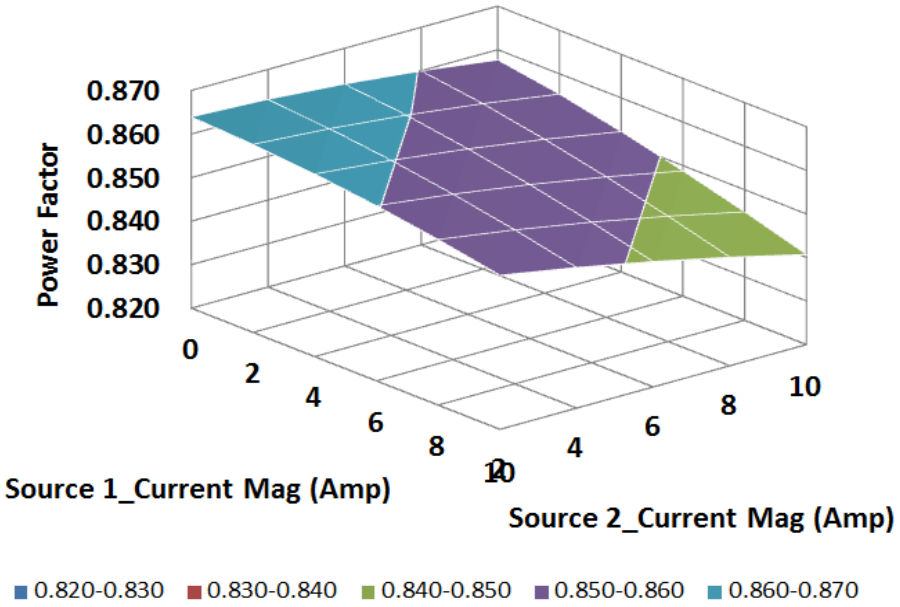

Figure 5-7 Multiple harmonic source total power factor for phase A for different current magnitudes

The presented results show how two harmonic source magnitudes increment interactively increases the total harmonic distortion and energy loss in distribution networks. Simulation results for phase B and phase C show the similar trend for THDV, THDI, IPHV and TPF.

5.4.3. Impact of Multiple Harmonic Source Angles

In systems with multiple harmonic sources, the injected harmonic current from each source add vectorally. Therefore, it is crucial to study the impact of each harmonic source phase angle on the total harmonic distortion. To perform a sensitivity analysis against phase angle values, a number of harmonic simulations were performed with the phase angles steps for both harmonic sources being varied as follows: (0°, 15°, 30°, 45°, 60°, 75°, 90°). These angles steps are added to the phase angle sequences presented in Table 5-1. When varying the angles of the harmonic sources, the magnitudes of both harmonic sources are maintained at 4 amps. Figure 5-8, Figure 5-9 and Figure 5-10 depict the THDV for different phase angle values.

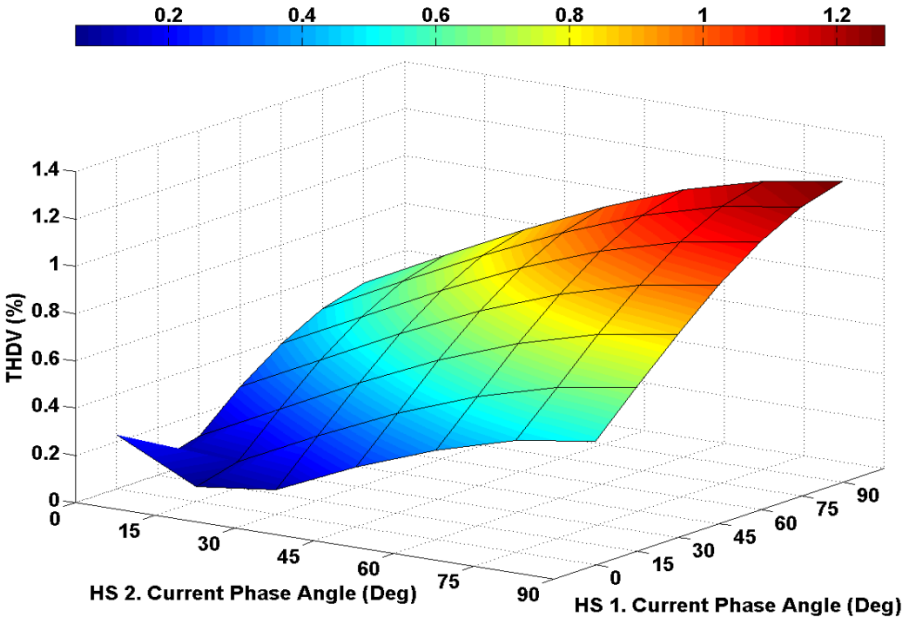

Figure 5-8 Harmonic source 1 and 2 THDV for phase A

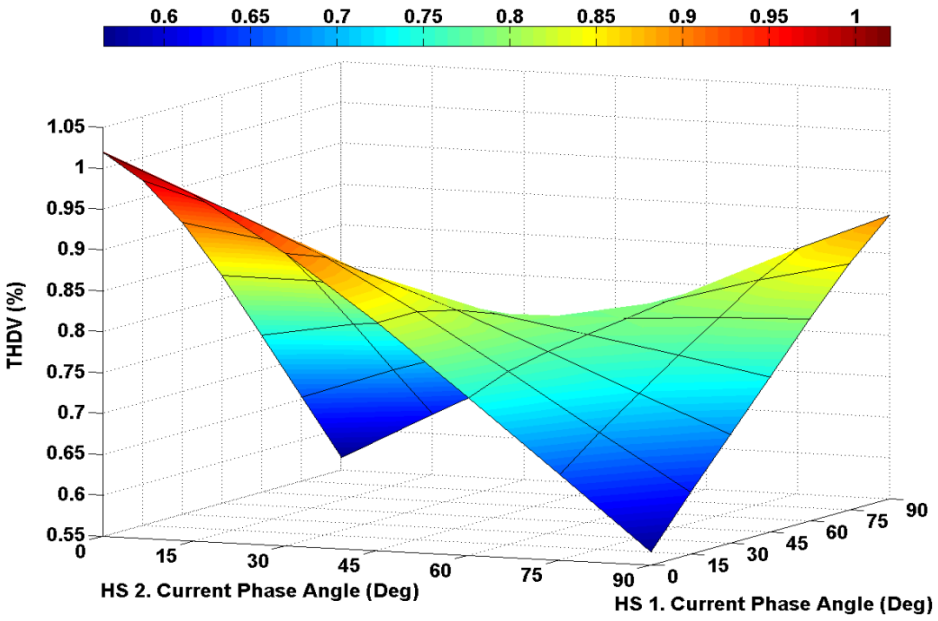

Figure 5-9 Harmonic source 1 and 2 THDV for phase B

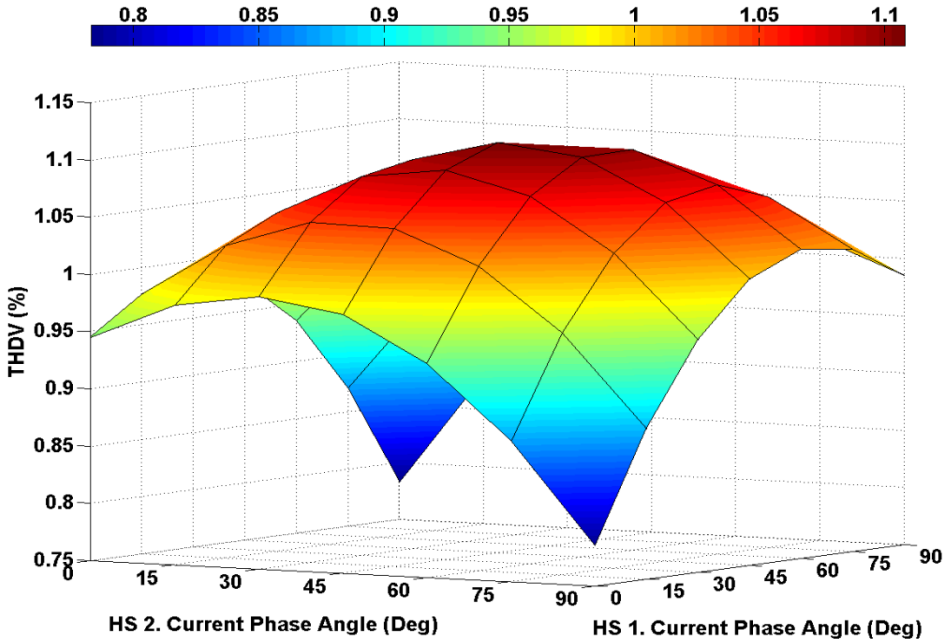

Figure 5-10 Harmonic source 1 and 2 THDV for phase C

Figure 5-8, Figure 5-9 and Figure 5-10 present THDV for each of the three phases. As may be seen from these figures, the THDV vs. angle plot for each phase is significantly different than the other phases. Reasons for this are the different phase loadings (see Table 5-2), the three phase mutual couplings (see Table 5-3), and network topology. Moreover, the portion of single phase lines and underground cables in the distribution network affect the harmonic emissions because of the capacitance characteristics of such conductors.

Table 5-2 Unbalanced Circuit Loading

	Ph. A	Ph. B	Ph. C
Connected Load (kW)	818.25	429.58	476.29
Connected Load (kVar)	468.53	254.45	273.17
Current Flow (Amps)	126.86	67.31	73.29

The distribution network is unbalanced. Its phase loading at the substation is presented in Table 5-2. The values are achieved from the power flow analysis at the fundamental frequency. Table 5-2 shows the network sequential Thevenin impedance as seen by harmonic source 1 and the harmonic source 2 in the circuit.

Table 5-3 Network Thevenin Impedance as Seen by Harmonic Sources

		0	1	2
Harmonic Source 1	0	0.8063+ 2.9308j	-0.0102+ 0.0138j	0.0086+ 0.0155j
	1	0.0086+ 0.0155j	0.8063+ 2.9308j	-0.0102+ 0.0138j
	2	-0.0102+ 0.0138j	0.0086+ 0.0155j	0.8063+ 2.9308j
Harmonic Source 2	0	1.0368+ 3.6547j	-0.0122 +0.0155j	0.0098+ 0.0179j
	1	0.0098+ 0.0179j	1.0368 + 3.6547j	-0.0122+ 0.0155j
	2	-0.0122+ 0.0155j	0.0098 + 0.0179j	1.0368+ 3.6547j

The THDV surface shapes are similar to the hyperbolic geometrical functions. Figure 5-8 shows the THDV for phase A. It is a semispherical cliff with the minimum values at zero phase angles for both sources. The maximum values achieved with 90 ° phase angle in both sources (THDV=1.27). Figure 5-9 presents THDV for phase B. It is a saddle-shaped surface with saddle point at 45° phase angle in both sources (THDV=0.799), the maximum THDV values happen in 0° and 90° angles for both sources. Figure 5-10 is similar to a hemispherical plane with its maximum at 45° phase angle for both sources (THDV=1.1).

Figure 5-11, Figure 5-12, and Figure 5-13show the THDI surfaces for the phases at the substation for the variation over the harmonic source phase angles.

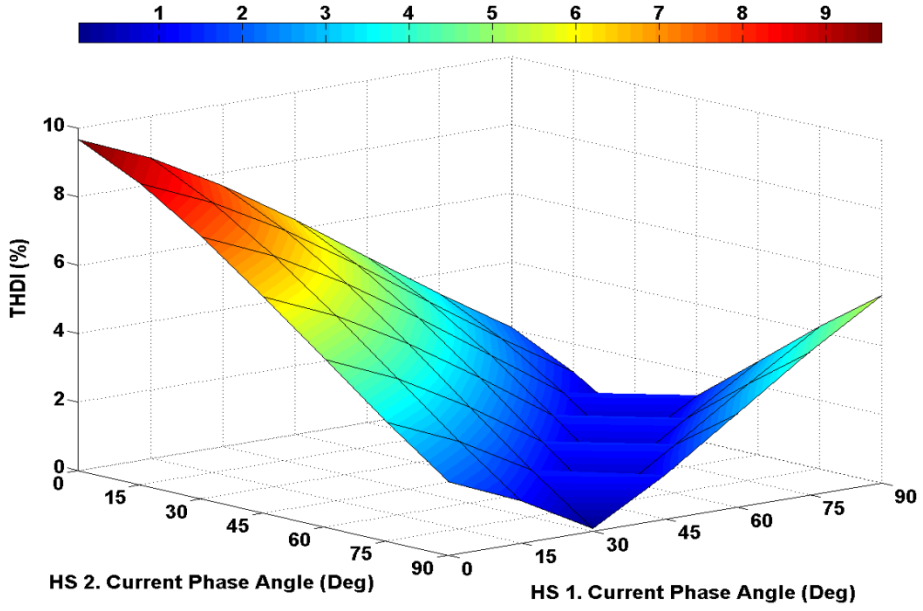

Figure 5-11 THDI for phase A for different angles

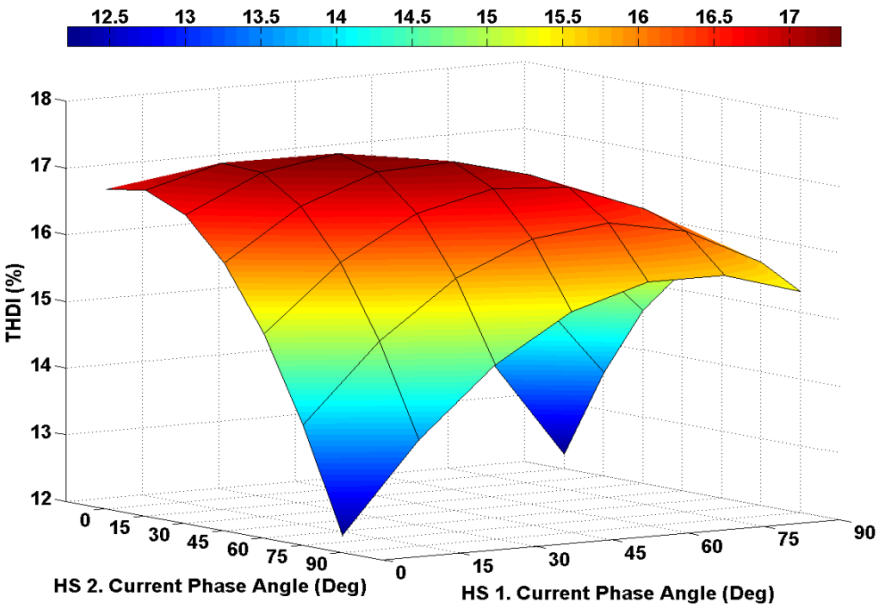

Figure 5-12 THDI for phase B for different angles

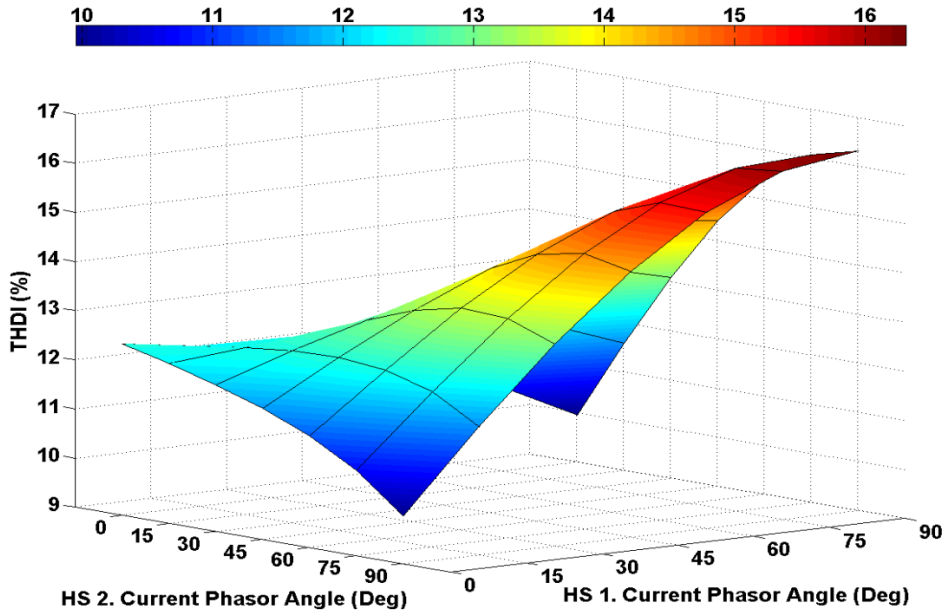

Figure 5-13 THDI for phase C for different angles

Figure 5-11 especially has interesting characteristics. There is a canyon on the surface where the THDI values are almost zero. In those near zero points, the harmonic sources cancel out each other and

cause the minimum current harmonic distortion. It is an important observation for harmonic distortion cancelation in mutli-source harmonic analysis. Table 5-4 shows the near zero points (minimum THDI points) for phase A that the canyon in Figure 5-11 passes through.

Table 5-4 THDI Cancelation for Phase A with Different Phase Angles

	H Source 1. Angle (Deg)	H Source 2. Angle (Deg)	Delta Angle	THDI (%)
Min THDI 1	30	90	- 60	0.074
Min THDI 2	45	75	- 30	0.049
Min THDI 3	60	60	00	0.042
Min THDI 4	75	45	+ 30	0.039
Min THDI 5	90	30	+ 60	0.043

Figure 5-12 is THDI for phase B. It has semi- hemispherical plane with its maximum at 45° phase angle for both sources (THDI=17.23). Figure 5-13 is a semispherical cliff with the minimum values at (source 1 phase angle 90° – source 2 phase angle 0°) and (source 1 phase angle 0° – source 2 phase angle 90°) with THDI = 9.95. The maximum values achieved with 90° phase angle in both sources (THDV=16.13).

The THDV and THDI observations show the maximum distortion values are around 0°, 45°, and 90° phase angles. For these harmonic source angles, the maximum THDV versus phase angle has the following trend: (Max THDV- Phase A at 90°, Max THDV-Phase B at 0°, Max THDV- Phase C at 45°). A similar trend for THDI is: (Max THDI-Phase A at 0°, Max THDI-Phase B at 45°, Max THDI-Phase C at 90°). The presented THD sensitivity analysis shows the harmonic sources' critical angles for voltage and current distortion. It is a helpful tool for harmonic minimization and harmonic control purposes.

Figure 5-14, Figure 5-15, and Figure 5-16 show the proposed Index of Phase Harmonic for Voltage (IPHV) which is defined in (5-10). Because of the contribution of the phase angle in the IPH numerator, IPH contains more information than THD. The IPH values are smaller or equal to 1, because of the "Triangle Inequality" property in a vector space.

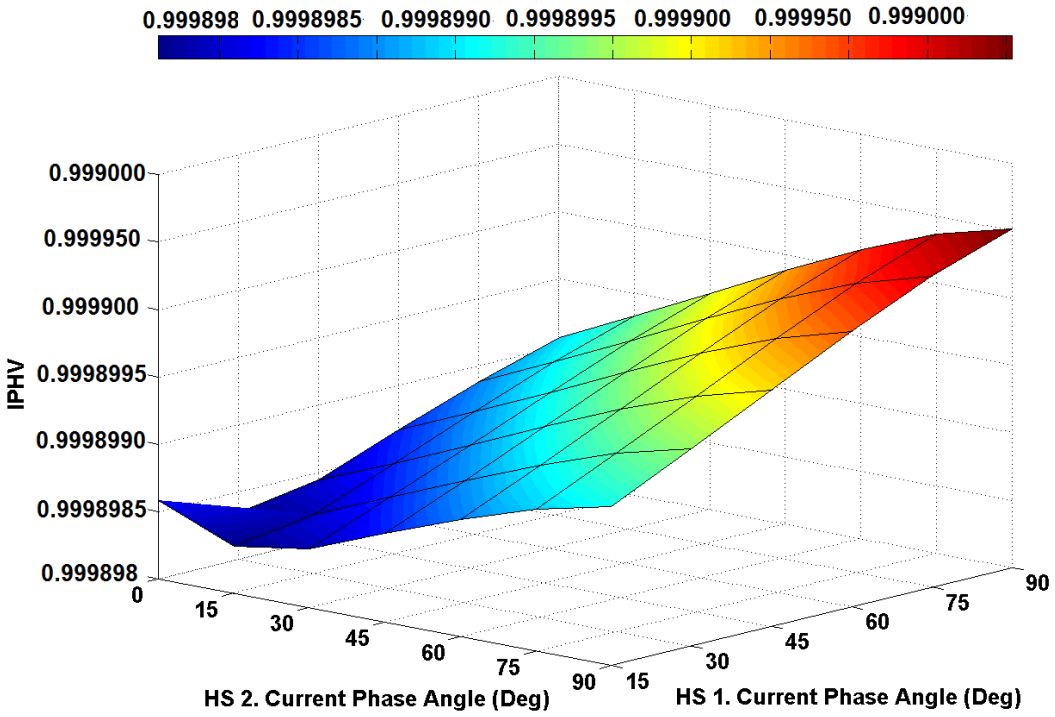

Figure 5-14 Phase A multiple harmonic source IPHV for different angles

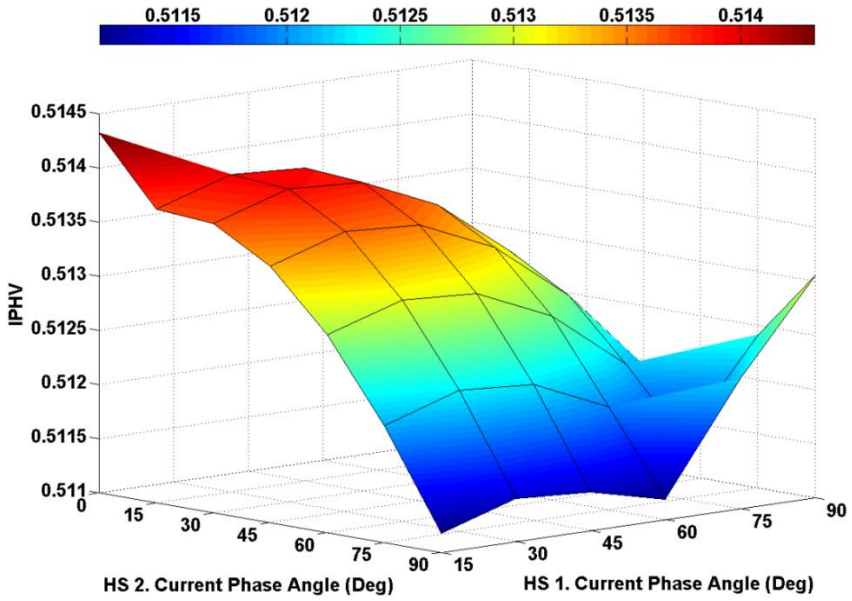

Figure 5-15 Phase B multiple harmonic source IPHV for different angles

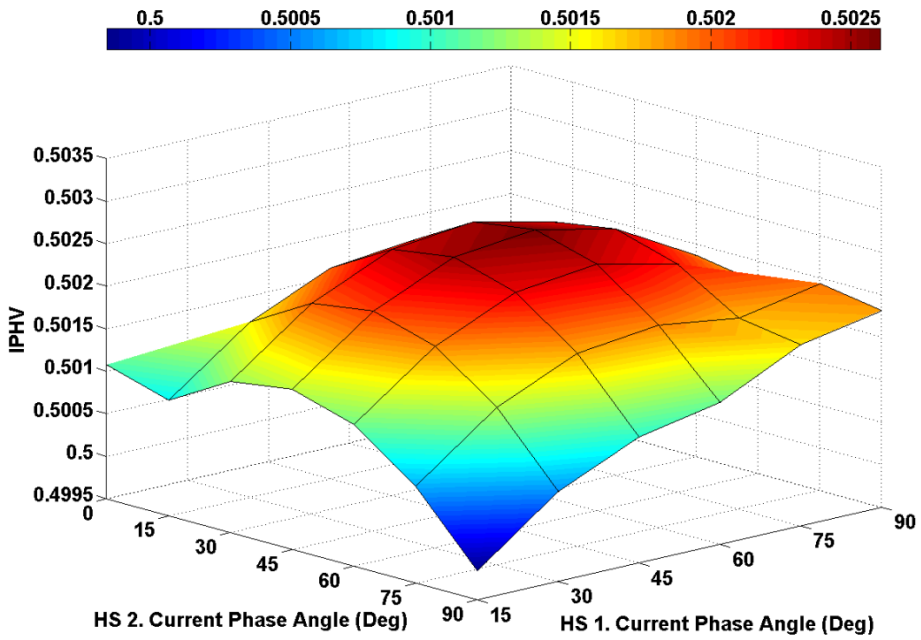

Figure 5-16 Phase C multiple harmonic source IPHV for different angles

Comparing the IPHV surfaces in and THDI and THDV surfaces shows an interesting relationship between IPHV, THDV and THDI geometrical representations for each phase. (Compare Figure 5-14 with Figure 5-8 plus Figure 5-11), (Compare Figure 5-15 with Figure 5-9 plus Figure 5-12) and (Compare Figure 5-16 with Figure 5-10 plus Figure 5-13). The IPHV surface geometry is similar to the summation of THDI and THDV surfaces with a different scale.

Figure 5-14 presents IPHV for phase A. It shows IPHV increases with phase angle increase in both sources. The trend is less curvy than the THDV. In Figure 5-15, higher IPHVs occur in smaller phase angles. Its geometrical shape is a mix of THDV and THDI. Figure 5-16 depicts the IPHV for phase C. It shows the highest IPHV happens at a 45° phase angle for both harmonic sources. The IPHV observations illustrate that IPH has more information than THDI and THDV, because it contains phase and magnitude values. It simultaneously quantifies aspects of the THDI and THDV characteristics in one index.

Figure 5-17 shows the total power factor (TPF) for phase A. The surface has a semi-hilltop form. Higher total power factors means less loss which leads to more profit for distribution network operator.

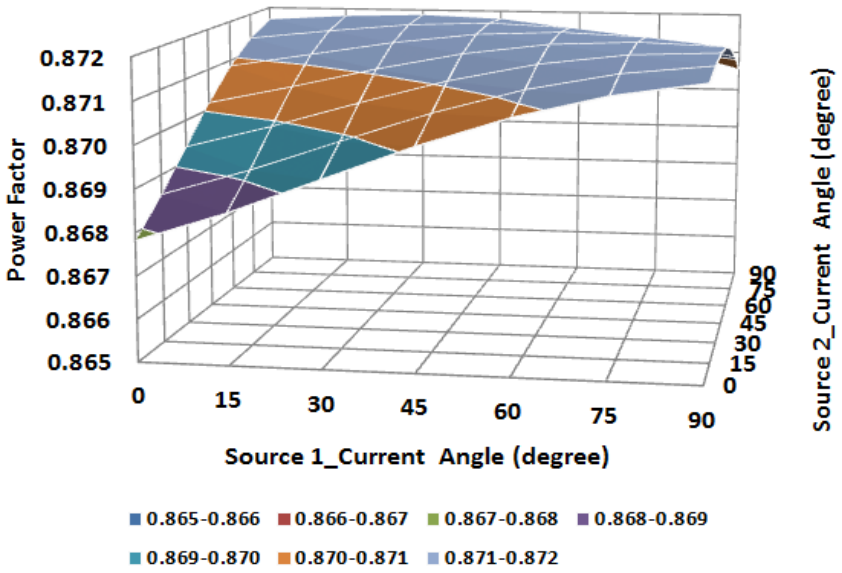

Figure 5-17 Multiple harmonic source total power factor for phase A for different current phase angles

The maximum total power factor points are presented in Table 5-5.

Table 5-5 Maximum TPF Points for Phase A with Different Phase Angles

	H Source 1. Angle (Deg)	H Source 2. Angle (Deg)	Delta Angle	TPF
Max TPF 1	30	90	- 60	0.871
Max TPF 2	45	75	- 30	0.871
Max TPF 3	60	60	00	0.871
Max TPF 4	75	45	+ 30	0.871
Max TPF 5	90	30	+ 60	0.871

Figure 5-18 illustrates TPF for phase B. The TPF plot is similar to a semi-spherical surface with minimum value at 30° phase angle for both harmonic sources (TPF=0.8406). The maximum TPF happen at (0°, 90°) and (90°, 0°) points with TPF=0.846.

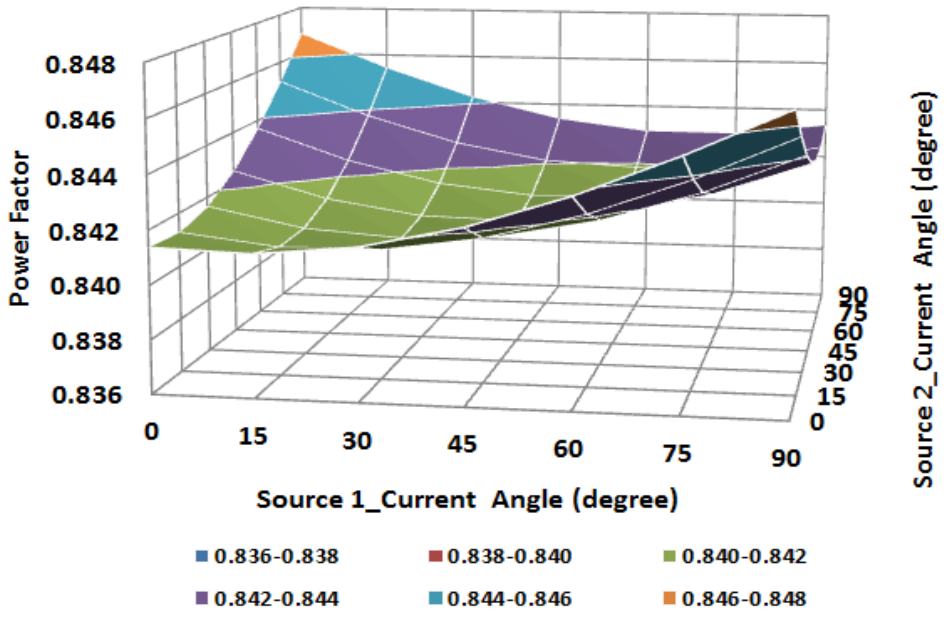

Figure 5-18 Multiple harmonic sources total power factor_phase B for different current phase angles

Figure 5-19 shows TPF values for phase C. It has a saddle-shaped surface. The maximum TPF points occurs at (0°, 90°) and (90°, 0°) points with TPF=0.865.

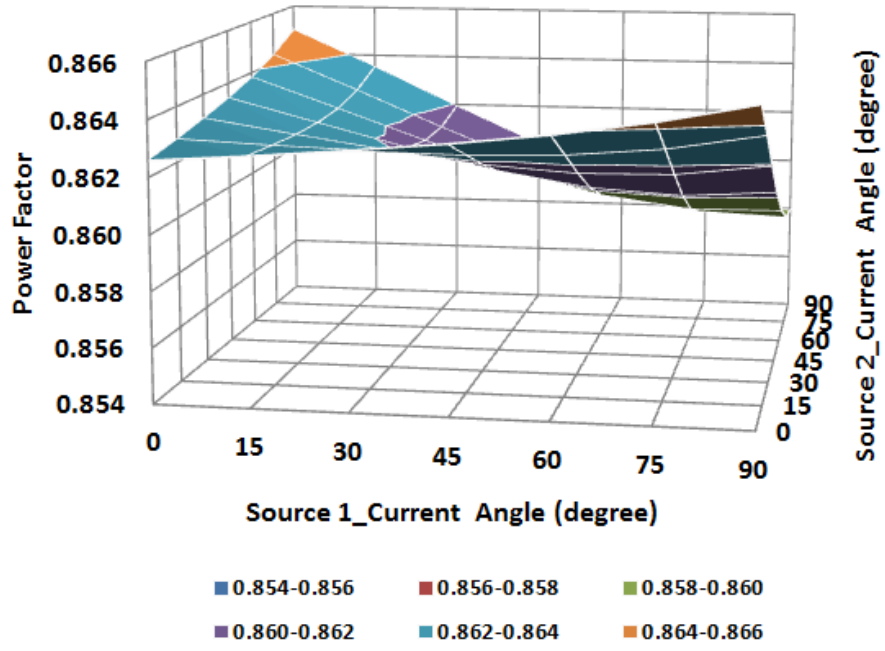

Figure 5-19 Multiple harmonic sources total power factor_phase C for different current phase angles

The presented observations show that considering Total Power Factor (TPF) in addition to the Total Harmonic Distortion (THD) provides a better picture of multiple-harmonic sources impacts and interactions. The impact of phase angle variation on interactive multiple source harmonic distortion is especially helpful for harmonic distortion minimization and power factor improvement. Any improvement in power factor via the multiple harmonic sources' control has economic value for distribution network operators and stockholders.

It is worthwhile to mention that the presented investigation on harmonic source phase angle variations aims to show how phase angle of each harmonic source can impact the overall harmonic distortion at the substation (or other locations in distribution network). However, the inverter control and active filter design are not subjected in this research. To implement harmonic controller, the power electronic constraints for harmonic control and active filter design considerations should be taken into account.

5.5. Chapter Outcomes and Conclusions

The domain of harmonic propagation in distribution networks needs to be extended due to the steady increase in inverter based components in the smart grid. In this chapter, the authors evaluate multiplesource harmonic distortions with the help of a detailed distribution network model with secondary system customer loading modeled. Moreover, a new index, Index of Phasor Harmonics (IPH), is proposed for harmonic analysis in multiple harmonic source cases. Several simulations and analysis were performed on the distribution network model based on commonly used harmonic indices and the proposed IPH index. The main outcomes of this chapter are as follows.

1) The proposed IPH index presents more information than THD because it incorporates phase angle information in addition to the harmonic source magnitudes, which is crucial in multiple harmonic source cases. The geometrical visualization approach is used to show the effectiveness of IPH in comparison with THDI and THDV.

2) Multiple harmonic source magnitudes act together to change the harmonic distortion in the circuit. In the case of harmonic source magnitude increases, the distortion increases at the substation with increases in the harmonic source magnitudes. The harmonic source that is closer to the substation has more impact.

3) Multiple harmonic source phase angles have a more complex impact on harmonic propagation because of the vectorial impact of injected harmonic currents. The way that phase angles act together is highly dependent on the network topology, mutual conductor impedances and phase balance. The

resultant harmonic distortion in the distribution network can increase or decrease due to the deviation of phase angles in different harmonic sources. In some cases, phase angles can result in canceling out the interactive multiple harmonic source distortion. Moreover, the phase angles that apparently boost harmonic distortion need to be observed precisely. In this chapter, the THD and IPH indices along with the geometrical data visualization show how phase angle variations affect harmonic distortion.

4) Phase balance is a significant factor for harmonic emission in distribution networks. In this chapter it is demonstrated that phase balance can help reduce harmonic distortion.

Finally, multiple-source harmonic impact studies can help distribution network planners and operators have a better picture of the potential effects of harmonic interactions.

Chapter 6 : Topological Assessment of Interactive Harmonics from Distributed Energy Resources

6.1. Introduction

The advent of Smart Grid is bringing a steady increase in inverter-based components like Distributed Energy Resources (DER), energy storage systems, and plug-in electric vehicles. The resultant harmonics from DER inverters and the spread of power electronic-based appliances create concerns for power system operators and engineers. Harmonic propagation causes distortion in voltage and current waveforms in different parts of distribution networks. Harmonics generated by different harmonic sources can interact to either increase or decrease the effects of harmonics.

The harmonic impact on power systems is a well-researched topic. Harmonic measurement and filtering in power systems are discussed in [136, 137]. However, existing research mostly considers harmonics as a local phenomenon with local effects [64, 138]. There are a few papers that focus on DER harmonics [67-69]. Authors in [96, 139] focus on harmonic filter design for DER units. However, the proposed solutions are local approaches for controlling each inverter.

Even less literature investigates the impact of harmonic propagation in distribution networks. Authors in [61] proposed a method to find harmonic source locations in distribution networks. However, the authors use the Norton equivalent model for the distribution network. [73] analyzes harmonic distortion in different distribution transformer types. [74] conducts a sensitivity analysis to find vulnerable buses in distribution networks. But, the authors use the Thevenin equivalent model at each bus instead of the full topological model of the circuit. [60, 62] show the impact of aggregated harmonics from Distributed Generation units in distribution networks. However, they use single-phase equivalent line models and do not consider multi-phase line models.

The harmonic investigation in this dissertation benefits from the detailed distribution network model employed. The model employed has large numbers of single phase, multi-phase, and unbalanced equipment and loads. This detailed model provides for more realistic harmonic propagation simulations. This detail of distribution system modeling is not addressed in previous harmonic analysis literature. This dissertation seeks to investigate the impact of distribution network topology and phase couplings on harmonic propagation more precisely and realistically.

This dissertation also seeks to investigate the interactions of multiple harmonic sources. The way DER inverters can work together to either decrease or increase harmonic distortion throughout the distribution network is investigated.

There are a few papers that consider the impact of phase balance on harmonics [71, 72, 140]. However, they are all at the device level. That is, they focus on harmonic and load balancing in transformers and inverters. The other novelty of this dissertation is analyzing the impact of phase balance on harmonic distortion.

In terms of harmonic distortion quantization, the Total Harmonic Distortion (THD) is the most common index in standards and literature [65, 66]. But, THD is based only on the magnitude of the distorted waveforms. In this dissertation a new index is proposed called the Index of Phasor Harmonics (IPH). IPH incorporates both magnitude and phase angle information in evaluating distorted waveforms resulting from the interaction of multiple harmonic sources. The advantages of IPH as compared to common harmonic indexes are illustrated in case studies. As harmonics from different harmonic sources propagate and interact, the interactions can result in harmonics being reduced or increased. This dissertation seeks to provide further insight into such interactions.

The chapter is organized as follows: Section 2 discusses harmonics analysis. Section 3 describes the analysis of harmonic propagation from multiple sources and topology and loading effects on harmonics. Section 4 presents simulations and results.

6.2. Harmonic Analysis Architecture

The ISM architecture for the harmonic analysis is illustrated in Figure 6-1.

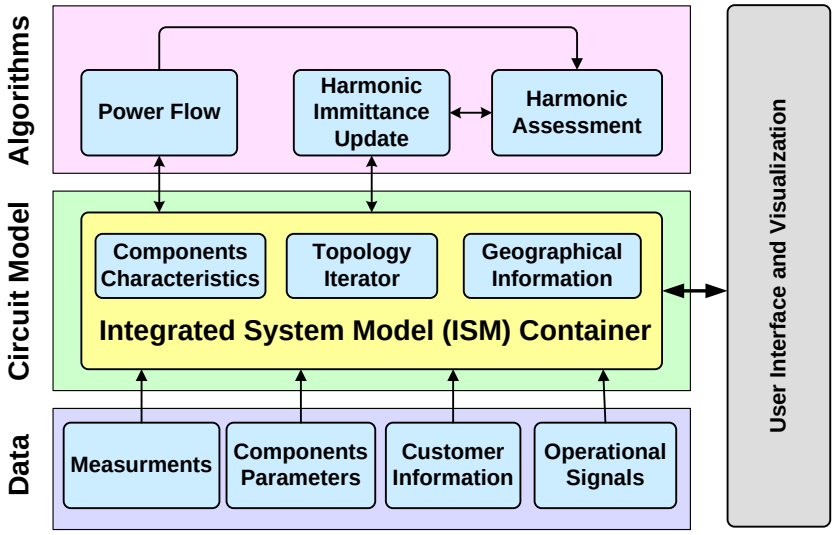

Figure 6-1. Architecture of Harmonic Analysis

The data layer contains data interfaces for the distribution network model. The measurements, component parameters, customer information, and operational signals, like distribution network operator commands, are attached to the ISM model. The ISM is explained in section 2.1. The customer information includes customers' class and time varying load data.

The harmonic assessment algorithm first uses power flow analysis to calculate the fundamental voltage and current waveforms. Then, the circuit is modified to represent the next higher frequency to be analyzed. The circuit modifications involve revising the network component impedances and the harmonic current injections for the harmonic order to be analyzed. Next the power flow runs to determine the harmonic current and voltage emissions in the circuit for the given harmonic order. This type of analysis is continued until all harmonic orders to be analyzed are completed.

Harmonics are affected by configuration, impedance, and loading of conductors, transformers, and other circuit components. Figure 6-2 illustrates the flow of the harmonic assessment algorithm.

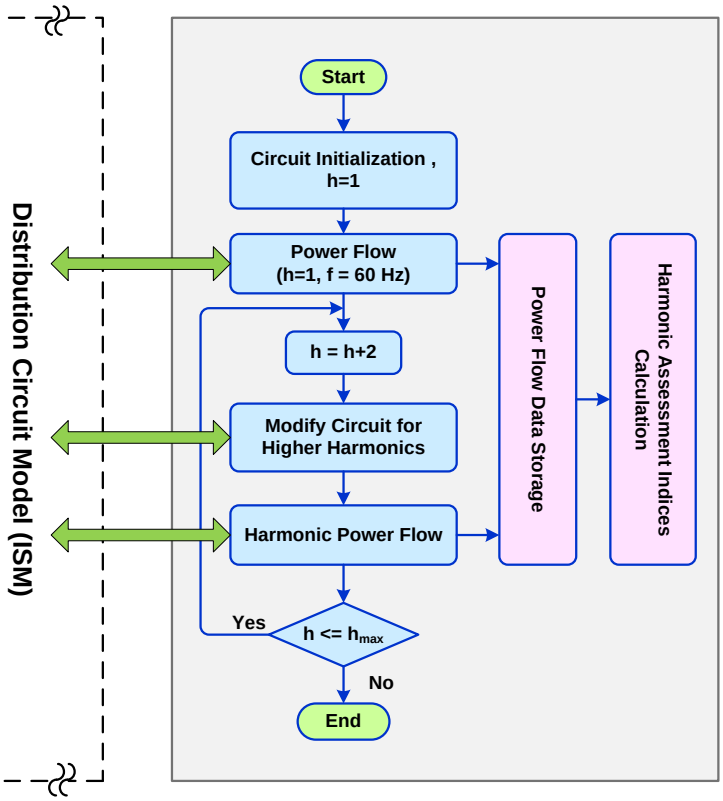

Figure 6-2. Flow chart for Harmonic Assessment

For the power flow calculation, the Distributed Engineering Workstation (DEW) software package is used. The "Power Flow Data Storage" stores fundamental and higher order harmonic power flow results that are used to calculate harmonic assessment indices. In the work here, hmax is 11 and the odd harmonic orders are taken into account.

6.3. Topological Analysis of Harmonic Propagation from Multiple Sources

Harmonic propagation in distribution networks with a number of harmonic sources, like DERs, depend on a number of factors related to harmonic sources and distribution network characteristics. In this section the impact of harmonic source phase angle on harmonic propagation with multiple sources is addressed. In addition, how network topology, variations in harmonic phase angle injections, and load balance impact harmonic propagation are investigated.

6.3.1. Salient Features of Simulation

The research objective is the harmonic impact study apart from the harmonic source technology. There are two 3-phase harmonic sources in the distribution network. All phases of the harmonic sources have the same magnitudes. The harmonic magnitudes are based on measurement data from field tests as shown in Figure 6-3. The dominant current and voltage harmonic observed through the simulation are of the 3rd, 5th, 7th, 9th and 11th orders. Harmonics of higher orders are neglected due to their small values. The phase rotation sequences of the harmonic source phase angles are presented in Table 6-1, where positive, zero, and negative sequence rotations are indicated with +, 0, and -, respectively.

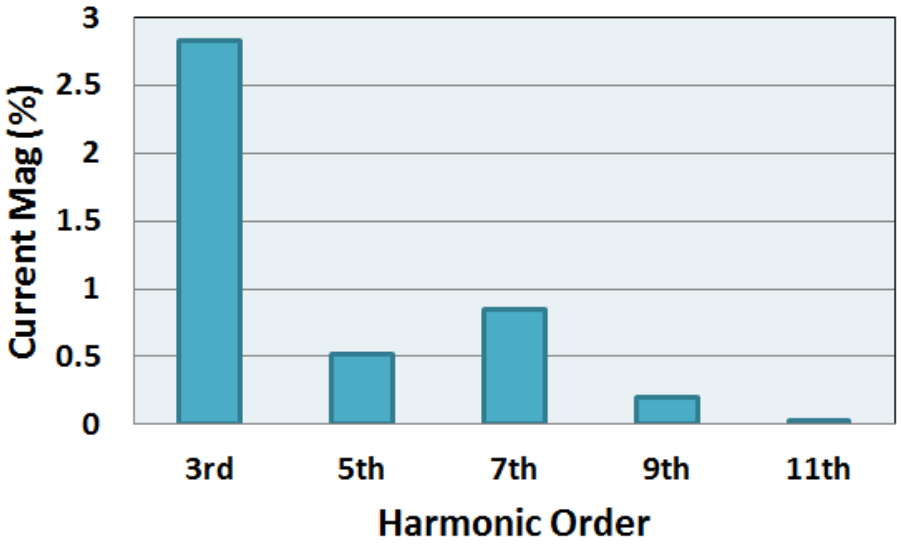

Figure 6-3. Harmonic source magnitudes from field measurement data

Table 6-1 Three Phase harmonic Angle Sequences

Order	Frequency	Sequence
0	60	+
3	180	0
5	300	-
7	420	+
9	540	0
11	660	-

In this chapter, a geographically based, full-topology model is applied as shown in Figure 6-4. The circuit is 13.2 kV with 329 residential and commercial customers. The peak load is 9.5 MVA. The model contains unbalanced, single phase and multi-phase loads, and includes distribution transformers. The two harmonic sources studied are indicated with triangular symbols. The harmonic calculations are presented at two points indicated by arrows in Figure 1. The first point is the substation, and the second point is at the secondary of a distribution transformer between the two harmonic sources.

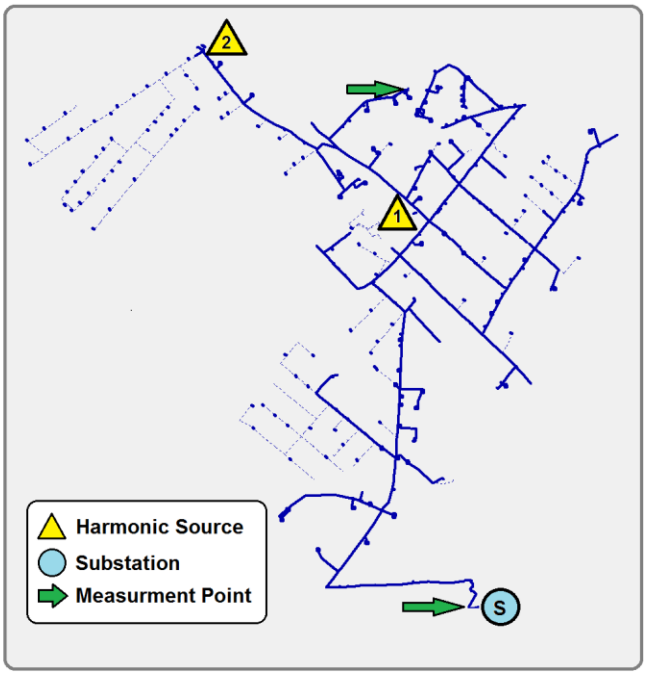

Figure 6-4. Schematic of distribution network model used for studying interactions of multiple harmonic sources, Triangle indicate locations of harmonic sources and arrows indicate locations where harmonics are evaluated.

6.3.2. Impact of Phase Angle Variation on Harmonic Emission Interactions

In systems with multiple harmonic sources, the harmonic distortion interactions are impacted by the vectorial characteristics of the injected harmonic currents. The impact of each harmonic source's phase angle is investigated in this section. For sensitivity analysis purposes, harmonic source phase angles vary as follows: (0°, 15°, 30°, 45°, 60°, 75°, 90°). These steps in angle are added to the phase angle sequences

presented in **Error! Reference source not found.**. When varying the phase angles of the harmonic sources, the magnitudes of both harmonic sources are maintained as given in Figure 6-3. Figure 6-5 shows THDV for different phase angle values at the substation point for each of the three phases.

As illustrated in Figure 6-5, there are significant differences between THDV for the different phases. One reason for the variation of THDV is the different phase loading as presented in . Three phase mutual coupling is another reason for the difference in the harmonic current propagations. Also, the network topology impacts the harmonic propagation. For example, the portion of single phase lines and underground cables in the distribution network affects the harmonic emissions because of the capacitance characteristics of such conductors. The impact of network topology will be discussed in following sections.

Table 6-2. Unbalanced circuit loading at substation

	Ph. A	**Ph. B**	**Ph. C**
Connected Load (kW)	818.25	429.58	476.29
Connected Load (kVar)	468.53	254.45	273.17
Current Flow (Amps)	126.86	67.31	73.29

The THDV surface plots in Figure 6-5 are similar to hyperbolic geometrical functions. Figure 6-5-A shows THDV for phase A with a semispherical cliff with the minimum values at zero phase angle for both sources. The maximum values are achieved with 90° phase angle for both sources (THDV=1.596). For Phase B, Figure 6-5-B, the saddle-shaped surface has the saddle point at 45° phase angle in both sources (THDV=0.873), and the maximum THDV values occur at 0° and 90° for both sources. Phase C has a hemispherical plane with its maximum at 45° phase angle for both sources (THDV=1.484). Observations show that the phase angles of the two harmonic sources affect the minimum and maximum THDV points at the substation.

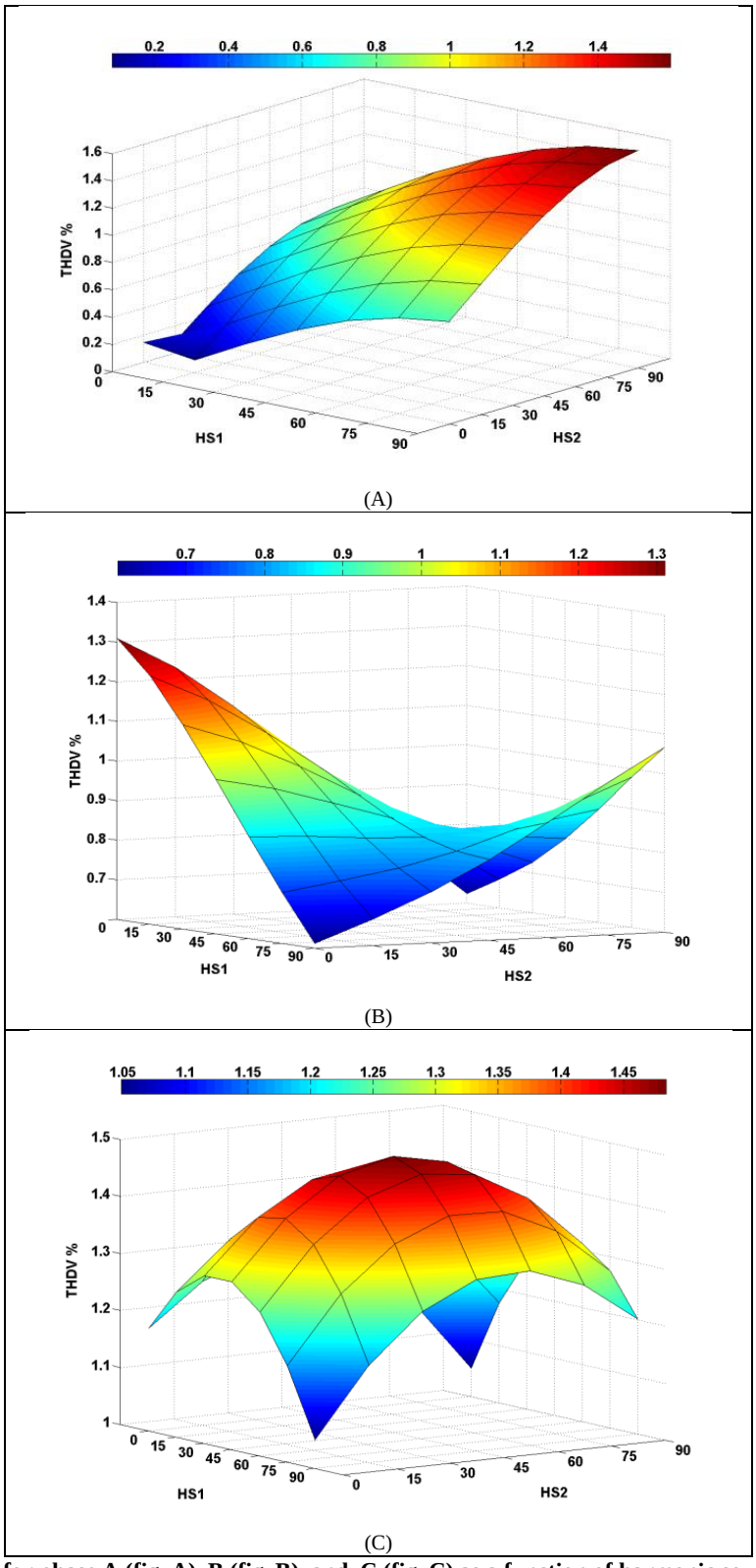

Figure 6-5. THDV for phase A (fig. A), B (fig. B), and C (fig. C) as a function of harmonic source 1 (HS1) and harmonic source 2 (HS2) phase angles.

The THDI surfaces in Figure 6.6 illustrate that the first harmonic source has a larger impact on the harmonic current distortion at the substation. This observation reflects that the first harmonic source is closer to the substation than the second harmonic source. In Figure 6.6-A, the maximum THDI occurs at 0° for the first harmonic source and 90° for the second harmonic source. There is a canyon on the THDI surface for points with minimum THDI values at 45° for the first harmonic source. Finding points with minimum harmonic current distortion is important for harmonic control. At these points, the harmonic source contributions cancel each other out and cause the minimum current harmonic distortion. The THDV and THDI sensitivity analysis shows that the extreme points occur around 0°, 45°, and 90° phase angles.

The THDI and THDV minimum and maximum points are different, as are shown in Figure 6-5 and Figure 6.6. Relying on THDI and THDV brings more complexity to harmonic control in terms of focusing on voltage or current distortion. THDI and THDV are only based on harmonic source magnitudes. The IPHV index (equation 9) results are presented in Figure 6-7.

The IPHV geometrical variations for all phases show more correlation with the THDV surfaces in Figure 6-5 and THDI surfaces in Figure 6.6. However, the maximum IPHV area for each phase is shifted slightly from the high THDV area to the high THDI area. Because the IPHV incorporates phase angle information, it is based on more information than THDV or THDI and this is reflected in the figures.

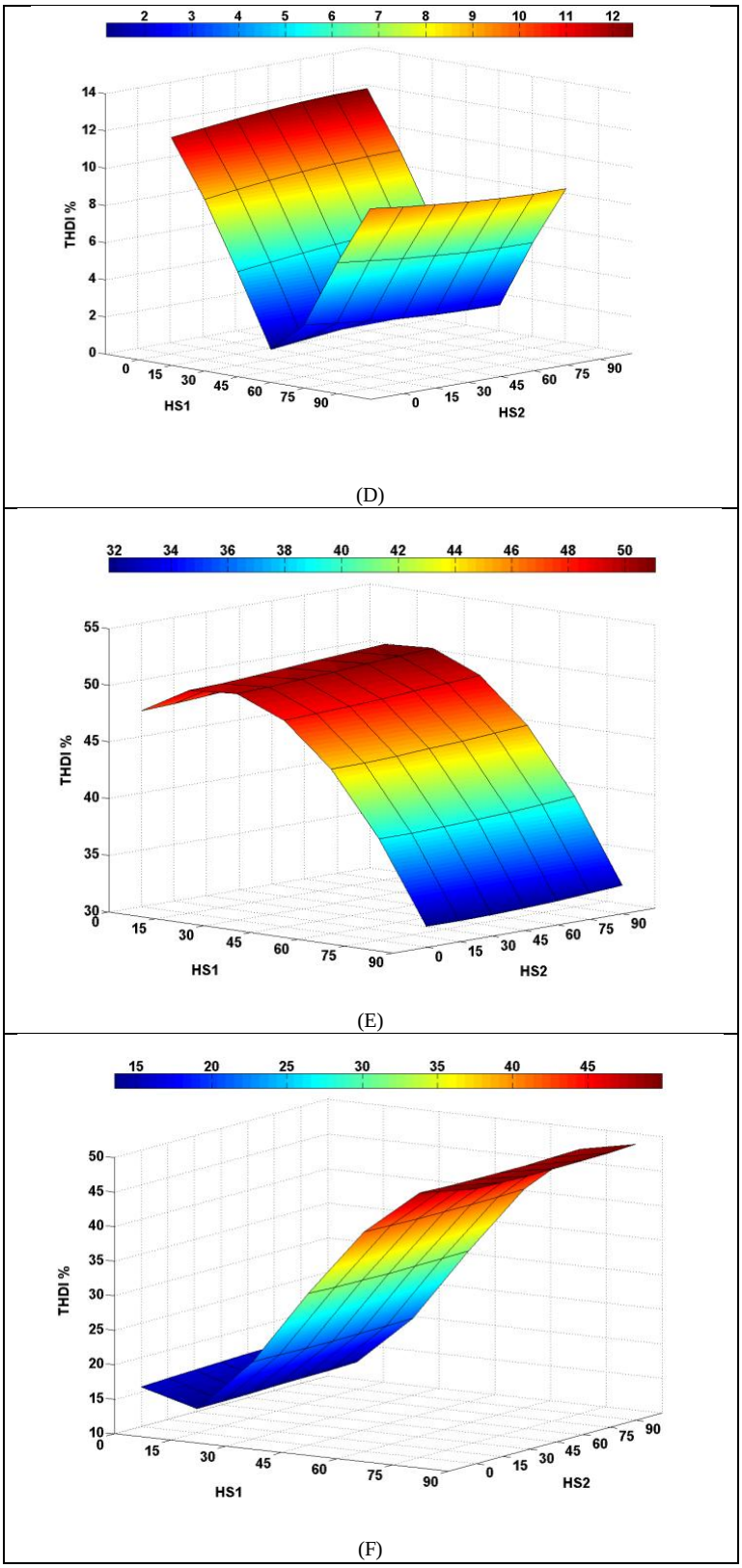

Figure 6-6.THDI for phase A (fig. A), phase B (fig. B), and phase (fig. C) as a function of harmonic source 1 (HS1) and harmonic source 2 (HS2) phase angle.

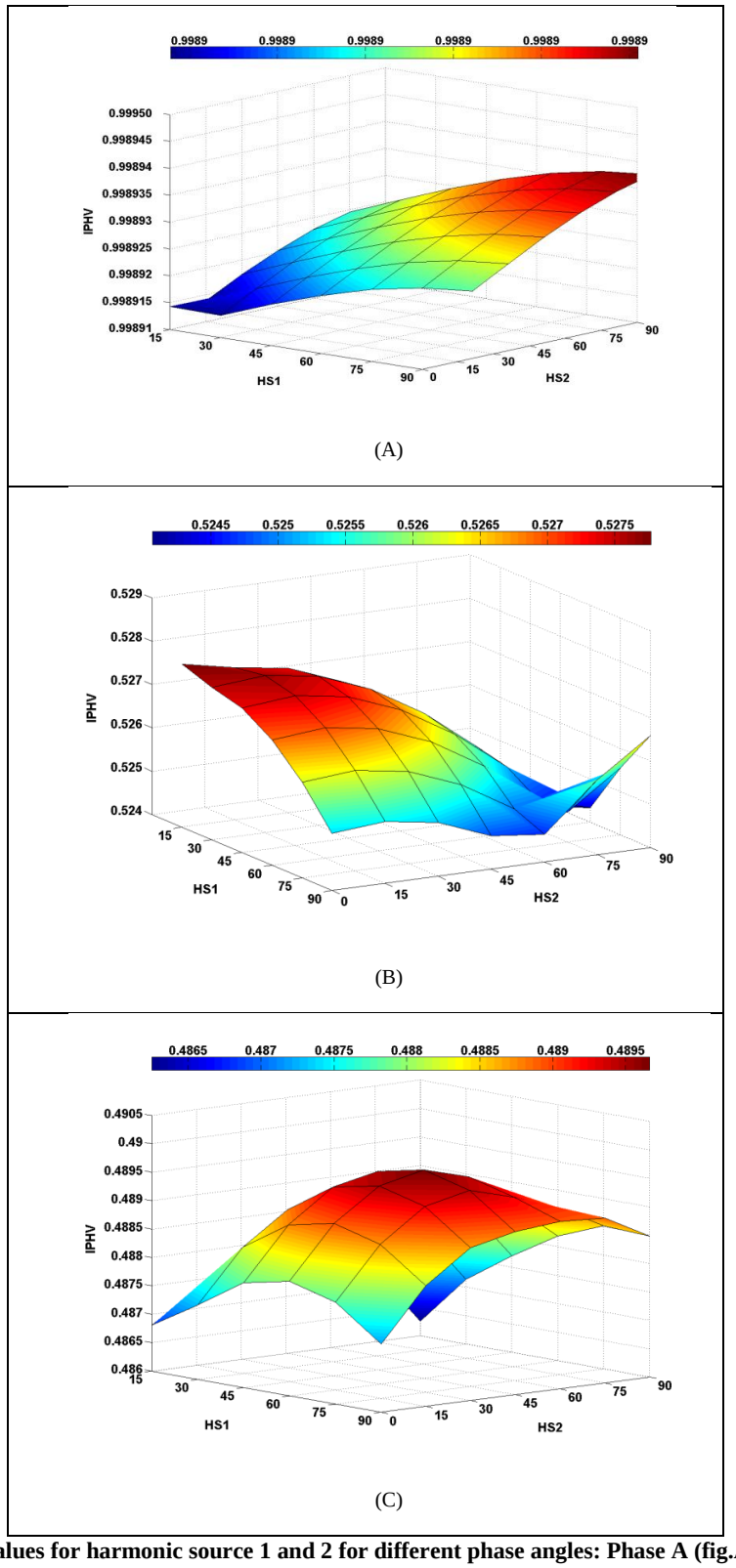

Figure 6-7, IPHV values for harmonic source 1 and 2 for different phase angles: Phase A (fig.A), Phase B (fig.B), and Phase C (fig. C).

The IPHV observation for phase A, Figure 6-7-A, shows more distortion around 90° phase angle for both harmonic sources. In phase B, Figure 6-7-B, the higher distortion area is extended to 0°-45° for both harmonic sources. The IPHV for Phase C, Figure 6-7-C, shows high distortion near 90° for both harmonic sources, as is in the THDI.

6.3.3. Impact of Network Immittance on Harmonic Interactions

Distribution network multi-phase structures, connection types, unbalanced loading and variety of equipment in some ways make for more complexity than transmission networks. The Thevenin equivalent impedance as seen by harmonic sources is applied in this section for sensitivity analysis purposes.

The Phase Thevenin Matrix (PTM) is a 3x3 matrix. It is derived by numerical approaches presented in [141]. To achieve the PTM, a test load is attached between phase and ground in grounded nodes and between two phases in ungrounded nodes. For each test load attachment, power flow is calculated to obtain voltage and current changes caused by the coupling between the phases and the connection point phase. The PTM is

$$\begin{bmatrix} V_{an} \\ V_{bn} \\ V_{cn} \end{bmatrix} = \begin{bmatrix} Z_{aa} & Z_{ab} & Z_{ac} \\ Z_{ba} & Z_{bb} & Z_{bc} \\ Z_{ca} & Z_{ca} & Z_{cc} \end{bmatrix} \times \begin{bmatrix} I_{an} \\ I_{bn} \\ I_{cn} \end{bmatrix} \qquad (6-1)$$

$$\bar{V} = PTM_n \times \bar{I} \qquad (6-2)$$

where the diagonal elements represent, zii, self-impedance of each phase and off-diagonal elements, zij, represent coupling between phases i and j. Equation (13) is the matrix form of (12). The PTMn is the calculated Thevenin impedance at node n. I and V are the three phase current and voltage vectors. The Thevenin impedance matrixes in this section are in the form of ABC impedances. The PTM impedance seen by harmonic sources are as follows:

$$PTM_{HS1} = \begin{bmatrix} 1.5111 + 4.7840j & 0.1528 + 0.6197j & 0.1519 + 0.5121j \\ 0.1528 + 0.6197j & 1.5095 + 4.7573j & 0.1536 + 0.6148j \\ 0.1519 + 0.5121j & 0.1536 + 0.6148j & 1.5089 + 4.7714j \end{bmatrix}$$

$$PTM_{HS2} = \begin{bmatrix} 1.7328 + 5.4966j & 0.2391 + 0.9180j & 0.2376 + 0.7603j \\ 0.2391 + 0.9180j & 1.7325 + 5.4627j & 0.2399 + 0.9097j \\ 0.2376 + 0.7603j & 0.2399 + 0.9097j & 1.7304 + 5.4831j \end{bmatrix}$$

As illustrated in Figure 6-4, the second harmonic source is farther from the substation. Figure 6-8 shows a schematic of the three-phase system equivalent PTM.

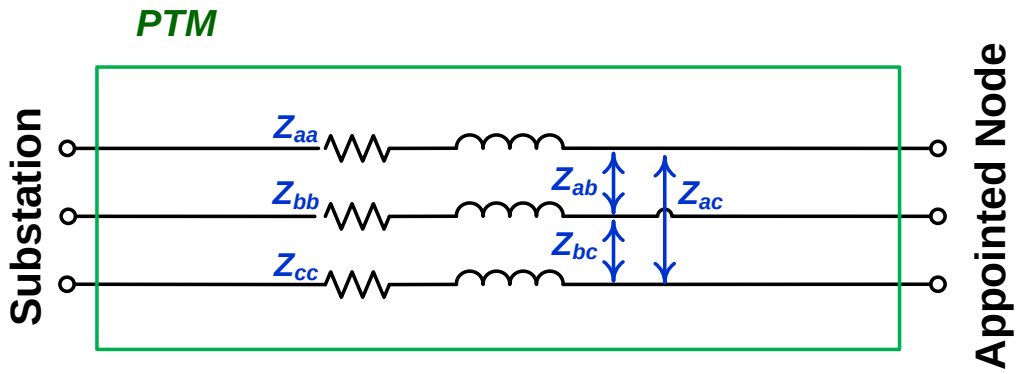

Figure 6-8. Three-phase system PTM equivalent

The PTM depends on network topology and three phase coupling. To analyze the impacts of three phase network impedance on harmonic propagation, the PTM is calculated for four cases. The first case neglects the admittance terms in conductor lines. The shunt admittance of overhead lines is usually small and can be neglected [29]. The second case neglects mutual coupling elements in the PTM impedance. The PTM impedance matrix is diagonal in this case. The PTM impedance calculation in this case reduces the impact of topology on the harmonic propagation. The third case considers balanced impedance values for three phases. The last case calculates the PTM without the previously mentioned simplifications. Table 6-3 shows the PTM impedance as seen by the first harmonic source for the four cases.

Figure 6-9 shows the THDV for the four cases of Table 6-3 at the substation. The phase angle for harmonic source 1 varies from 0° to 90° and phase angle for the second harmonic source is maintained at 0°. Figure 6-9 shows that case 2, which ignores mutual coupling, has less voltage distortion than the other

cases. Cases 1 and 3 have very close THDV results. However, case 4, the complete model, has slightly less THDV values than cases 1 and 3.

Table 6-3, PTM values for different cases

Case	Description	PTM for HS1
1	Neglect Shunt Admittance	$\begin{bmatrix} 1.5102 + 4.7827j & 0.1528 + 0.6196j & 0.1518 + 0.5121j \\ 0.1528 + 0.6196j & 1.5090 + 4.7566j & 0.1537 + 0.6148j \\ 0.1518 + 0.5121j & 0.1537 + 0.6148j & 1.5084 + 4.7707j \end{bmatrix}$
2	Neglect Mutual Coupling	$\begin{bmatrix} 1.5111 + 4.7840j & 0 & 0 \\ 0 & 1.5094 + 4.7574j & 0 \\ 0 & 0 & 1.5094 + 4.7574j \end{bmatrix}$
3	Force Balanced Impedances	$\begin{bmatrix} 1.5132 + 4.7691j & 0.1529 + 0.5822j & 0.1531 + 0.5821j \\ 0.1529 + 0.5822j & 1.5075 + 4.7722j & 0.1525 + 0.5823j \\ 0.1531 + 0.5821j & 0.1525 + 0.5823j & 1.5089 + 4.7713j \end{bmatrix}$
4	Complete Model Values	$\begin{bmatrix} 1.7328 + 5.4966j & 0.2391 + 0.9180j & 0.2376 + 0.7603j \\ 0.2391 + 0.9180j & 1.7325 + 5.4627j & 0.2399 + 0.9097j \\ 0.2376 + 0.7603j & 0.2399 + 0.9097j & 1.7304 + 5.4831j \end{bmatrix}$

Figure 6-10 shows the THDI for presented cases in Table 6-3, PTM values for different cases. For THDI values, case 2 has the highest THDI. Similar to the THDV values, cases 1 and 3 have very close THDI values. However, case 4 is less than cases 1 and 3. The presented THDV and THDI values show that for this circuit ignoring admittance to simplify the PTM calculation does not make a big change in THDI and THDV values. Moreover, forcing balanced values for the three phases impedance matrix as in case 3 does not make a big change, because harmonic source 1 is connected to the three phase line and the three phase conductors from the harmonic source to the substation have similar specifications in terms of length and conductivity. But case 2 shows that the phase coupling values cannot be ignored due to the considerable differences from the original case (case 4) in THDV and THDI achieved in the case 2 simulations.

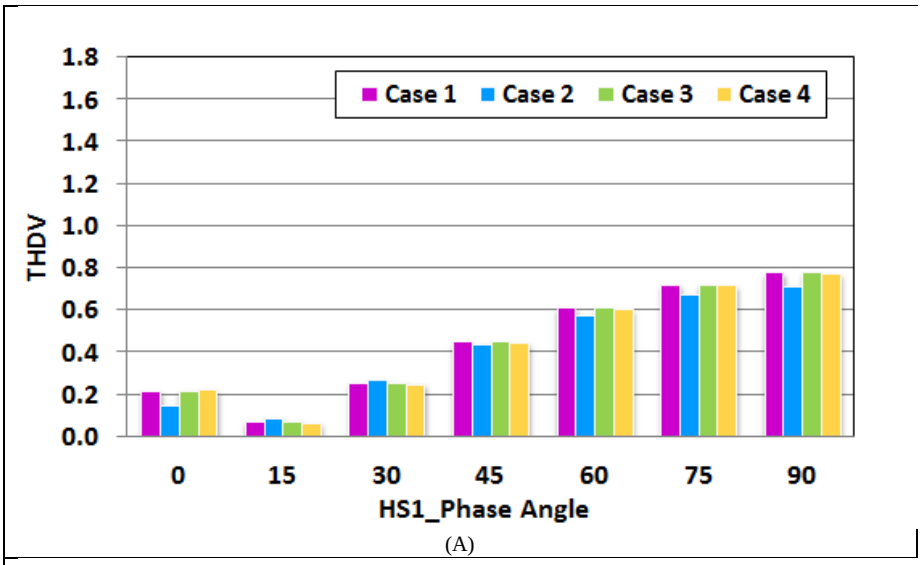

(A)

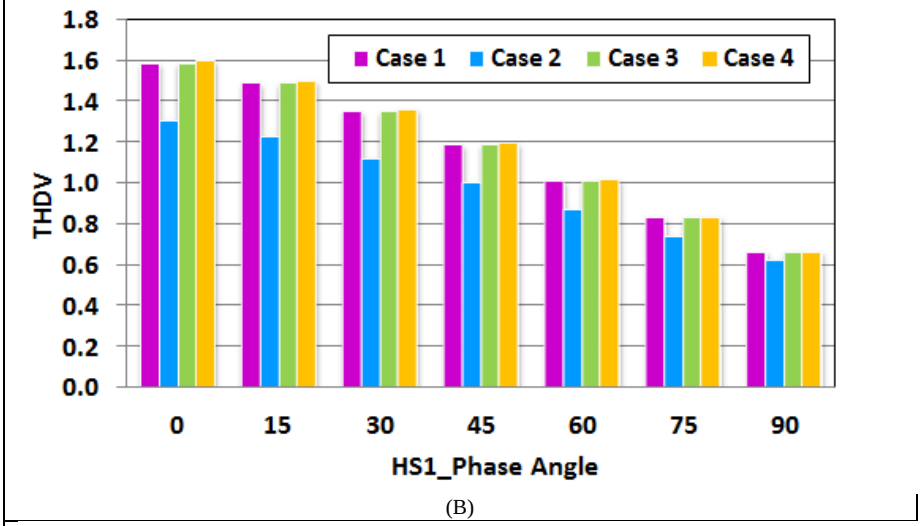

(B)

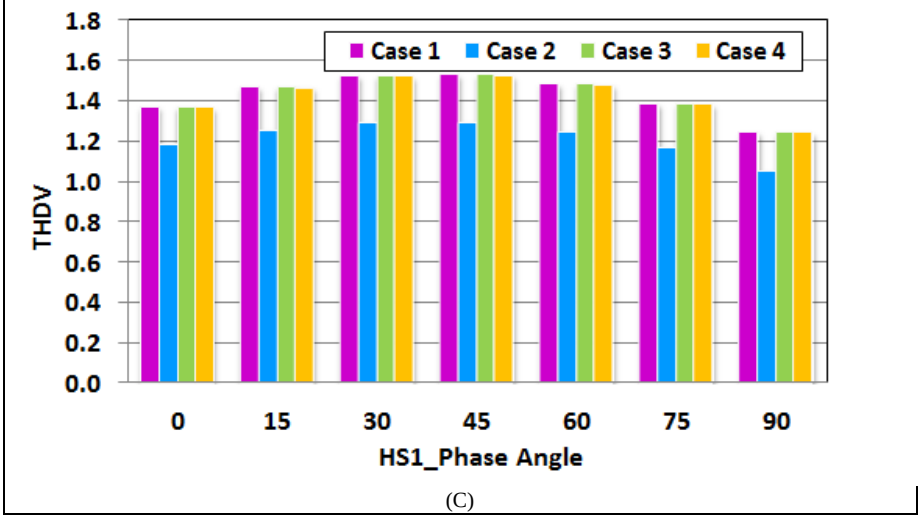

(C)

Figure 6-9. THDV for phase A (A), phase B (B), phase C (C) for different Thevenin impedance calculation cases

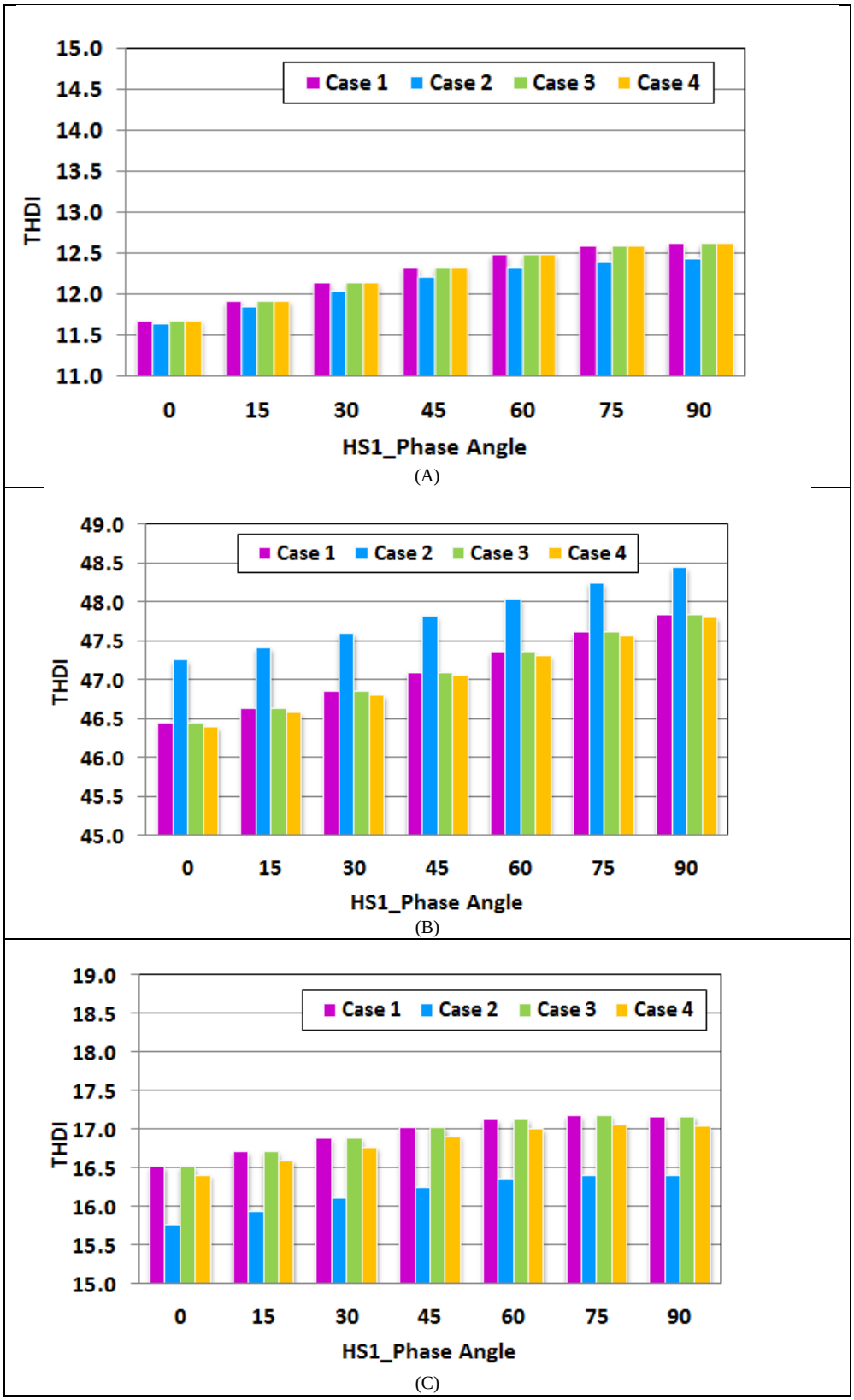

Figure 6-10. THDV for phases A (A), B (B), and C (C) for different Thevenin impedance calculation cases

6.3.4. Single Phase Harmonic Sources and Mutual Coupling Effects

In this section, harmonic sources attached to one phase are analyzed to determine the impact on other phases. The single phase harmonic sources are located at the same place as the three phase harmonic sources (see Figure 6-4). THDV and THDI are calculated at the substation. With harmonic current injections in only one phase, THDV and THDI indices for the other phases than the phase with the harmonic source are almost zero. However, mutual couplings do cause distortion in coupled voltage and current waveforms, but these are not reflected in the THDV and THDI indices. The IPHI index does provide non-zero harmonic distortion values for coupled phases.

Figure 6-11 depicts the statistical comparison of IPHI at the substation for the three phase harmonic source and the harmonic source considered in each phase separately. In Figure 6-11, the IPHI values for different phase angles (0° to 90°) of both harmonic sources are classified as a data set presented in the form of a Box Plot. The Box Plots show minimum, maximum, mean, and median values of IPHI calculated over the different phase angles. In Figure 6-11-A, IPHI is measured in phase A. For cases of three phase harmonic sources and phase A harmonic sources, the IPHI values are very similar. IPHI values for phase B and phase C are less than phase A, however they are not zero. In Figure 6-11-B and C there is a similar situation for phases B and C, respectively. The greater distance between the minimum and maximum values of IPHI in phase C shows that phase C has more sensitivity than the other phases to the harmonic source phase angle variations.

These types of sensitivity analyses are not possible with THDV and THDI indices because of the extremely small values of THD in the coupled phases that do not contain the harmonic source.

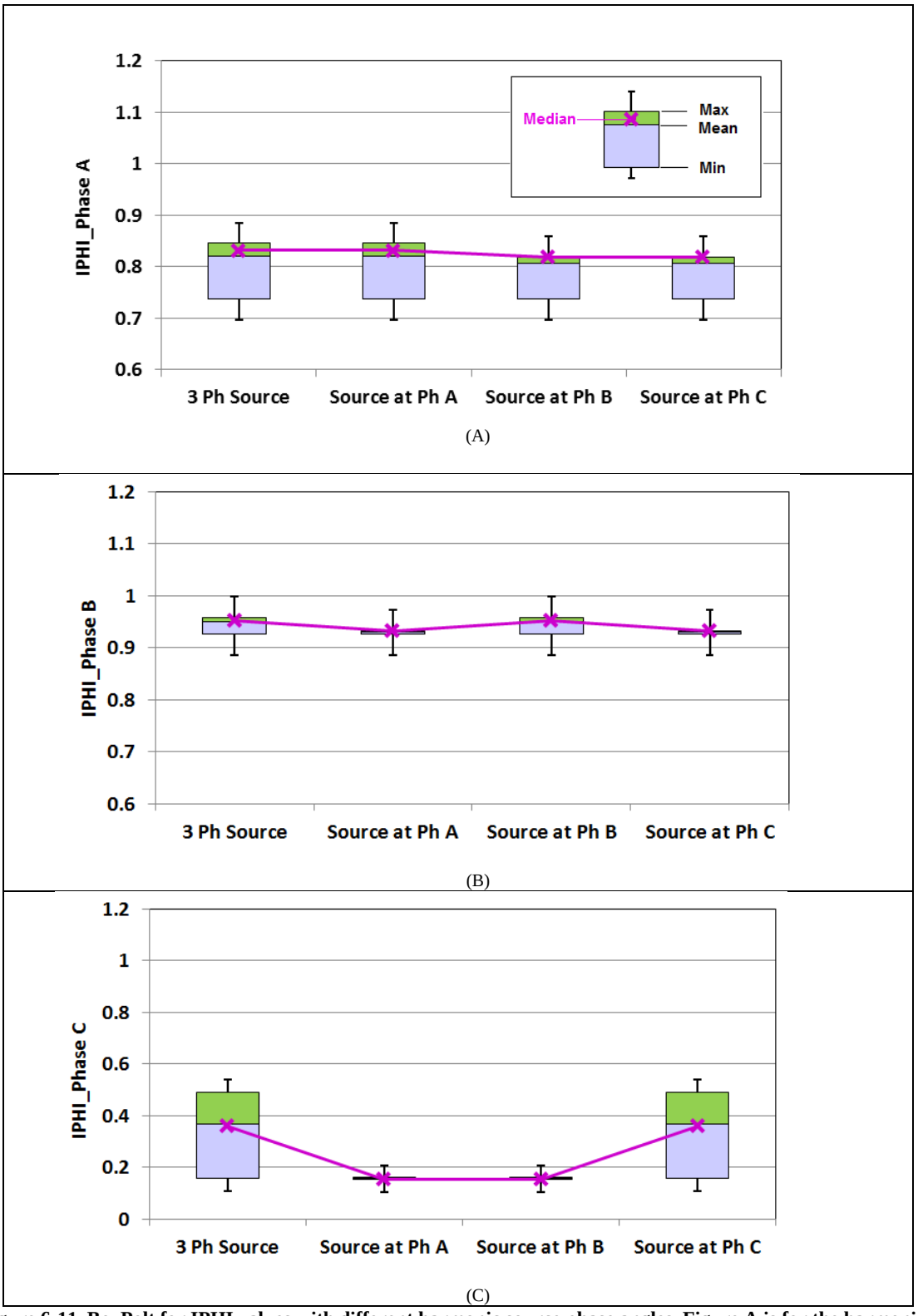

Figure 6-11. BoxPolt for IPHI values with different harmonic source phase angles. Figure A is for the harmonic source injections in only phase A, Figure B is for the harmonic source injections in only phase B, and Figure C is for the harmonic source injections in only phase C.

6.3.5. Phase Balance and Harmonic Propagation

Phase balance affects harmonic propagation due to the change in power flow and the interphase couplings [30]. Phase balancing results in neutral current reduction and a decline in third harmonic currents [31]. In this section the impact of phase balancing on harmonic distortion is analyzed with the help of THDV, THDI and IPHV indices. Table 6-4 shows the substation loading before and after phase balancing.

Table 6-4. Three phase lording in substation level before and after phase balance

Currents at Substation	Ph. A (Amp)	Ph. B (Amp)	Ph. C (Amp)
Before Phase balance	126.86	67.31	73.29
After Phase balance	93.52	84.03	90.46

The phase balancing in this study includes re-phasing single-phase or double-phase laterals in the case study circuit model. After performing phase balancing, part of phase A lateral branches moved to phase B and C. There are totally 9 phase moves to balance the circuit. Figure 6-12 depicts phase moves and their location in the distribution network. Phases are indicated in the figure with different colors. Locations in the circuit where phase moves occurred are numbered, and the associated graphic indicates the phase move that occurred at each numbered location. The arrows represent phase movements in different branches of the circuit. The arrows are colored based on phase changes (phase A -> green, phase B -> blue, phase C-> yellow).

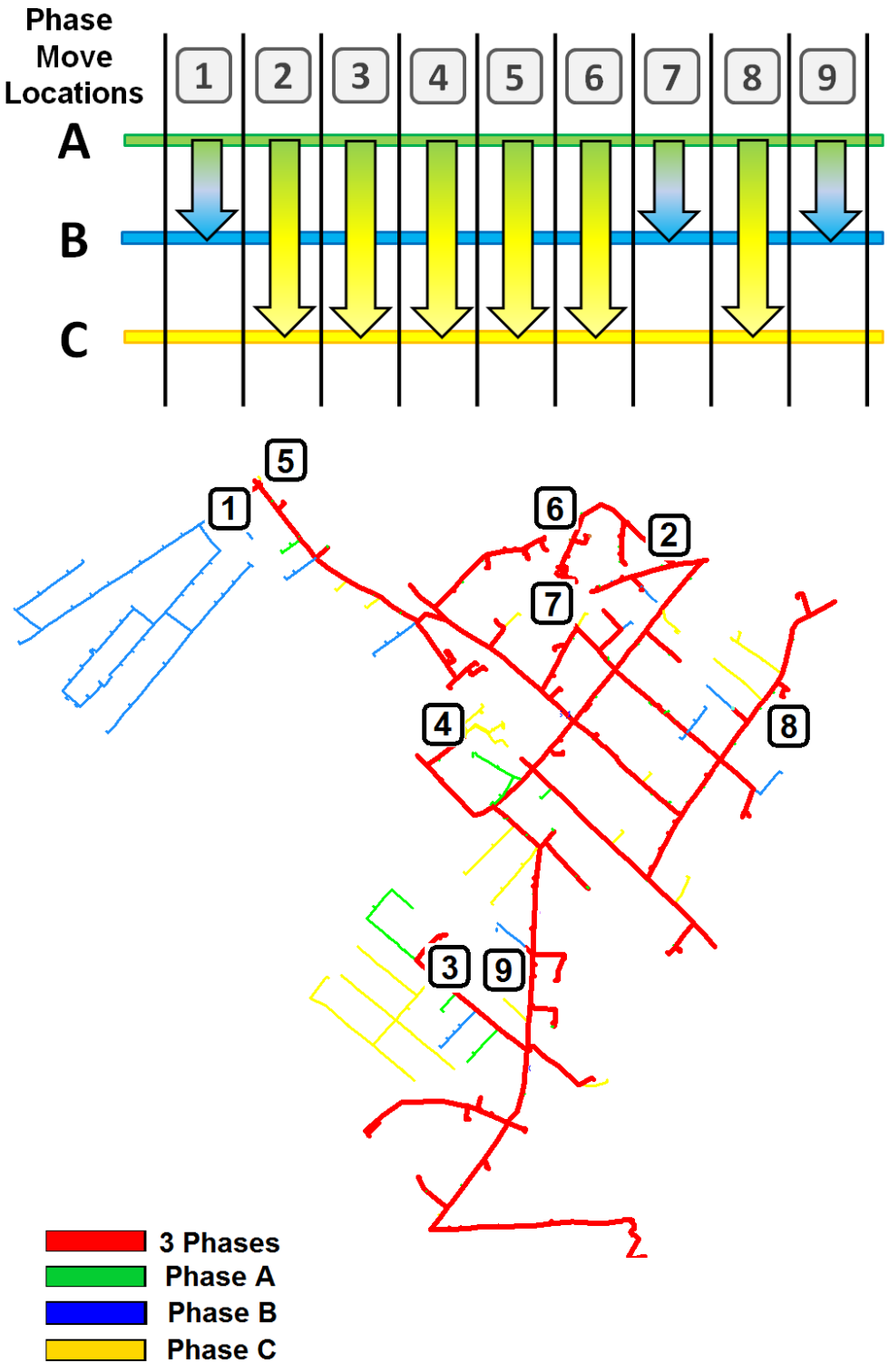

Figure 6-12. Phase movements for circuit phase balance

The substation THDV comparison of balanced and unbalanced circuit is presented in Figure 6-13. The THDV shows a small decrease for the balanced circuit.

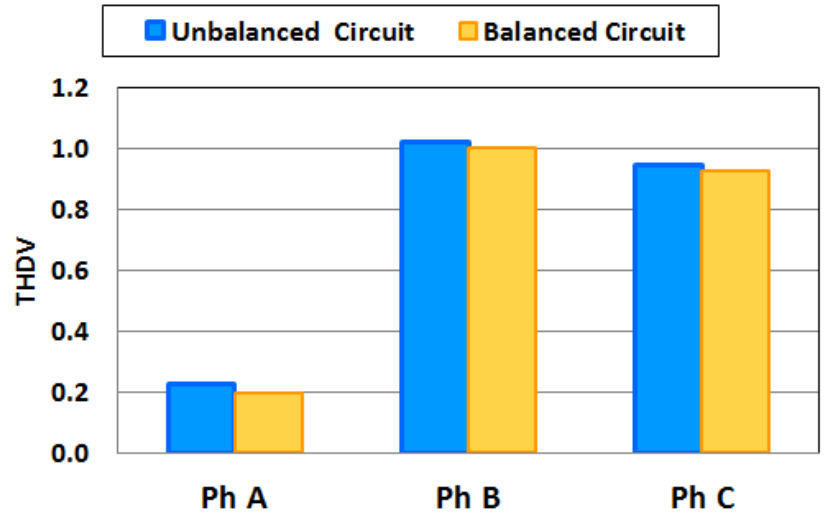

Figure 6-13. THDV for balanced and unbalanced circuit

The THDI calculations are presented in Figure 6-14. There is a decline in THDI for phases B and C, but phase A has an increase in THDI. However, the maximum THDI for the unbalanced case is 16.79 in phase B, and for the balanced case the maximum THDI is 13.42 in phase A. Thus, the maximum THDI over all of the phases decreased from the unbalanced case to the balanced case.

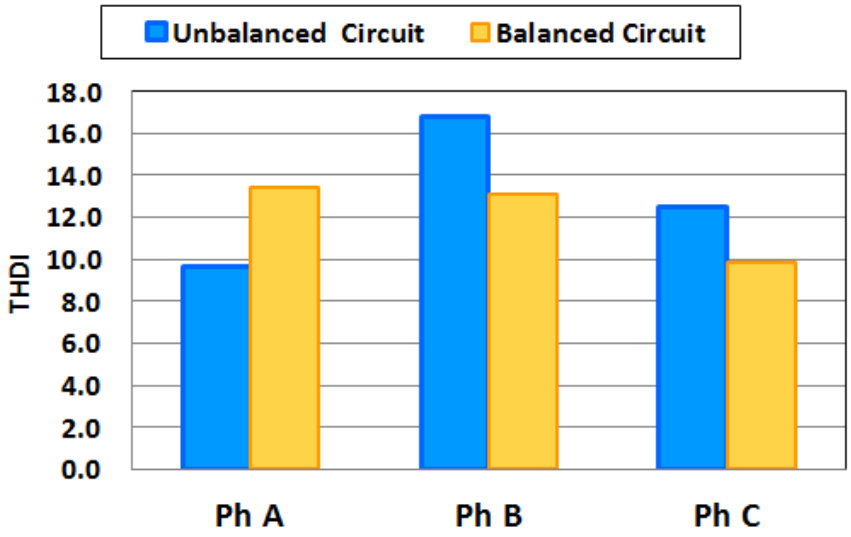

Figure 6-14. THDI for balanced and unbalanced circuits

As illustrated in Figure 6-13 and Figure 6-14 , THDV and THDI have different trends in phase balance. The visual observation of THDI could create doubts about the positive impact of phase balance on harmonic distortion. Table 6-5 presents the IPHV calculation for the balanced and unbalanced circuit.

Table 6-5. IPHV calculations for balanced and unbalanced cases

IPHV	Ph. A	Ph. B	Ph. C
Balanced Circuit	0.99990	0.51432	0.50107
Unbalanced Circuit	0.99994	0.51608	0.49953
Δ IPHV (Bal- UnBal)	- 0.00004	- 0.00176	+ 0.00154
Σ (Δ IPHV) = **- 0.00026**			

Table 6-5 shows that the change in IPHV from the balanced case to the unbalanced case for Phase A and phase B have a negative IPHV, and phase C has a positive IPHV. The sum of the changes in IPHV shows a net decrease in harmonic distortion. Such a calculation cannot be performed with THDV and THDI.

6.3.6. Harmonic Distortion Levels at Customer Loads

To demonstrate the harmonic distortion at different locations of the circuit, harmonic calculations are conducted at a customer load (secondary of distribution transformer) in this section. The measurement point is illustrated in Figure 6-4. The customer side measurement point is between the harmonic sources. Figure 6-15 shows THDV values at the substation and at a customer load.

Figure 6-16 presents the THDI values at the substation and at a customer load. It shows the substation experiences more distortion in current than the customer load. However, the customer load is exposed to higher harmonic voltage distortion. To explain these results, Figure 6-17 depicts the equivalent circuit with measurement points and harmonic sources.

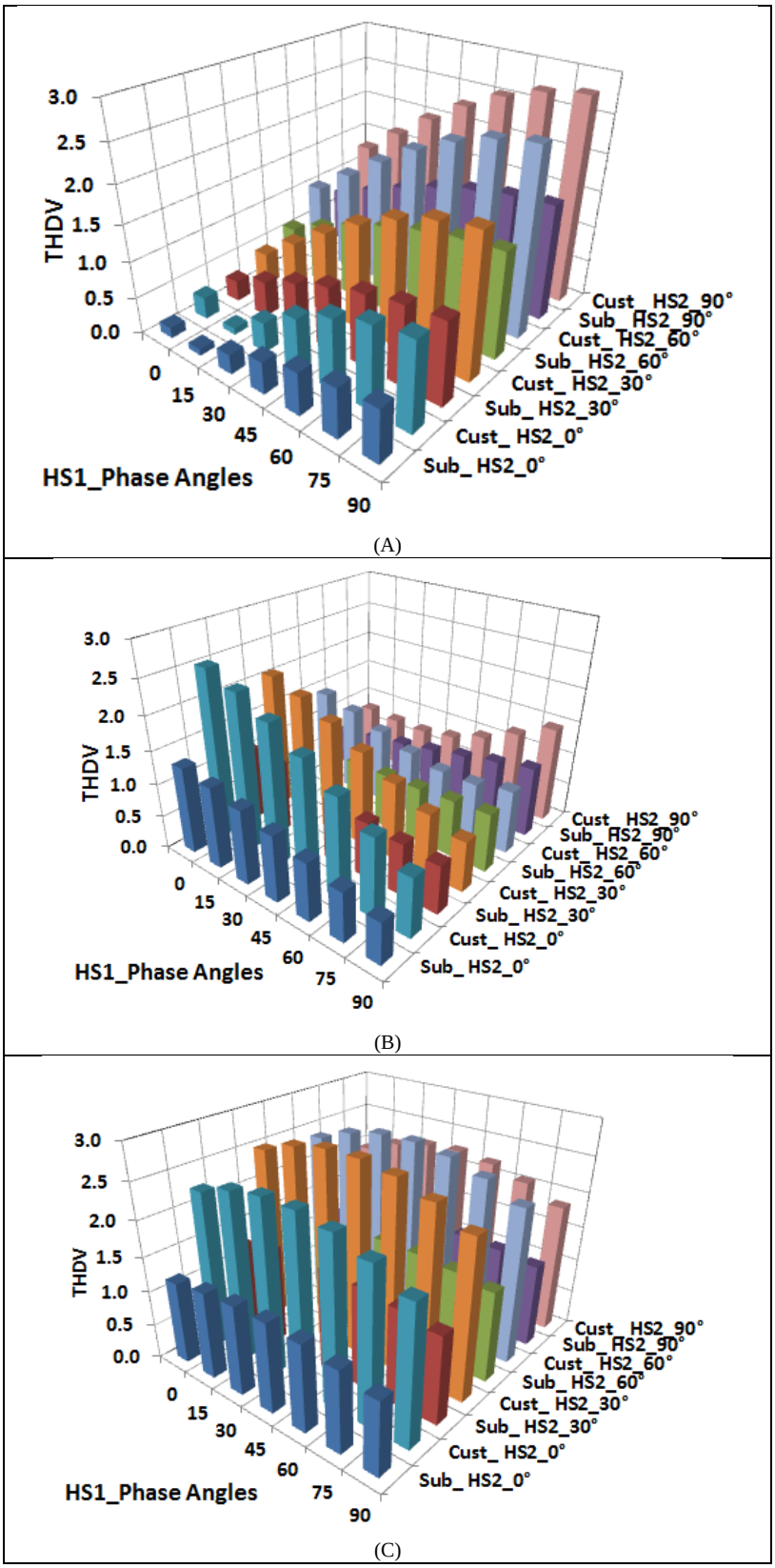

Figure 6-15. THDV at the substation and a customer load point for each of the phases

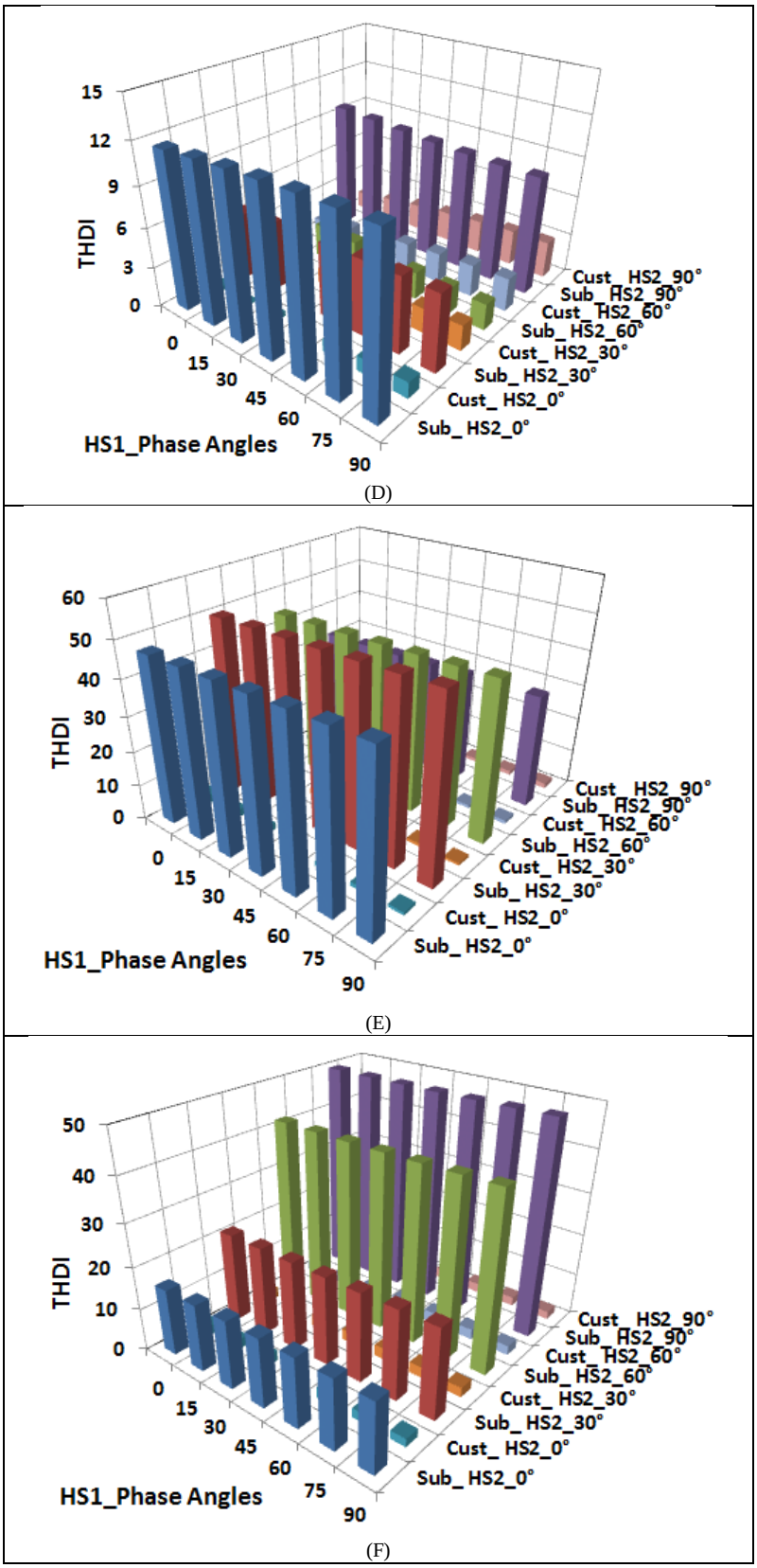

Figure 6-16. THDI at the substation and a customer load point for each of the three phases

Since the impedance looking back into the substation is much smaller than the customer load impedance, a higher portion of harmonic currents flow to the substation than to the customer site. Therefore, the substation has more THDI. In this case study, the voltage distortion is larger at the customer load. Voltage is the product of impedance and current. The customer load impedance is much larger than the impedance of the path to the substation. The current through the load side is less, but the product of current and impedance for the customer side is higher than for the substation side. Therefore, more voltage distortion is realized at the customer side. This observation is illustrated in Figure 6-17.

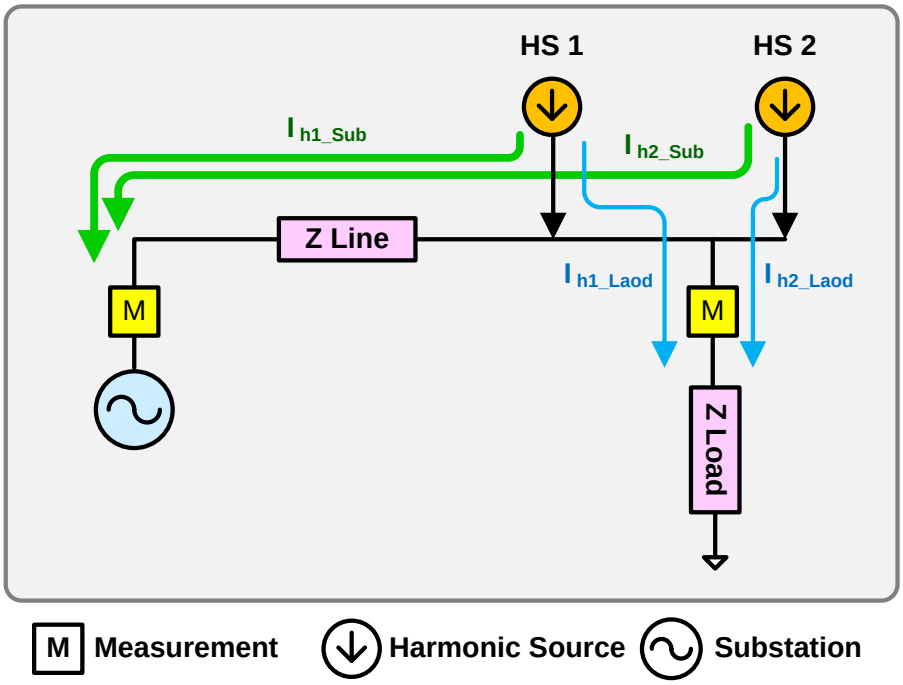

Figure 6-17. The harmonic current distribution between load and substation

6.3.7. Chapter Conclusions and Observations

In this dissertation, the impact of distribution network topology on interactive harmonic distortion from multiple harmonic sources is investigated. A detailed model of the distribution network is employed in the harmonic analysis. Several simulations and sensitivity analyses are presented that consider commonly used harmonic indices and a new proposed index that takes into account information concerning angle differences. The major outcomes and uniqueness of this dissertation are:

1) Understanding the way that multiple harmonic sources interact to increase or decrease the harmonic distortion is crucial to minimizing harmonic problems in distribution networks and microgrids with large numbers of Distributed Energy Resources.

2) The new proposed index, IPH, provides more information than THDV and THDI in the sensitivity analysis conducted in this chapter. IPH considers the phase angles of the distorted voltage and current waveforms in the harmonic quantization, and the phase angle plays a significant role in the interactions of the harmonic sources.

3) Phase angles of harmonic sources have complex impacts on the overall harmonic distortion because of the vectorial summation of the injected harmonic currents. The phase angle impacts also vary with the distribution network topology and components characteristics. In some cases, phase angle variations of different harmonic sources result in reduced harmonic impacts. However, phase angle variations that increase harmonic distortion need to be understood.

4) The detailed circuit model employed paves the ground for the topological sensitivity analysis performed. Single phase, multiphase, and unbalanced loads in addition to the three phase conductors' model help to demonstrate realistic harmonic propagation in distribution networks.

5) The impact of phase balance on harmonic propagation in the distribution network is analyzed via a number of simulations. The results demonstrate that phase balancing can have a positive impact on harmonic reduction in distribution networks.

6) In quantizing the impact of single phase harmonic sources on other phases than its own phase, THDV and THDI values are very small. But, the equivalent Thevenin impedance analysis shows that the mutual coupling creates harmonic propagation in all phases. The proposed IPHI index is helpful in quantizing harmonic distortion in all phases with single phase harmonic sources present.

7) Harmonic impacts on customer loads and at the substation are evaluated. The THD observation shows more current distortion at the substation than at the customer load. However, more harmonic voltage distortion is experienced at the customer load. In harmonic studies and in making harmonic measurements, harmonic values should be considered throughout the circuit.

Chapter 7 : Conclusions and Future Work

7.1. Conclusions

The advent of smart grid brings new trends to power systems, like distributed renewable energy resource integration, electric vehicles, decentralized management and control, and deregulation of electricity markets. The need for modern electricity infrastructures and more capable grid components brings attention to distributed energy storage systems because of their bidirectional power flow capability. This dissertation focuses on three different aspects of distributed energy storage system applications in distribution networks. It starts with flywheel energy storage system modeling and analysis for application in microgrid facilities. Then, a market-based optimal controller is proposed to enhance the operational profit of distributed energy storage devices in distribution networks. Finally, impact of multiple distributed energy storage devices on harmonic propagation in distribution networks is investigated.

The first task of the dissertation (Chapter 3) is devoted to investigating energy storage technologies for ride-through applications in facility microgrids, and in particular comparing batteries with flywheels. The major outcomes of this section can be summarized as follows:

- This dissertation presents a comparison between batteries and flywheels for critical microgrid facilities like data centers. Literatures and manufacturer documents show flywheels have higher efficiency, less footprint and longer life cycle than batteries. This is to account for the fact that the life of flywheels is estimated at 20 years, whereas that life of batteries is estimated at three to five years [79]. Although the initial capital cost of the flywheel is more that of the battery of equivalent size, the 20-year life cycle cost calculation shows that flywheels have less cumulative ownership cost than batteries after three to four years.
- Conventionally, backup power units consist of batteries and diesel generators. Batteries handle critical loads before diesel generators startup. The conducted simulations demonstrate

that, flywheels in combination with micro generators, are a better fit for critical microgrid facilities in spite of their shorter discharging time. The 15-minute ride-through time of batteries is not needed because the common practice in data centers is that micro generators start within 5-6 seconds after an outage. Therefore, a flywheel with 15-30 seconds ride-through time is sufficient for data center applications.

- The conducted simulations demonstrate how a 750kW FES in conjunction with a diesel generator improves the load serving capability, providing a highly reliable ride-through capability for a data center in Virginia. Data centers cannot tolerate even a momentary interruption. The analysis shows flywheels can handle critical loads in milliseconds which is faster than equivalent size batteries. Moreover, simulations show that flywheels can significantly decrease the system frequency deviation during diesel engine start-up.
- In comparison with batteries, the application of FES for power security is new. This limits the availability of experimental data. The software tool developed in this dissertation enables analysis of short-term ride-through applications of FES during an islanded operation of a facility microgrid. As a result, it can provide a guideline for facility engineers in data centers or other types of facility microgrids to design their backup power systems based on FES technology. The proposed tool includes a library of available commercial FES systems. The user can also create any customer-defined flywheels by entering appropriate mechanical and electrical parameters.

The second task of the dissertation (Chapter 4) focused on optimal economic operation of community energy storage systems. The outcomes of this task are:

- CES has the potential to improve capacity, efficiency and reliability of distribution circuits. Since, CES units are located at the secondary of distribution transformers, they provide more controllability and quality of services for utilities. Peak shaving and renewable energy

resource firming are also of financial interest. This dissertation presents a real-time control scheme that maximizes the revenue attainable by energy storage systems without sacrificing the benefits related to improvements in reliability and reduction in peak feeder loading.

- This dissertation presents a means of realizing additional benefits for utilities by taking advantage of the fluctuating cost of energy in competitive energy markets. By combining electricity market information with real-time control of energy storage devices, utilities may enjoy year-round economic benefits from the CES market-based operation. Simulations using real-time LMP pricing show market-based operation of CES units can provide up to $180 per month profit per CES unit for utilities in addition to the reliability and grid support benefits.
- In this dissertation, a novel combination of trade-offs related to transformer loading, feeder loss, and LMP price prediction is considered that is not addressed in other literature. In terms of distribution transformer loading associated with a CES unit, the conducted analyses shows that greater profits can be realized by placing the CES units on more lightly loaded transformers. When the load is higher, more energy must be saved in case of an outage, so there is lower availability for participation in the electricity market, resulting in smaller profits. The simulations show that increasing transformer loading from 10% to 40% leads to a 50% drop in monthly benefit for each CES unit operation.
- The dissertation analysis shows that the CES operational profit is highly dependent on the accuracy of the LMP prediction and load forecasting. If market operators provide more accurate day-ahead market prices, CES is able to take more advantage of fluctuations in market prices. The analysis presented in this dissertation shows that the monthly profit of each CES unit can improve up to 45% with accurate LMP forecasting.
- The conducted simulations illustrate dependency between reliability requirements and CES operational profits. The utility can achieve longer outage recovery with storing more energy in CES units. The reserve capacity of CES units can be based on a fixed reserve energy level (static reserve capacity) or specific time duration of outage serving (dynamic reserve

capacity). The presented optimization solution shows that higher reserved energy in CES units for outage recovery means less energy is available for market participation. Based on analysis for static reserve capacity, increasing reserve energy from 10 kWh to 20 kWh in each CES units can result in a 15% decline in monthly operational profits for each CES unit. For dynamic reserve capacity, analysis shows that increasing the number of supported hours from 2 to 5 hours decreases the CES monthly profit around 35%.

- This dissertation uses a detailed, multi-phase model of the distribution network that considers all circuit components, including distribution transformers and secondary distribution. The detailed network model is needed to schedule community energy storage (CES) units based on the customer loads and the loading of transformers associated to each CES unit. This detailed model provides more realistic analysis results than previous studies. Moreover, the detailed model helps to investigate the advantage of the proposed optimal control algorithm for CES in circuits with a high adoption of Plugged-in Electric Vehicles (PEV) and Distributed Photovoltaic (DPV) sources. In the case of high levels of PEV adoption, CES prevents the distribution transformers from overloading. Moreover, DPV source penetration are addressed in case studies. The results show that the proposed optimal control system can improve the distribution network operational profit with a combination of DPV and CES adoptions.

The third task of the dissertation (Chapters 5 and 6) investigates harmonic interactions from multiple inverter-based Distributed Energy Resources (DER) like PV and CES. The outcomes of this part of dissertation are as follows:

- In this dissertation, the impact of distribution network topology on harmonic propagation due to the interaction of multiple harmonic sources is investigated. Understanding how multiple harmonic sources interact to increase or decrease the harmonic distortion is crucial in distribution networks with a large number of Distributed Energy Resources. Through a

number of analyses, this dissertation shows how harmonic distortion at substations or at the customer side can go beyond the standard levels or can drop due to multiple harmonic source interactions.

- In this dissertation, a new index, Index of Phasor Harmonics (IPH), is proposed for harmonic analysis in multiple harmonic source cases. The proposed IPH index presents more information than Total Harmonic Distortion (THD) and Individual Harmonic Distortion (IHD) because the IPH incorporates phase angle information in addition to the harmonic source magnitudes. A number of simulations and analyses are performed on the distribution network model to show IPH advantages in comparison with conventional harmonic quantization indices. For example, mutual coupling causes distortion in coupled voltage and current waveforms, but these are not reflected in the THDV and THDI indices. The IPHI index does provide non-zero harmonic distortion values for coupled phases.
- This dissertation investigates the correlation between magnitude and phase angle variations of harmonic sources and overall harmonics propagation. The analysis shows that multiple harmonic sources act together to change the harmonic distortion in the circuit. In the case of harmonic source magnitudes, the harmonic distortion increases at a different rate than that of each of the harmonic source magnitude rates. Phase angles of harmonic sources have complex impacts on the overall harmonic distortion due to the vectorial summation of the injected harmonic currents. Phase angle impacts also vary with the distribution network topology and component characteristics. In some cases, phase angle variations of different harmonic sources result in reduced harmonic impacts. However, phase angle variations that increase harmonic distortion need to be understood.
- The simulations demonstrate that the substation and customers experience different impacts from the interactions of multiple harmonic sources. THD observations show more current distortion at the substation than at the customer load. However, more harmonic voltage distortion is experienced at the customer load.

- The impact of three phase balance on harmonic propagation in the distribution network is analyzed in this dissertation. The THD and IPH calculations show that phase balance has a positive impact on harmonic reduction in distribution networks.
- The detailed circuit model employed in the analysis paves the ground for the topological sensitivity analysis performed. It provides for more realistic harmonic propagation analysis. The detailed mode helps in investigating harmonic propagation between phases in different locations of the circuit. Moreover, the applied model facilities impact studies based on phase balance.

7.2. Future Work

The presented results and observations in this dissertation are starting points for further research and investigations related to distributed energy resource adoption and operation in distribution networks. The research is a combination of distribution network modeling and topology, energy storage, optimization and control techniques, electricity market-based operation, distributed energy resources and harmonic propagation. This dissertation points to future work as follows:

1) Flywheel technology application in distributed energy storage system for ancillary services in distribution networks

2) Analyzing the field test data for community energy storage to improve the capability of economic operation in real condition for islanding and grid connected modes

3) Participating in day ahead market bidding with aggregated community energy storage systems

4) Considering reliability cost in the objective function for CES optimal operation

5) Investigating the impact of volt-var control devices like voltage regulator and switchable capacitor banks on harmonic propagation

6) Developing an active harmonic filtering system for each DER to minimize overall harmonics at the substation

References:

[1] S. Massoud Amin and B. F. Wollenberg, "Toward a smart grid: power delivery for the 21st century," *Power and Energy Magazine, IEEE,* vol. 3, pp. 34-41, 2005.

[2] E. A. Committee, "Smart grid: Enabler of the new energy economy," *EB/OL,* pp. 12-01, 2008.

[3] D. Kathan, C. Daly, E. Eversole, M. Farinella, J. Gadani, R. Irwin, C. Lankford, A. Pan, C. Switzer, and D. Wright, "National action plan on demand response," *The Federal Energy Regulatory Commission Staff, Federal Energy Regulatory Commission, Washington, DC, Tech. Rep. AD09-10,* 2010.

[4] F. Rahimi and A. Ipakchi, "Demand response as a market resource under the smart grid paradigm," *Smart Grid, IEEE Transactions on,* vol. 1, pp. 82-88, 2010.

[5] R. Lasseter and M. Erickson, "Integration of Battery-Based Energy Storage Element in the CERTS Microgrid," *CERTS Report,* 2009.

[6] A. Nourai and C. Schafer, "Changing the electricity game," *Power and Energy Magazine, IEEE,* vol. 7, pp. 42-47, 2009.

[7] J. Tomić and W. Kempton, "Using fleets of electric-drive vehicles for grid support," *Journal of Power Sources,* vol. 168, pp. 459-468, 2007.

[8] M. C. W. Kintner-Meyer, P. J. Balducci, C. Jin, T. B. Nguyen, M. A. Elizondo, V. Viswanathan, X. Guo, and F. Tuffner, *Energy Storage for Power Systems Applications: A Regional Assessment for the Northwest Power Pool (NWPP)*: Pacific Northwest National Laboratory, 2010.

[9] L. W. Chung, M. F. M. Siam, A. B. Ismail, and Z. F. Hussien, "Modeling and simulation of sodium sulfur battery for battery-energy storage system and custom power devices," in *Power and Energy Conference, 2004. PECon 2004. Proceedings. National*, 2004, pp. 205-210.

[10] Z. F. Hussien, W. C. Lee, M. F. M. Siam, and A. B. Ismail, "Modeling of sodium sulfur battery for power system applications," *Elektrika Journal of Electrical Engineering,* vol. 9, pp. 66-72, 2007.

[11] L. Joerissen, J. Garche, C. Fabjan, and G. Tomazic, "Possible use of vanadium redox-flow batteries for energy storage in small grids and stand-alone photovoltaic systems," *Journal of Power Sources,* vol. 127, pp. 98-104, 2004.

[12] B. Roberts, "Capturing grid power," *Power and Energy Magazine, IEEE,* vol. 7, pp. 32-41, 2009.

[13] E. Karden, S. Ploumen, B. Fricke, T. Miller, and K. Snyder, "Energy storage devices for future hybrid electric vehicles," *Journal of Power Sources,* vol. 168, pp. 2-11, 2007.

[14] M. Wakihara and O. Yamamoto, *Lithium ion batteries*: Wiley-Vch, 2008.

[15] R. Arghandeh, M. Pipattanasomporn, and S. Rahman, "Flywheel Energy Storage Systems for Ride-through Applications in a Facility Microgrid," *Smart Grid, IEEE Transactions on,* vol. 3, pp. 1955-1962, 2012.

[16] H. Shaalan, J. Thompson, R. Broadwater, M. Ellis, and H. Ng, "Distribution engineering tool features a flexible framework," *Computer Applications in Power, IEEE,* vol. 8, pp. 21-24, 1995.

[17] L. R. Feinauer, K. J. Russell, and R. P. Broadwater, "Graph trace analysis and generic algorithms for interdependent reconfigurable system design and control," *Naval Engineers Journal,* vol. 120, pp. 29-40, 2008.

[18] D. Cheng, D. Zhu, R. P. Broadwater, and S. Lee, "A graph trace based reliability analysis of electric power systems with time-varying loads and dependent failures," *Electric power systems research,* vol. 79, pp. 1321-1328, 2009.

[19] D. Cheng, Y. Liang, D. Zhu, and R. P. Broadwater, "Real-Time Power Electric System Modeling, Assessment and Reliability Prediction," in *Power Systems Conference and Exposition, 2009. PSCE'09. IEEE/PES*, 2009, pp. 1-6.

[20] J. Hambrick and R. Broadwater, "Advantages of Integrated System Model-Based Control for Electrical Distribution System Automation," in *World Congress*, 2011, pp. 6117-6120.

[21] K. Russell and R. Broadwater, "Model-based automated reconfiguration for fault isolation and restoration," in *Innovative Smart Grid Technologies (ISGT), 2012 IEEE PES*, 2012, pp. 1-4.
[22] D. G. Hart, "Using AMI to realize the Smart Grid," in *Power and Energy Society General Meeting-Conversion and Delivery of Electrical Energy in the 21st Century, 2008 IEEE*, 2008, pp. 1-2.
[23] F. Alvarez and H. Rudnick, "Impact of energy efficiency incentives on electricity distribution companies," *Power Systems, IEEE Transactions on*, vol. 25, pp. 1865-1872, 2010.
[24] A. T. Le, "New UPS system configuration that will improve energy efficiency," *Power Apparatus and Systems, IEEE Transactions on*, pp. 829-834, 1985.
[25] R. Billinton, "Evaluation of different operating strategies in small stand-alone power systems," *Energy Conversion, IEEE Transactions on*, vol. 20, pp. 654-660, 2005.
[26] M. Ross, R. Hidalgo, C. Abbey, and G. Joos, "Energy storage system scheduling for an isolated microgrid," *Renewable Power Generation, IET*, vol. 5, pp. 117-123, 2011.
[27] M. Zackrisson, L. Avellán, and J. Orlenius, "Life cycle assessment of lithium-ion batteries for plug-in hybrid electric vehicles–Critical issues," *Journal of Cleaner Production*, vol. 18, pp. 1519-1529, 2010.
[28] R. Thelen, A. Gattozzi, D. Wardell, and A. Williams, "A 2-MW Motor And ARCP Drive for High-Speed Flywheel," in *Applied Power Electronics Conference, APEC 2007-Twenty Second Annual IEEE*, 2007, pp. 1690-1694.
[29] M. Ahrens, L. Kucera, and R. Larsonneur, "Performance of a magnetically suspended flywheel energy storage device," *Control Systems Technology, IEEE Transactions on*, vol. 4, pp. 494-502, 1996.
[30] G. Genta, *Kinetic energy storage: theory and practice of advanced flywheel systems*: Butterworths, 1985.
[31] S. Samineni, B. K. Johnson, H. L. Hess, and J. D. Law, "Modeling and analysis of a flywheel energy storage system for voltage sag correction," *Industry Applications, IEEE Transactions on*, vol. 42, pp. 42-52, 2006.
[32] L. Zhou and Z. ping Qi, "Modeling and control of a flywheel energy storage system for uninterruptible power supply," in *Sustainable Power Generation and Supply, 2009. SUPERGEN'09. International Conference on*, 2009, pp. 1-6.
[33] A. Rajapakshe, U. K. Madawala, and D. Muthumani, "A model for a fly-wheel driven by a grid connected switch reluctance machine," in *Sustainable Energy Technologies, 2008. ICSET 2008. IEEE International Conference on*, 2008, pp. 1025-1030.
[34] T. T. Leung, "Concept of a modified flywheel for megajoule storage and pulse conditioning," *Magnetics, IEEE Transactions on*, vol. 27, pp. 403-408, 1991.
[35] K. Divya and J. Østergaard, "Battery energy storage technology for power systems—An overview," *Electric power systems research*, vol. 79, pp. 511-520, 2009.
[36] B. P. Roberts and C. Sandberg, "The Role of Energy Storage in Development of Smart Grids," *Proceedings of the IEEE*, vol. 99, pp. 1139-1144, 2011.
[37] B. Roberts and J. McDowall, "Commercial successes in power storage," *Power and Energy Magazine, IEEE*, vol. 3, pp. 24-30, 2005.
[38] P. Grünewald, T. Cockerill, M. Contestabile, and P. Pearson, "The role of large scale storage in a GB low carbon energy future: Issues and policy challenges," *Energy Policy*, vol. 39, pp. 4807-4815, 2011.
[39] P. F. Ribeiro, B. K. Johnson, M. L. Crow, A. Arsoy, and Y. Liu, "Energy storage systems for advanced power applications," *Proceedings of the IEEE*, vol. 89, pp. 1744-1756, 2001.
[40] N. W. Miller, R. S. Zrebiec, R. W. Delmerico, and G. Hunt, "Battery energy storage systems for electric utility, industrial and commercial applications," in *Battery Conference on Applications and Advances, 1996., Eleventh Annual*, 1996, pp. 235-240.

[41] D. F. Daly, "20 MW battery power conditioning system for Puerto Rico Electric Power Authority," in *Battery Conference on Applications and Advances, 1995., Proceedings of the Tenth Annual*, 1995, pp. 233-237.
[42] S. M. Lukic, J. Cao, R. C. Bansal, F. Rodriguez, and A. Emadi, "Energy storage systems for automotive applications," *Industrial Electronics, IEEE Transactions on,* vol. 55, pp. 2258-2267, 2008.
[43] A. F. Burke, "Batteries and ultracapacitors for electric, hybrid, and fuel cell vehicles," *Proceedings of the IEEE,* vol. 95, pp. 806-820, 2007.
[44] J. Eyer and G. Corey, "Energy Storage for the Electricity Grid: Benefits and Market Potential Assessment Guide," Sandia National Laboratories, New Mexico, USA2010.
[45] C. A. Hill, M. C. Such, C. Dongmei, J. Gonzalez, and W. M. Grady, "Battery Energy Storage for Enabling Integration of Distributed Solar Power Generation," *Smart Grid, IEEE Transactions on,* vol. 3, pp. 850-857, 2012.
[46] "Functional Specification For Community Energy Storage (CES) Unit " American Electric Power2009.
[47] A. Nourai and D. Kearns, "Batteries Included," *Power and Energy Magazine, IEEE,* vol. 8, pp. 49-54, 2010.
[48] K. Dietrich, J. M. Latorre, L. Olmos, and A. Ramos, "Demand Response in an Isolated System With High Wind Integration," *Power Systems, IEEE Transactions on,* vol. 27, pp. 20-29, 2012.
[49] E. Sortomme and M. A. El-Sharkawi, "Optimal Power Flow for a System of Microgrids with Controllable Loads and Battery Storage," in *Power Systems Conference and Exposition, 2009. PSCE '09. IEEE/PES*, 2009, pp. 1-5.
[50] C. Marnay, G. Venkataramanan, M. Stadler, A. S. Siddiqui, R. Firestone, and B. Chandran, "Optimal Technology Selection and Operation of Commercial-Building Microgrids," *Power Systems, IEEE Transactions on,* vol. 23, pp. 975-982, 2008.
[51] C. Changsong, D. Shanxu, C. Tao, L. Bangyin, and H. Guozhen, "Optimal Allocation and Economic Analysis of Energy Storage System in Microgrids," *Power Electronics, IEEE Transactions on,* vol. 26, pp. 2762-2773, 2011.
[52] H. Sugihara, K. Yokoyama, O. Saeki, K. Tsuji, and T. Funaki, "Economic and Efficient Voltage Management Using Customer-Owned Energy Storage Systems in a Distribution Network With High Penetration of Photovoltaic Systems," *Power Systems, IEEE Transactions on,* vol. 28, pp. 102-111, 2013.
[53] c. chen, S. Duan, T. Cai, B. Liu, and G. Hu, "Smart energy management system for optimal microgrid economic operation," *Renewable Power Generation, IET,* vol. 5, pp. 258-267, 2011.
[54] X. Yixing, X. Le, and C. Singh, "Optimal scheduling and operation of load aggregators with electric energy storage facing price and demand uncertainties," in *North American Power Symposium (NAPS), 2011*, 2011, pp. 1-7.
[55] A. A. Hussein, N. Kutkut, Z. J. Shen, and I. Batarseh, "Distributed Battery Micro-Storage Systems Design and Operation in a Deregulated Electricity Market," *Sustainable Energy, IEEE Transactions on,* vol. 3, pp. 545-556, 2012.
[56] R. Niemi and P. Lund, "Decentralized electricity system sizing and placement in distribution networks," *Applied Energy,* vol. 87, pp. 1865-1869, 2010.
[57] D. Hung, N. Mithulananthan, and R. Bansal, "Multiple distributed generators placement in primary distribution networks for loss reduction," 2011.
[58] C. Abbey and G. Joos, "A Stochastic Optimization Approach to Rating of Energy Storage Systems in Wind-Diesel Isolated Grids," *Power Systems, IEEE Transactions on,* vol. 24, pp. 418-426, 2009.
[59] S. Jalal Kazempour and M. P. Moghaddam, "Economic viability of NaS battery plant in a competitive electricity market," in *Clean Electrical Power, 2009 International Conference on*, 2009, pp. 453-459.

[60] J. H. R. Enslin and P. J. M. Heskes, "Harmonic interaction between a large number of distributed power inverters and the distribution network," *Power Electronics, IEEE Transactions on,* vol. 19, pp. 1586-1593, 2004.
[61] M. Farhoodnea, A. Mohamed, H. Shareef, and H. Zayandehroodi, "An enhanced method for contribution assessment of utility and customer harmonic distortions in radial and weakly meshed distribution systems," *International Journal of Electrical Power & Energy Systems,* vol. 43, pp. 222-229, 2012.
[62] W. Fei, J. L. Duarte, M. A. M. Hendrix, and P. F. Ribeiro, "Modeling and Analysis of Grid Harmonic Distortion Impact of Aggregated DG Inverters," *Power Electronics, IEEE Transactions on,* vol. 26, pp. 786-797, 2011.
[63] "Modeling and simulation of the propagation of harmonics in electric power networks. I. Concepts, models, and simulation techniques," *Power Delivery, IEEE Transactions on,* vol. 11, pp. 452-465, 1996.
[64] R. N. Ray, D. Chatterjee, and S. K. Goswami, "Reduction of voltage harmonics using optimisation-based combined approach," *Power Electronics, IET,* vol. 3, pp. 334-344, 2010.
[65] "IEEE Recommended Practices and Requirements for Harmonic Control in Electrical Power Systems," *IEEE Std 519-1992*, p. 0_1, 1993.
[66] F. C. De La Rosa, *Harmonics And Power Systems*: CRC Press INC, 2006.
[67] M. Farhoodnea, A. Mohamed, and H. Shareef, "A new method for determining multiple harmonic source locations in a power distribution system," in *Power and Energy (PECon), 2010 IEEE International Conference on*, 2010, pp. 146-150.
[68] I. T. Papaioannou, A. S. Bouhouras, A. G. Marinopoulos, M. C. Alexiadis, C. S. Demoulias, and D. P. Labridis, "Harmonic impact of small photovoltaic systems connected to the LV distribution network," in *Electricity Market, 2008. EEM 2008. 5th International Conference on European*, 2008, pp. 1-6.
[69] H. E. Mazin, X. Wilsun, and H. Biao, "Determining the Harmonic Impacts of Multiple Harmonic-Producing Loads," *Power Delivery, IEEE Transactions on,* vol. 26, pp. 1187-1195, 2011.
[70] A. Ulinuha, M. A. S. Masoum, and S. Islam, "Hybrid genetic-fuzzy algorithm for volt/var/total harmonic distortion control of distribution systems with high penetration of non-linear loads," *Generation, Transmission & Distribution, IET,* vol. 5, pp. 425-439, 2011.
[71] P. S. Moses and M. A. S. Masoum, "Three-Phase Asymmetric Transformer Aging Considering Voltage-Current Harmonic Interactions, Unbalanced Nonlinear Loading, Magnetic Couplings, and Hysteresis," *Energy Conversion, IEEE Transactions on,* vol. 27, pp. 318-327, 2012.
[72] M. A. S. Masoum and P. S. Moses, "Impact of balanced and unbalanced direct current bias on harmonic distortion generated by asymmetric three-phase three-leg transformers," *Electric Power Applications, IET,* vol. 4, pp. 507-515, 2010.
[73] A. Mansoor, "Lower order harmonic cancellation: impact of low-voltage network topology," in *Power Engineering Society 1999 Winter Meeting, IEEE,* 1999, pp. 1106-1109 vol.2.
[74] A. Mau Teng and V. M. Jovica, "Planning Approaches for the Strategic Placement of Passive Harmonic Filters in Radial Distribution Networks," *Power Delivery, IEEE Transactions on,* vol. 22, pp. 347-353, 2007.
[75] J. Hayes, "Data centres 2020," *Engineering & Technology,* vol. 4, pp. 54-58, 2009.
[76] J. Van Mierlo, P. Van den Bossche, and G. Maggetto, "Models of energy sources for EV and HEV: fuel cells, batteries, ultracapacitors, flywheels and engine-generators," *Journal of Power Sources,* vol. 128, pp. 76-89, 2004.
[77] "Flywheel vs. battery for medical center IT infrastructure," Mazzetti Nash Lipsy Burch Company, San Francisco, CA2008.
[78] "Reliability Assessment of Integrated Flywheel UPS vs. Double Conversion UPS with Batteries," Active Power Inc., Austin, TX2008.
[79] "Cost Comparison for a 20 MW Flywheel-based Frequency Regulation Power Plant," Beacon Power Corporation, Tyngsboro, MA2007.

[80] "Flywheel Energy Storage," Department of Energy2003.
[81] G. K. Singh, "A six-phase synchronous generator for stand-alone renewable energy generation: Experimental analysis," *Energy*, vol. 36, pp. 1768-1775, 2011.
[82] M. Olsen. (2008) 15 Seconds vs. 15 Minutes. *The international magazine of 7x24 Exchange*.
[83] A. Ruddell, "Investigation on storage technologies for intermittent renewable energies: Evaluation and recommended r&d strategy," *Storage Technology report ST6: Flywheel, Chilton Didcot www. itpower. co. uk/investire/pdfs/flywheelrep. pdf*, 2003.
[84] "Understanding Flywheel Energy Storage: Does High Speed Really Imply a Better Design?," Active power Inc., Austin, TX2008.
[85] T. Siostrzonek, A. Penczek, and S. Pirog, "The control and structure of the power electronic system supplying the Flywheel Energy Storage " presented at the 2007 European Conference on Power Electronics and Applications, Aalborg, Denmark, 2007.
[86] E. Furlong and W. Wiltsch, "Performance and Operational Characteristics of an Advanced Power System," *GE library*.
[87] R. S. Weissbach, G. G. Karady, and R. G. Farmer, "A combined uninterruptible power supply and dynamic voltage compensator using a flywheel energy storage system," *Power Delivery, IEEE Transactions on*, vol. 16, pp. 265-270, 2001.
[88] S. Eckroad and I. Gyuk, "EPRI-DOE Handbook of Energy Storage for Transmission & Distribution Applications," *Electric Power Research Institute, Inc*, 2003.
[89] "UNIBLOCK UBR - Hybrid Rotary UPS from 150 kVA up to 1300 kVA," Piller UPS Company, Osterode, Germany2011.
[90] "Technical data sheet, UNIBLOCK UBT 1300," P. U. Company, Ed., ed. Osterode, Germany Piller UPS Company, 2005.
[91] I. Alan and T. A. Lipo, "Induction machine based flywheel energy storage system," *Aerospace and Electronic Systems, IEEE Transactions on*, vol. 39, pp. 151-163, 2003.
[92] H. F. Hofmann, *High-speed synchronous reluctance machine for flywheel applications*, 1998.
[93] P. Liu and H. P. Liu, "Permanent-magnet synchronous motor drive system for electric vehicles using bidirectional z-source inverter," *Electrical Systems in Transportation, IET*, vol. 2, pp. 178-185, 2012.
[94] "VAZATA Data Centers Specifications," VAZATA Solutions, Plano, TX 2012.
[95] "IEEE Recommended Practice for the Design of Reliable Industrial and Commercial Power Systems," *IEEE Std 493-2007 (Revision of IEEE Std 493-1997)*, pp. 1-689, 2007.
[96] P. HESKES and J. DUARTE, "Harmonic reduction as ancillary service by inverters for distributed energy resources (DER) in electricity distribution networks," in *Proc. CIRED*, 2007, pp. 1-4.
[97] A. Fodor, A. Magyar, and K. M. Hangos, "Control-oriented modeling of the energy-production of a synchronous generator in a nuclear power plant," *Energy*, vol. 39, pp. 135-145, 2012.
[98] "FACT SHEET: COMMUNITY ENERGY STORAGE FOR GRID SUPPORT (OCTOBER 2012)," ed: Office of Electricity Delivery & Energy Reliability, Department of Energy, 2012.
[99] A. Nourai, R. Sastry, and T. Walker, "A Vision & Strategy for Deployment of. Energy Storage in Electric Utilities," in *Power and Energy Society General Meeting, 2010 IEEE*, 2010, pp. 1-4.
[100] S. Beer, T. Gomez, D. Dallinger, I. Momber, C. Marnay, M. Stadler, and J. Lai, "An Economic Analysis of Used Electric Vehicle Batteries Integrated Into Commercial Building Microgrids," *Smart Grid, IEEE Transactions on*, vol. 3, pp. 517-525, 2012.
[101] A. Nourai, "Distributed Bulk Storage: The future of batteries in grid applications," in *Power and Energy Society General Meeting, 2011 IEEE*, 2011, pp. 1-1.
[102] R. Arghandeh, A. Onen, and R. P. Broadwater, "Distributed energy storage system control for optimal adoption of electric vehicles," in *Power and Energy Society General Meeting, 2012 IEEE*, 2012, pp. 1-8.
[103] D. Gautam and M. Nadarajah, "Influence of distributed generation on congestion and LMP in competitive electricity market," *Int. Jour. Electr. Power Eng*, vol. 3, pp. 228-235, 2010.

[104] E. Litvinov, "Design and operation of the locational marginal prices-based electricity markets," *Generation, Transmission & Distribution, IET,* vol. 4, pp. 315-323, 2010.
[105] R. P. Broadwater, A. Sargent, A. Yarali, H. E. Shaalan, and J. Nazarko, "Estimating substation peaks from load research data," *Power Delivery, IEEE Transactions on,* vol. 12, pp. 451-456, 1997.
[106] A. Sargent, R. Broadwater, J. Thompson, and J. Nazarko, "Estimation of diversity and kWHR-to-peak-kW factors from load research data," *Power Systems, IEEE Transactions on,* vol. 9, pp. 1450-1456, 1994.
[107] T. DcDermott, I. Drezga, and R. Broadwater, "A heuristic nonlinear constructive method for distribution system reconfiguration," *Power Systems, IEEE Transactions on,* vol. 14, pp. 478-483, 1999.
[108] R. P. Broadwater, P. A. Dolloff, T. L. Herdman, R. Karamikhova, and A. F. Sargent, "Minimum loss optimization in distribution systems: discrete ascent optimal programming," *Electric power systems research,* vol. 36, pp. 113-121, 1996.
[109] Y. Liang, K. S. Tam, and R. Broadwater, "Load Calibration and Model Validation Methodologies for Power Distribution Systems," *Power Systems, IEEE Transactions on,* vol. 25, pp. 1393-1401, 2010.
[110] J. Wengler, *Managing energy risk: a nontechnical guide to markets and trading*: PennWell Books, 2001.
[111] G. Li, C. C. Liu, C. Mattson, and J. Lawarrée, "Day-ahead electricity price forecasting in a grid environment," *Power Systems, IEEE Transactions on,* vol. 22, pp. 266-274, 2007.
[112] S. Y. Park, "Performance of differentiated rate scheduling using contention-based CSI feedback," *Vehicular Technology, IEEE Transactions on,* vol. 59, pp. 3143-3148, 2010.
[113] M. Erol-Kantarci, J. Sarker, and H. Mouftah, "Communication-based Plug-In Hybrid Electrical Vehicle load management in the smart grid," in *Computers and Communications (ISCC), 2011 IEEE Symposium on*, 2011, pp. 404-409.
[114] Z. Darabi and M. Ferdowsi, "Aggregated impact of plug-in hybrid electric vehicles on electricity demand profile," *Sustainable Energy, IEEE Transactions on,* vol. 2, pp. 501-508, 2011.
[115] S. Shao, M. Pipattanasomporn, and S. Rahman, "Challenges of PHEV penetration to the residential distribution network," in *Power & Energy Society General Meeting, 2009. PES'09. IEEE*, 2009, pp. 1-8.
[116] C. Camus, C. Silva, T. Farias, and J. Esteves, "Impact of Plug-in Hybrid Electric Vehicles in the Portuguese electric utility system," in *Power Engineering, Energy and Electrical Drives, 2009. POWERENG'09. International Conference on*, 2009, pp. 285-290.
[117] J. Jung, H. Asgeirsson, T. Basso, J. Hambrick, M. Dilek, R. Seguin, and R. Broadwater, "Evaluation of DER adoption in the presence of new load growth and energy storage technologies," in *Power and Energy Society General Meeting, 2011 IEEE*, 2011, pp. 1-8.
[118] N. C. McDonald, "Critical factors for active transportation to school among low-income and minority students: evidence from the 2001 National Household Travel Survey," *American journal of preventive medicine,* vol. 34, pp. 341-344, 2008.
[119] "2001 National Household Travel Survey User's Guide," NHTS2004.
[120] K. Clement-Nyns, E. Haesen, and J. Driesen, "The impact of charging plug-in hybrid electric vehicles on a residential distribution grid," *Power Systems, IEEE Transactions on,* vol. 25, pp. 371-380, 2010.
[121] K. Morrow, D. Karner, and J. Francfort, "Plug-in hybrid electric vehicle charging infrastructure review," *US Departent of Energy-Vehicle Technologies Program,* 2008.
[122] *In My backyard Online Tool*. Available: http://www.nrel.gov/eis/imby/
[123] *PV Watts online tool*. Available: http://rredc.nrel.gov/solar/calculators/PVWATTS/version1
[124] *New York State Public Service Commission*.
[125] S. Kawasaki, "Analysis on harmonics of distribution network with distribution generators," presented at the International Conference on Electrical Engineering, Shenyang, China, 2009.

[126] S. Volut, *Electrical Installation Guide According to IEC Standards*. Franse: Schneider Electric, 2009.
[127] A. Cataliotti, V. Cosentino, and S. Nuccio, "Static Meters for the Reactive Energy in the Presence of Harmonics: An Experimental Metrological Characterization," *Instrumentation and Measurement, IEEE Transactions on,* vol. 58, pp. 2574-2579, 2009.
[128] X. Wilsun and L. Yilu, "A method for determining customer and utility harmonic contributions at the point of common coupling," *Power Delivery, IEEE Transactions on,* vol. 15, pp. 804-811, 2000.
[129] G. J. Wakileh, *Power Systems Harmonics Fundamentals, Analysis and Filter Design*. Germany: Springer, 2001.
[130] L. Cividino, "Power factor, harmonic distortion; causes, effects and considerations," in *Telecommunications Energy Conference, 1992. INTELEC '92., 14th International*, 1992, pp. 506-513.
[131] B. S. I. Staff, *Guide for the Application of the European Standard En 50160*: B S I Standards, 2004.
[132] S. M. Halpin, "Comparison of IEEE and IEC harmonic standards," in *Power Engineering Society General Meeting, 2005. IEEE*, 2005, pp. 2214-2216 Vol. 3.
[133] I. E. Commission, *IEC 61000-3-6: Electromagnetic compatibility (EMC) - limits - assessment of emission limits for distorting loads in MV and HV power systems - basic EMC publication*, 1996.
[134] "IEEE Application Guide for IEEE Std 1547, IEEE Standard for Interconnecting Distributed Resources with Electric Power Systems," *IEEE Std 1547.2-2008*, pp. 1-207, 2009.
[135] A. E. d. N. y. Certificación, *CEI/IEC 61000-2-11: Compatibilidad electromagnética(CEM). Parte 2-11, Entornos: clasificación de entornos IEMN-GA*: AENOR, 2002.
[136] F.-s. Kang, S.-J. Park, S. E. Cho, and J.-M. Kim, "Photovoltaic power interface circuit incorporated with a buck-boost converter and a full-bridge inverter," *Applied Energy,* vol. 82, pp. 266-283, 2005.
[137] A. Marzoughi, H. Imaneini, and A. Moeini, "An optimal selective harmonic mitigation technique for high power converters," *International Journal of Electrical Power & Energy Systems,* vol. 49, pp. 34-39, 2013.
[138] D. Salles, J. Chen, W. Xu, W. Freitas, and H. E. Mazin, "Assessing the Collective Harmonic Impact of Modern Residential Loads—Part I: Methodology," *Power Delivery, IEEE Transactions on,* vol. 27, pp. 1937-1946, 2012.
[139] X. Wang, F. Blaabjerg, and Z. Chen, "Synthesis of Variable Harmonic Impedance in Inverter-Interfaced Distributed Generation Unit for Harmonic Damping Throughout a Distribution Network," *Industry Applications, IEEE Transactions on,* vol. 48, pp. 1407-1417, 2012.
[140] A. Ghosh and A. Joshi, "The use of instantaneous symmetrical components for balancing a delta connected load and power factor correction," *Electric Power Systems Research,* vol. 54, pp. 67-74, 2000.
[141] M. Dilek, R. Broadwater, and R. Sequin, "Computing distribution system fault currents and voltages via numerically computed Thevenin equivalents and sensitivity matrices," in *Power Systems Conference and Exposition, 2004. IEEE PES*, 2004, pp. 244-251.